2004

Catalytic applications of rhenium compounds and hydrogen atom transfer reactions of substituted phthalimide N-oxyl radicals

Yang Cai
Iowa State University

Catalytic applications of rhenium compounds and hydrogen atom transfer reactions of substituted phthalimide N-oxyl radicals

by

Yang Cai

A dissertation submitted to the graduate faculty

in partial fulfillment of the requirements for the degree of

DOCTOR OF PHILOSOPHY

Major: Inorganic Chemistry

Program of Study Committee:
James H. Espenson, Major Professor
Victor Shang-Yi Lin
Gordon J. Miller
Nicola L. Pohl
Mark S. Hargrove

Iowa State University

Ames, Iowa

2004

Graduate College

Iowa State University

This is to certify that the doctoral dissertation of

Yang Cai

has met the dissertation requirements of Iowa State University

Signature was redacted for privacy.

Major Professor

Signature was redacted for privacy.

For the Major Program

TABLE OF CONTENTS

GENERAL INTRODUCTION

Introduction

The chemistry and reactivities of transition metal oxo complexes have attracted great attention due to their applications in catalysis.[1] One category is the high-valent rhenium oxo compounds. Indeed, there are many rhenium oxo compounds reported to be good catalysts for oxygen atom transfer reactions.[2-5] Among them, methyltrioxorhenium $MeReO_3$, abbreviated as MTO, has been used for catalytic oxygen atom transfer reactions.[6,7] It has the ability to activate hydrogen peroxide to form two active rhenium peroxo species, both of which are able to transfer oxygen atoms to various substrates.[8-13]

Recently, we found that MTO also catalyzes the reduction of hydronium ions from acidic europium(II) solutions to evolve hydrogen. Although the reaction between Eu^{2+} and H^+ is thermodynamically favorable, kinetically they are sufficiently stable with each other for lengthy periods. Since Eu^{2+} is a strong single-electron reductant, the chemistry of dihydrogen formation would entail intermediate formation of H_{aq}•, which is not thermodynamically feasible, E° for H•/H_2 being 2.3 V.[14,15] So the actual process for proton reduction must avoid the intermediacy of H radicals. In Chapter I, we describe the kinetic studies of the reaction of Eu^{2+} and H^+ with MTO as catalyst and propose a possible mechanism for hydrogen evolution. In this mechanism, a hydrido rhenium species is suggested, from which H_2 is generated by a proton-hydride reaction pathway. During the study, chromium(II) ions are also investigated for the same reaction and were shown not to evolve H_2, even though they have similar reduction potentials -0.43 V and -0.38 V respectively.[16,17] Besides, we also report the reaction mechanism of MTO catalyzed reduction of perchlorate ions by europium(II) ions in acid solution in this chapter. Perchlorate has a powerful thermodynamic tendency for

reduction in dilute aqueous solution: $E°(ClO_4^-/ClO_3^-) = 1.19$ V. However, it is usually very slow. To our knowledge, the only exception for fast reduction of aqueous perchlorate ions is a system involving the reactive reductant, methylrhenium dioxide (MDO), which is produced by MTO and H_3PO_2 in aqueous solution.[18] Now we use hydrated Eu^{2+} or Cr^{2+} as the reducing agents and they can reduce MTO to MDO, followed by its fast reduction of perchlorate ions. Such an oxygen transfer reaction is summarized in Scheme 1. All the results are presented in Chapter I.

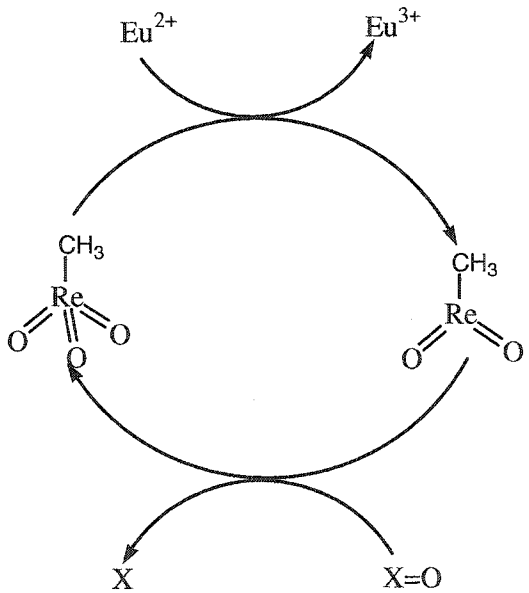

Scheme 1. Oxygen transfer reactions by Eu^{2+} with MTO as catalyst.

Chapter II reports the synthesis of a new oxorhenium(V) compound **1**, MeReO(edt)(bpym), and its kinetics for catalyzing oxygen atom transfer from picoline N-oxide to triarylphosphines. Before this, numbers of oxorhenium(V) compounds have been synthesized in our group. Some of them are found to be active catalysts for the oxygen atom transfer reaction, such as the Re(V) dithiolato complex MeReO(mtp)PPh_3 **2**, where $mtpH_2$ is 2-(mercaptomethyl)thiophenol (o-$HSC_6H_4CH_2SH$).[19-21] However, those active catalysts are

all five-coordinate oxorhenium compounds. Other oxorhenium(V) complexes with six-coordinate ligands are completely inactive.[22] Based on previous findings, we postulate that there must be a steric requirement for the active catalysts, which is that the O-atom donor must be able to coordinate to an active site on the rhenium center. Thus, the potential catalyst should have an already-vacant position, or have a position which can become vacant by the departure of an existing ligand.[23]

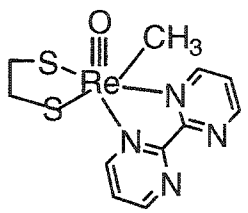

MeReO(edt)(bpym)

1

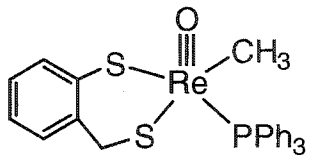

MeReO(mtp)PPh_3

2

In order to confirm this hypothesis, compound **1** was designed and prepared. The important feature is that it has a six-coordinate rhenium(V) center with a weakly-coordinating bidentate ligand, 2,2'-bipyrimidine, where the sixth coordination site can be opened during the catalytic cycle. The catalytic study shows that this compound catalyzes the oxygen atom transfer reaction between picoline N-oxide and triarylphosohines. Compared with those five-coordinate oxorhenium(V) compounds, it is less active. The details of kinetics and mechanism are illustrated in Chapter II.

Chapter III shows the kinetic studies for three distinct types of reactions of phthalimide N-oxyl radicals (PINO•) and N-hydroxylphthalimide (NHPI) derivatives (Chart 1). In 2001, Ishii discovered a remarkable catalytic reactivity of NHPI for the autoxidation of mehyl arenes.[24] After that, a number of related NHPI-catalyzed reactions have been reported.[24-26] In that cataylic system, PINO•, which is the one-electron oxidized form of

NHPI, plays a very important role. It abstracts a hydrogen atom from hydrocarbons. The kinetics for hydrogen abstraction reactions by PINO• from methyl arenes and other organic substrates have been studied in our group.[27,28] In this study, we present new kinetic data by using ring-substituted NHPI derivatives for three different type reactions, which are self-decomposition reactions, hydrogen atom self-exchange reactions and hydrogen abstraction reactions from *para*-xylene and toluene.

Chart 1.

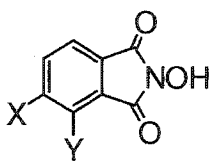

	X	Y
NHPI	H	H
4-Me-NHPI	Me	H
4-Cl-NHPI	Cl	H
4-F-NHPI	F	H
3-F-NHPI	H	F

Dissertation Organization

The dissertation consists of three chapters. Chapters I and II have been submitted to *Inorganic Chemistry*. Chapter III has been submitted to *Journal of Organic Chemistry*. Each chapter is self-contained with its own equations, figures, tables and references. Following the last chapter are the general conclusions and acknowledgements. With exception of Chapter III, small parts of which were performed with Dr. Nobuyoshi Koshino and Dr. Basudeb Saha, all the work in this dissertation was performed by the author.

References

(1) Casey, C. P. *Science* **1993**, *259*, 1552.

(2) Huang, R.; Espenson, J. H. *Inorg. Chem.* **2001**, *40*, 994.

(3) Arias, J.; Newlands, C. R.; Abu-Omar, M. M. *Inorg. Chem.* **2001**, *40*, 2185.

(4) Abu-Omar, M. M.; McPherson, L. D.; Arias, J.; Bereau, V. M. *Angew. Chem. Int. Ed. Engl.* **2000**, *39*, 4310.

(5) Gunaratne, H. D.; McKervey, M. A.; Feutren, S.; Finlay, J.; Boyd, J. *Tetrahedron Lett.* **1998**, *39*, 5655.

(6) Espenson, J. H. *J. Chem. Soc. Chem. Commun.* **1999**, 479.

(7) Herrmann, W. A.; Kratzer, R. M.; Fisher, R. W. *Angew. Chem. Int. Ed. Engl.* **1997**, *36*, 2652.

(8) Murray, R. W.; Lyanar, K. *Tetrahedron Lett.* **1997**, 335.

(9) Zhu, Z.; Espenson, J. H. *J. Org. Chem.* **1995**, 1326.

(10) Zhu, Z.; Espenson, J. H. *J. Org. Chem.* **1995**, 7728.

(11) Abu-Omar, M. M.; Espenson, J. H. *J. Am. Chem. Soc.* **1995**, 272.

(12) Vassell, K. A.; Espenson, J. H. *Inorg. Chem.* **1994**, 5491.

(13) Herrmann, W. A.; Fisher, R. W.; Rauch, M. U. *Angew. Chem. Int. Ed. Engl.* **1993**, 1157.

(14) Schwarz, H. A. *J. Chem. Educ.* **1981**, 101.

(15) Swallow, A. J. *Radiation Chemistry: An Introduction;* **1973**, Longman: London, 1973.

(16) Weaver, M. J.; Yee, E. L. *Inorg. Chem.* **1980**, *19*, 1936.

(17) Weaver, M. J. *J. Am. Chem. Soc.* **1979**, *101*, 1131.

(18) Abu-Omar, M. M.; Espenson, J. H. *Inorg. Chem.* **1995**, *34*, 6239.

(19) Lente, G.; Espenson, J. H. *Inorg. Chem.* **2000**, *39*, 4809.

(20) Wang, Y.; Espenson, J. H. *Inorg. Chem.* **2002**, *41*.

(21) Wang, Y.; Espenson, J. H. *Org. Lett.* **2000**, *2*, 3525.

(22) Espenson, J. H.; Shan, X.; Lahti, D. W.; Rockey, T. M.; Saha, B.; Ellern, A. *Inorg. Chem.* **2001**, *40*.

(23) Espenson, J. H. *Adv. Inorg. Chem.* **2003**, *54*, 157.

(24) Ishii, Y.; Sakaguchi, S.; Iwahama, T. *Adv. Synth. Catal.* **2001**, *343*, 393.

(25) Arends, I. W. C. E.; Sasidharan, M.; Duda, M.; Kuhnle, A.; Jost, C.; Sheldon, R. A. *Tetrahedron* **2002**.

(26) Amorati, R.; Lucarini, M.; Mugnaini, V.; Pedulli, G. F.; Minisci, F.; Recupero, F.; Fontana, F.; Astolfi, P.; Greci, L. *J. Org. Chem.* **2003**, *68*, 1747.

(27) Koshino, N.; Saha, B.; Espenson, J. H. *J. Org. Chem.* **2003**, *68*, 9364.

(28) Koshino, N.; Cai, Y.; Espenson, J. H. *J. Phys. Chem. A.* **2003**, *107*, 4262.

CHAPTER I. KINETICS AND MECHANISM OF HYDROGEN EVOLUTION AND PERCHLORATE REDUCTION IN ACIDIC EUROPIUM(II) SOLUTION CATALYZED BY METHYLRHENIUM TRIOXIDE (MTO)

A manuscript submitted to *Inorganic Chemistry*

Yang Cai and James H. Espenson

Introduction

Many species that lie below H^+/H_2 in the electrochemical series survive for lengthy periods in acidic solution because of substantial kinetic barriers. Indeed, among reduced metal ions, species such as the hydrated cations of Cr^{2+}, Eu^{2+}, and V^{2+} remain indefinitely unchanged provided the solutions are acidic and oxygen is rigorously excluded. However, these species are thermodynamically unstable because of the formation of M(III) and dihydrogen, shown as eq 1.

$$2M_{aq}^{2+} + 2H^+ \longrightarrow 2M_{aq}^{3+} + H_2 \qquad (1)$$

The driving forces $\Delta E°$ for these reactions are 0.415, 0.380, and 0.230 V for Cr^{2+}, Eu^{2+}, and V^{2+} respectively.[1,2] Since the potentials show the reactions are favorable, a kinetic barrier is responsible for the lack of reactivity. Because all of these metal ions are strong single electron reductants, single-electron chemistry of dihydrogen formation would entail intermediate formation of $H_{aq}•$, which is not thermodynamically feasible. Although V^{2+} ion can go through a two electron change to produce VO^{2+}, the reduction potential for VO^{2+}/V^{2+} is 0.08 V, more positive than that for H^+/H_2. That means the reaction

$$V_{aq}^{2+} + H_2O \longrightarrow VO_{aq}^{2+} + H_2 \qquad (2)$$

is thermodynamically unfavorable. Thus, any actual process for proton reduction must avoid the intermediacy of H radicals. Most hydrogen evolution reactions from a metal or a metal complex have one common feature, which is the formation of an intermediate hydridometal species. The metal hydride formation will lower the energy barrier for the production of H_2 and avoid hydrogen radical formation. Thus, hydrogen gas can be generated directly by a bimolecular reaction pathway[3,4] or by a proton-hydride reaction pathway.[4,5]

In 1986, the first example of a homogeneous, nonphotochemical process of proton reduction was reported, which evolves molecular hydrogen rapidly from acidic solutions of chromium(II), europium(II), or vanadium(II) ions in the presence of trace concentrations of the cobalt(II) macrocycle $Co(dmgBF_2)_2$.[6] The reaction follows Michaelis-Menten kinetics, which is summarized in eq 3-8. In this scheme, a $Co^{I}(dmgBF_2)_2^-$ intermediate is proposed, which produces a Co(III) hydride in the subsequent fast reaction. The hydride complex has the ability to evolve H_2 by both of the alternatives shown, eq 6 and 7. In such a system, the kinetics requires chloride, bromide, or a similar anion for hydrogen formation. Those halide ions serve as a bridge for inner-sphere electron transfer between the reducing metal and cobalt(II) to produce the cobalt(I) intermediate, as depicted in the equations.

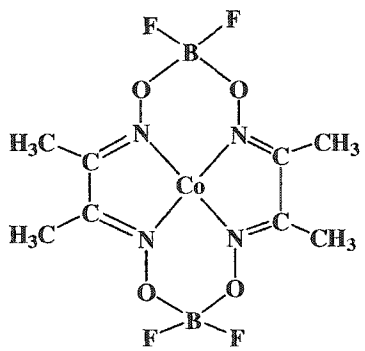

$$Cr^{2+} + Cl^- + Co^{II}(dmgBF_2)_2 \rightleftharpoons [Cr\text{-}Cl\text{-}Co(dmgBF_2)_2]^+ \quad (3)$$

$$[Cr\text{-}Cl\text{-}Co(dmgBF_2)_2]^+ \longrightarrow Co^{I}(dmgBF_2)_2^- + CrCl^{2+} \quad (4)$$

$$Co^{I}(dmgBF_2)_2^- + H^+ \xrightarrow{fast} HCo^{III}(dmgBF_2)_2 \quad (5)$$

$$2HCo^{III}(dmgBF_2)_2 \xrightarrow{fast} 2Co(dmgBF_2)_2 + H_2 \quad (6)$$

$$HCo^{III}(dmgBF_2)_2 + H^+ \xrightarrow{fast} H_2 + Co^{III}(dmgBF_2)_2^+ \quad (7)$$

$$Co^{III}(dmgBF_2)_2^+ + Cr^{2+} + Cl^- \xrightarrow{fast} CrCl^{2+} + Co(dmgBF_2)_2 \quad (8)$$

In 1988, Gould et al. noted that ReO_4^- can catalyze the reduction of H^+ to H_2 by vitamin B_{12s} (cobalt(I)alamin, the cobalt(I) analogue of B_{12}) as they studied the stoichiometry of the reaction between sodium perrhenate and B_{12s}. But they did not do further studies because of the difficulties in measuring the yield of H_2 formed and in determining the oxidation state of the rhenium species involved during the reaction process.[7] So the chemistry for this reaction remained unclear.

Recently, when we mixed $MeReO_3$ with Eu^{2+} in acidic aqueous solution, we made the unanticipated observation that H_2 is evolved fairly rapidly when the perchlorate ion is absent in the solution. In contrast to the $Co(dmgBF_2)_2$ system, this reaction does not require any chloride anion, which is necessary for the evolution of H_2 in the cobalt's case. Even though most of our experiments are carried out in chloride anion media, triflate anion solutions also evolve H_2. It is also interesting that no H_2 bubbles are observed when we used Cr^{2+} as the reducing agent. Because these observations are unprecedented, we have undertaken a study of the Eu^{2+} reaction to understand, principally by kinetics, the mechanism of catalyzed

hydrogen formation and also the reasons why Eu^{2+} but not Cr^{2+}, both of which have essentially the same value of E°, do not behave in the same way.

In the course of this research, we also found that perchlorate ion is reduced to chloride ion instead of H_2 formation when perchlorate ion is present in the solution. Perchlorate ion has a powerful thermodynamic tendency for reduction in dilute aqueous solution: $E°(ClO_4^-/ClO_3^-) = 1.19$ V. Although this reduction is very favorable in terms of $\Delta G°$, nevertheless, it is often very slow. Tables 1 and 2 list reduction potentials for a number of transition metal ions and their rate constants for the reduction of perchlorate ions.[8-14] The rates show no obvious correlation to the driving force. For instance, some metal ions and complexes react with perchlorate ion slowly, which include V_{aq}^{2+},[8] V_{aq}^{3+},[8] Ti_{aq}^{3+},[9] $Ru(OH_2)_6^{2+}$,[12] and $Ru(NH_3)_6^{2+}$.[10] In contrast, essentially no reaction has been measured for even stronger reducing agents, including Eu_{aq}^{2+} and Cr_{aq}^{2+}. An acceptable explanation is that an especially stable bond to O^{2-} is formed by the oxidized product during the reduction of ClO_4^- ion.[13]

To our knowledge, the only exception is the fast reduction of aqueous perchlorate ions provided by a system containing MTO and H_3PO_2.[14] These components react ($k_{298} = 0.028$ L $mol^{-1}s^{-1}$)[15] to form $MeReO_2(H_2O)_n$ (n=2, presumably) (MDO). Although there is no direct structural characterization for this metastable MDO species, it was speculated to be a five-coordinate oxorhenium(V) compound, based on several similar analogues in previous reports.[16-19] In 1994, Herrmann et al. characterized a solid compound of $MeReO_2(PPh_3)_2 \cdot MeReO_3$. There is a MDO fragment in it, where the rhenium(V) center takes five-coordinated trigonal bipyramidal structure with trans-disposed phosphine ligands. The Re(V) complex MDO prepared from MTO and H_3PO_2 in aqueous solution is a strong $2e^-$ reducing agent and it is able to subtract an oxygen atom from many substrates, including

perchlorate ion. Abu-Omar found that MDO reduces ClO_4^- rapidly, $k_{298} = 7.3\ M^{-1}\ s^{-1}$, which is by far the highest rate constant recorded for perchlorate reduction. In this study, we are using Eu_{aq}^{2+} or Cr_{aq}^{2+} as the reducing agent. These metal ions can reduce MTO to MDO, followed by fast reduction of perchlorate ion. Thus, the catalytic cycle can keep running until the reducing agent is completely consumed.

Table 1. Redox potential for some metal ion reagents

Redox couples	E° / V
VO_{aq}^{2+}/V_{aq}^{3+}	0.36
$Ru(H_2O)_6^{3+}/ Ru(H_2O)_6^{2+}$	0.23
$Ti_{aq}^{4+}/Ti_{aq}^{3+}$	~ 0.1
$Ru(NH_3)_5(H_2O)^{3+}/ Ru(NH_3)_5(H_2O)^{2+}$	0.065
$Ru(NH_3)_6^{3+}/ Ru(NH_3)_6^{2+}$	0.051
V_{aq}^{3+}/V_{aq}^{2+}	-0.23
$Eu_{aq}^{3+}/Eu_{aq}^{2+}$	-0.38
$Cr_{aq}^{3+}/Cr_{aq}^{2+}$	-0.43

Table 2. Rate constant for perchlorate ion reduction by using transition metal complexes.

Reducing agents	T / °C	k / M^{-1} s^{-1}
V_{aq}^{3+}	50	2.8×10^{-6}
$Ru(H_2O)_6^{2+}$	25	3.2×10^{-3}
Ti_{aq}^{3+}	50	1.5×10^{-3}
$Ru(NH_3)_5(H_2O)^{2+}$	25	2.7×10^{-2}
$Ru(NH_3)_6^{2+}$	25	3.0×10^{-4}
V_{aq}^{2+}	50	2.2×10^{-5}
Eu_{aq}^{2+}	28	~ 10^{-8}
Cr_{aq}^{2+}		no reaction

Experimental Section

Materials. High-purity water was obtained by passing laboratory distilled water through a Millipore-Q water purification system. Methyltrioxorhenium(VII), CH_3ReO_3, abbreviated as MTO, was synthesized from sodium perrhenate and tetramethyltin (Strem).[20] Europium(III) solutions were made by dissolving europium(III) oxide (99.97%) in hydrochloric acid or triflic acid. Solutions of europium(II) was prepared from europium(III) solutions either by reduction with amalgamated zinc, or by electro-chemical reduction at a mercury cathode. Europium(II) solutions were stored in pyrex bottles under argon with a positive pressure. The concentrations of europium(II) were measured by their UV absorbance at 321nm, where the molar absorptivity is 587 M^{-1} cm^{-1}.

Chromium(II) solutions were reduced from chromium(III) solutions with amalgamated zinc. Chromium(III) solution was obtained by dissolving $CrCl_3$ in hydrochloric acid. Its concentration was analyzed spectrophotometrically by UV at 408nm (ε = 15.8 M^{-1} cm^{-1}).[21]

Most other chemicals were reagent grade and obtained commercially: hydrochloric acid, triflic acid, lithium chloride, sodium perchlorate. The acid concentration was analyzed by titration with sodium hydroxide to a phenolphthalein endpoint. The acid concentration of electrochemically prepared Eu(II) solution was titrated by sodium hydroxide after it passed through a column of Dowex 50W-X8 H^+ cation exchange resin, eluting with purified water.

Instrumentation. UV-vis spectra and kinetic data were obtained with Shimadzu Model 3101 and OLIS RSM stopped-flow spectrophotometers. Optical cells of 1 cm path length were used throughout the study. A circulating water thermostatic system controlled the temperature variation to within $\pm$0.2 °C was used for the stopped-flow instrument and an

electronic thermostatic cell holder that maintained the temperature of the cell to ± 0.2 °C was used for the UV-vis spectrophotometer. Hydrogen was identified by gas chromatography. A Gow-Mac GC 350 with a thermal conductivity detector (TCD) was used with argon as the carrier gas and Molecular Sieve 13x as the stationary phase. The rate of H_2 formation was determined volumetrically using a recording microvolumeter apparatus, which is modified from the previously reported one (see Diagram 1).[22] The top part represents the glass apparatus, which is the heart of the system. Mercury is held in the glass capillary volumeter tube and is pushed into the mercury reservoir behind the tube when the reaction gas enters through the three-way stopcock at the right. A 30-gauge Nickel-80 resistance wire goes concentrically through the length of the volumeter tube. A simple circuit is applied to the wire, which is shown in the bottom of the diagram. As the mercury moves through the glass tube, the length of unshorted wire changes proportional to the change of the gas volume. Thus the voltage changes linearly with the volume of the gas, which is recorded by a HP 3457A multi-meter. A VICI Pressure-Lok gas syringe was used to make the calibration of volume against voltage. In order to get more accurate volume of the gas produced from the reaction, the dead volume in the reaction vessel and the connection tubing was made as small as possible. Chloride ion concentration from the reduction of perchlorate was determined quantitatively by ion chromatography using potentiometry.[23] In the experiments, a Weiss Research CL3005 combination chloride ion selective electrode and a Hanna Instruments HI 1131 combination pH electrode were connected to a Hanna Instruments pH302 pH-meter. The electrodes were calibrated before use with standard NaCl solutions and standard buffers, respectively.

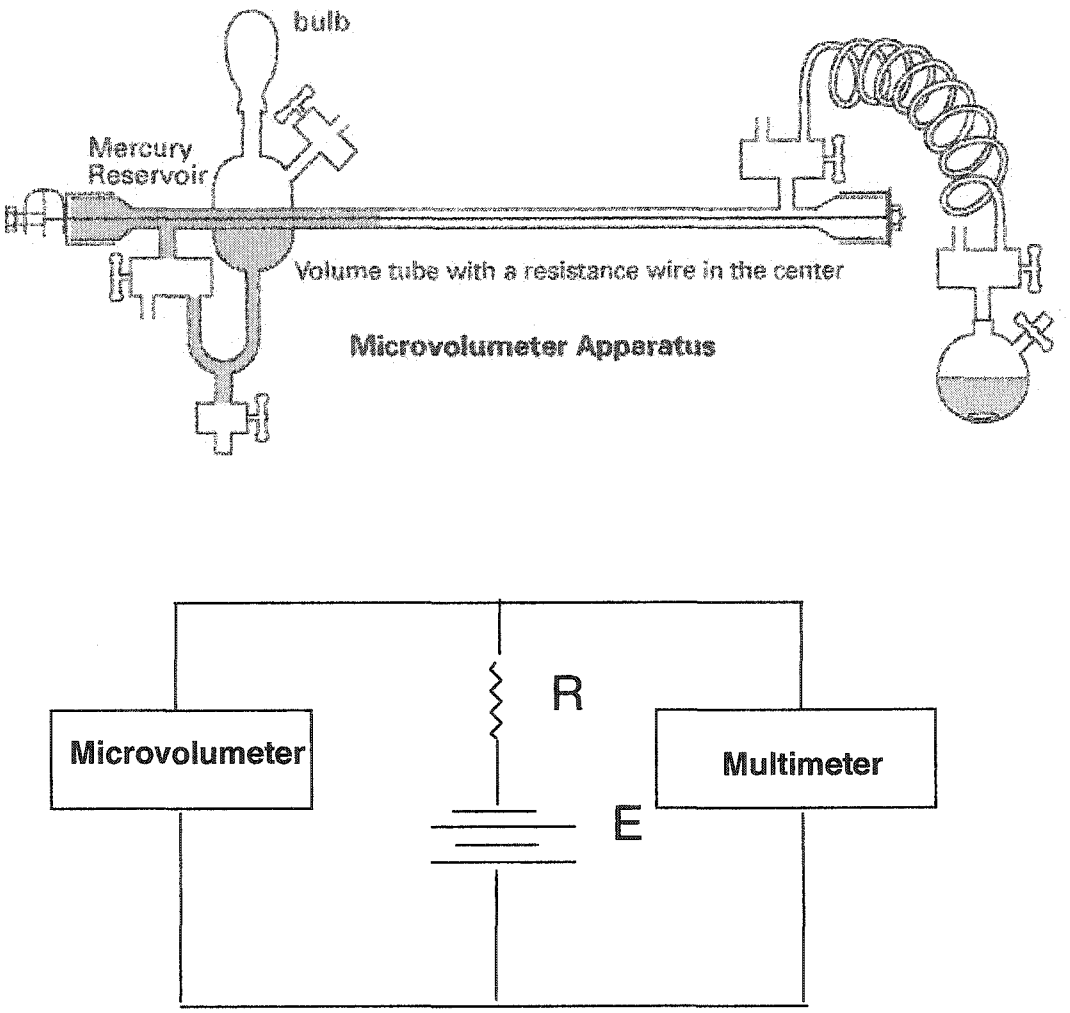

Diagram 1. A recording gas micorvolumeter system for hydrogen evolution. Top: the microvolumeter apparatus. Bottom: the circuit diagram. R, resistance; E, battery.

Results

Hydrogen evolution from acidic europium(II) solutions by MTO catalyst. When 0.3 mM MTO and 12 mM Eu^{2+} solutions were mixed in anaerobic 0.12 M HCl, a yellow color was produced instantaneously. Following that, a large amount of bubbles were produced, the number of which increases over 30 to 60 min. However, when Cr^{2+} was used instead, we only observed a color change from pale blue to yellow-green and no bubbles formed over 10 hours (see Picture 1).

Immediately after mixing MTO and Eu^{2+} solutions, there are two species evident in the UV-vis spectrum, Eu^{2+} and a species we call L410, named for the yellow intermediate with a maximum absorbance at 410 nm, shown in Figure 1. The peak at 321 nm, which belongs to Eu^{2+}, immediately begins to decrease in intensity while the L410 band remains stable until near the very end of the hydrogen evolution period (Figure 2). As a control experiment, an acidic Eu^{2+} solution was sealed in a cuvette; no bubbles were observed for 12 hours and the absorbance of Eu^{2+} remained unchanged, Figure3. But with MTO in the solution and 0.2 M H^+, the reaction finished in about 20 mins. The bubbles evolved were proved to be H_2 by GC. The buildup of H_2 gas was measured quantitatively by a microvolumeter apparatus. Quantitative measurements showed that the yield of H_2 is about 90% in several instances (Table 3), based on eq 9.

$$2Eu^{2+} + 2H^+ \xrightarrow{MTO} 2Eu^{3+} + H_2 \qquad (9)$$

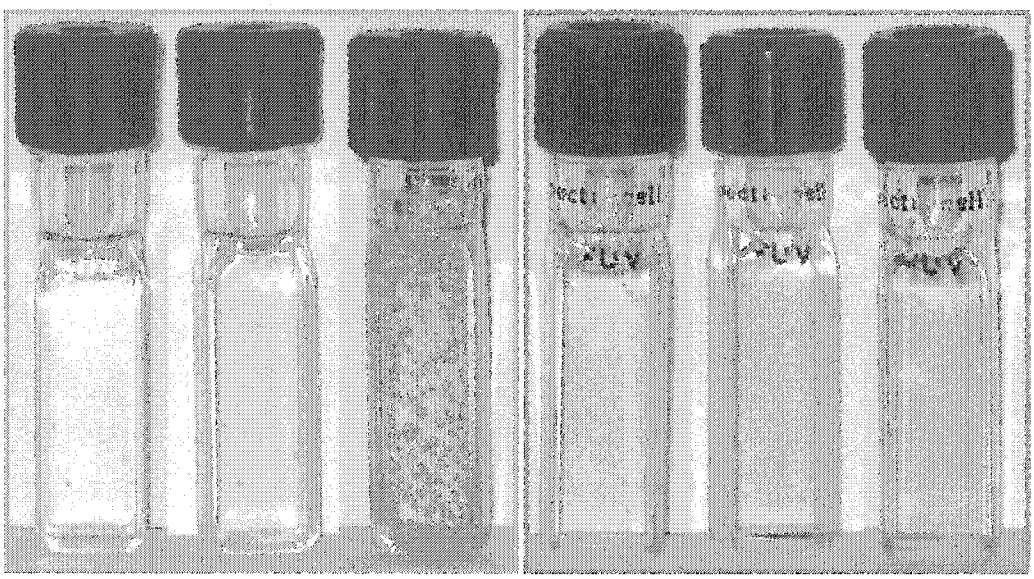

Picture 1. Visual changes in acidic solution, from left to right: 12 mM Eu^{2+}; 12 mM Eu^{2+} with 0.3 mM $MeReO_3$ after 1 min; 30 mins after, showing H_2 evolution; 12 mM Cr^{2+}; 12 mM Cr^{2+} with 0.3 mM $MeReO_3$ after 1 min; 1 hour later.

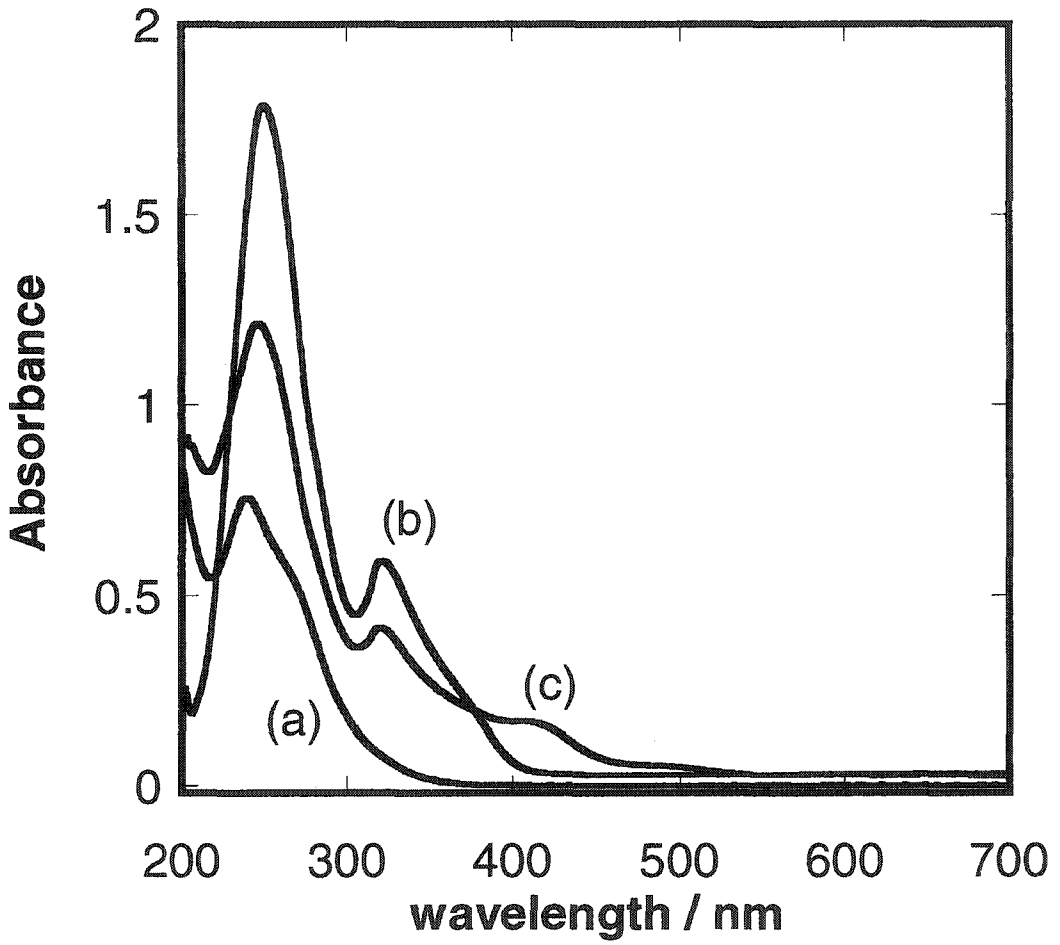

Figure 1. Spectral changes illustrating the formation of L410 from the reaction between MTO and Eu^{2+} in acid. (a) 0.4 mM MTO; (b) 1 mM Eu^{2+}; (c) 0.2 mM MTO with 1 mM Eu^{2+} at 0.14 M H^{+}.

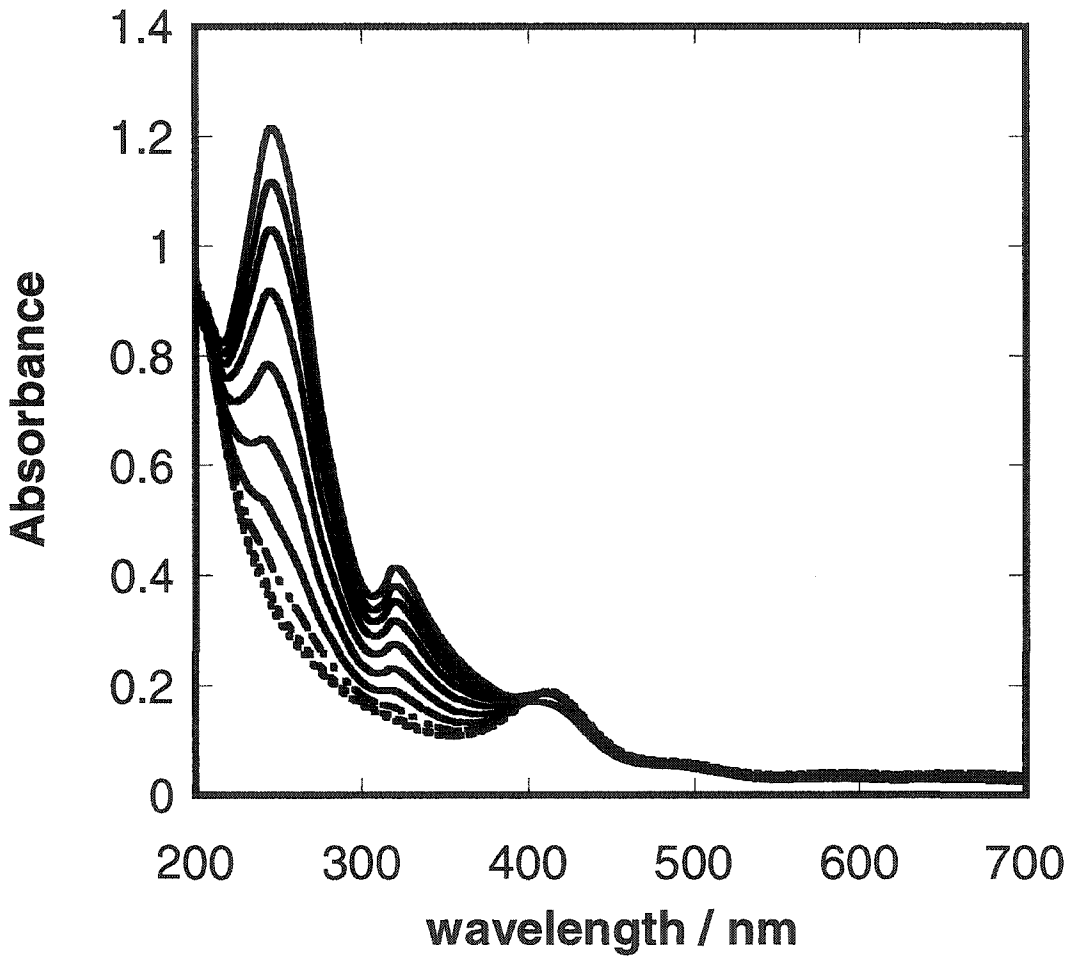

Figure 2. Spectral changes of 0.93 mM Eu^{2+} with 0.2 mM MTO at 0.14 M H^{+}, temp. = 25 °C, optical path length = 1.00 cm, and time-interval = 2 mins.

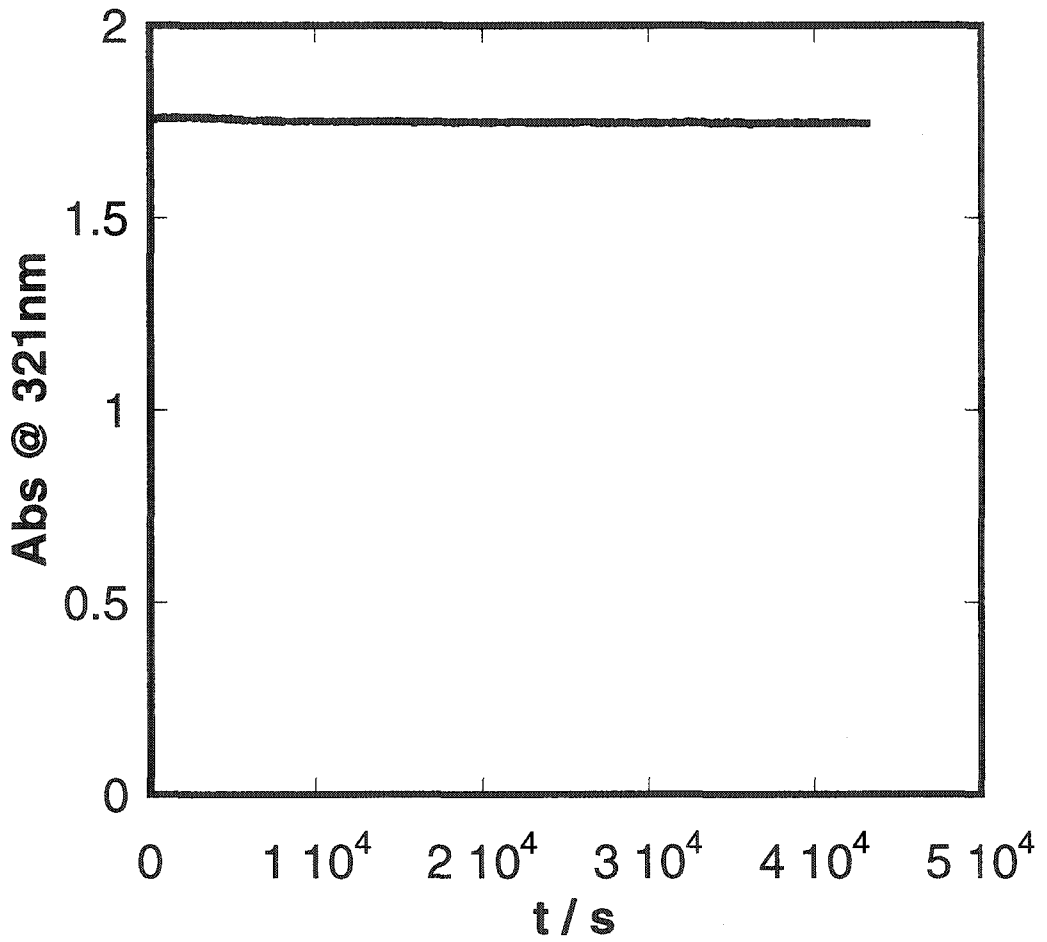

Figure 3. Control experiment of 3.2 mM Eu^{2+} in acidic solution at 25 °C for 12 hours, showing the stable absorbance in the absence of MTO.

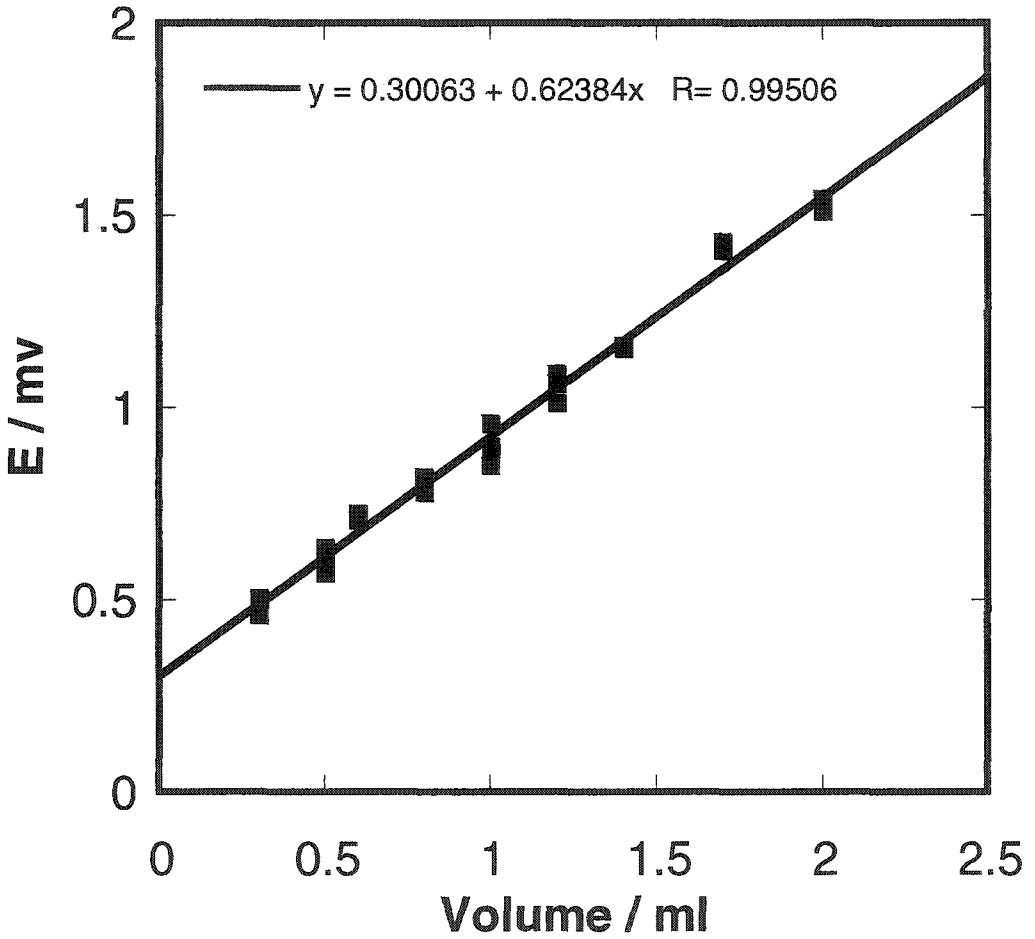

Figure 4. Calibration curve for hydrogen evolution.

Table 3. Quantitative measurements for hydrogen evolution by micorvolumeter apparatus. Volume(reaction vessel) = 20 mL.

$[Eu^{2+}] / 10^{-3}$ M	$[MTO] / 10^{-3}$M	E / mV	V_{H2} / mL	Yield %*
6	0.2	1.196	1.434	97.5
6	0.2	1.131	1.33	90.3
6	0.2	1.121	1.314	89.3
6	0.2	1.183	1.413	96.0
5	0.2	0.958	1.053	85.8
4	0.2	0.852	0.883	90.0
4	0.2	0.848	0.877	89.5

* Values come from the amount of H_2 measured over the calculations based on eq 9. All the values about 90% verify the net stoichiometry of the equation very well.

$$2Eu^{2+} + 2H^{+} \xrightarrow{MTO} 2Eu^{3+} + H_2$$

Formation of the intermediate L410. Figure 5 presents the results of a spectrophotometric titration of MTO by Eu^{2+}. From the plot, we found that when we used not more than 2 equiv Eu^{2+}, no L410 was formed. With one more Eu^{2+}, L410 peak appeared and the titration arrived at the endpoint. Thus, the spectrophotometric titration yields a ratio R = $[Eu^{2+}]$ / [MTO] of 3 to form L410, consistent with the stoichiometry of eq 10.

$$MTO + 3Eu^{2+} + 2H^{+} \longrightarrow L410 + 3Eu^{3+} + H_2O \quad (10)$$

Since Eu^{2+} serves as a one-electron reducing agent and the overall 3:1 stoichiometry in the L410 formation identifies L410 as a Re(IV) species, we formulate the sequence of reaction between MTO and Eu^{2+} as follows.

$$MTO + Eu^{2+} \xrightarrow{k_1} Re(VI) \quad (11)$$

$$Re(VI) + Eu^{2+} + 2H^{+} \xrightarrow{k_2} 2Eu^{3+} + MDO + H_2O \quad (12)$$

$$MDO + Eu^{2+} \xrightarrow{k_3} L410 + Eu^{3+} \quad (13)$$

In these equations, the oxidant MTO undergoes one-electron changes and the oxidation state of rhenium species changes from VII to IV. We assume the first two steps, eq 11-12, are very fast because the large driving force between Eu^{2+} and MTO and the rate-controlling step is the third step, L410 formation given in eq 13. This assumption was confirmed by studying the reactions with OLIS stopped-flow device. When we mixed 0.4 mM Eu^{2+} with excess MTO, the reaction reached completion in 0.1 s (Figure 6a) and the second-order rate constant k_1 is 2.7×10^4 M^{-1} s^{-1}, Figure 6b.

The formation of L410 was followed by monitoring an increase in absorbance at 410 nm due to L410, shown in Figure 7. The reaction obeyed first-order kinetics in the presence of an excess amount of Eu^{2+}, and the pseudo-first-order rate constant k_{obs} was plotted against the

concentration of Eu^{2+}, which was presented in Figure 8. The linear plot establishes that the rate of reaction is a simple first-order dependence on the concentration of Eu^{2+}, and the second-order rate constant k_3 equals 61.3 ± 0.2 M^{-1} s^{-1} at 25 °C obtained from the slope. In addition, variation of acid concentration did not alter k_{obs}. All the kinetic results are listed in Table 4.

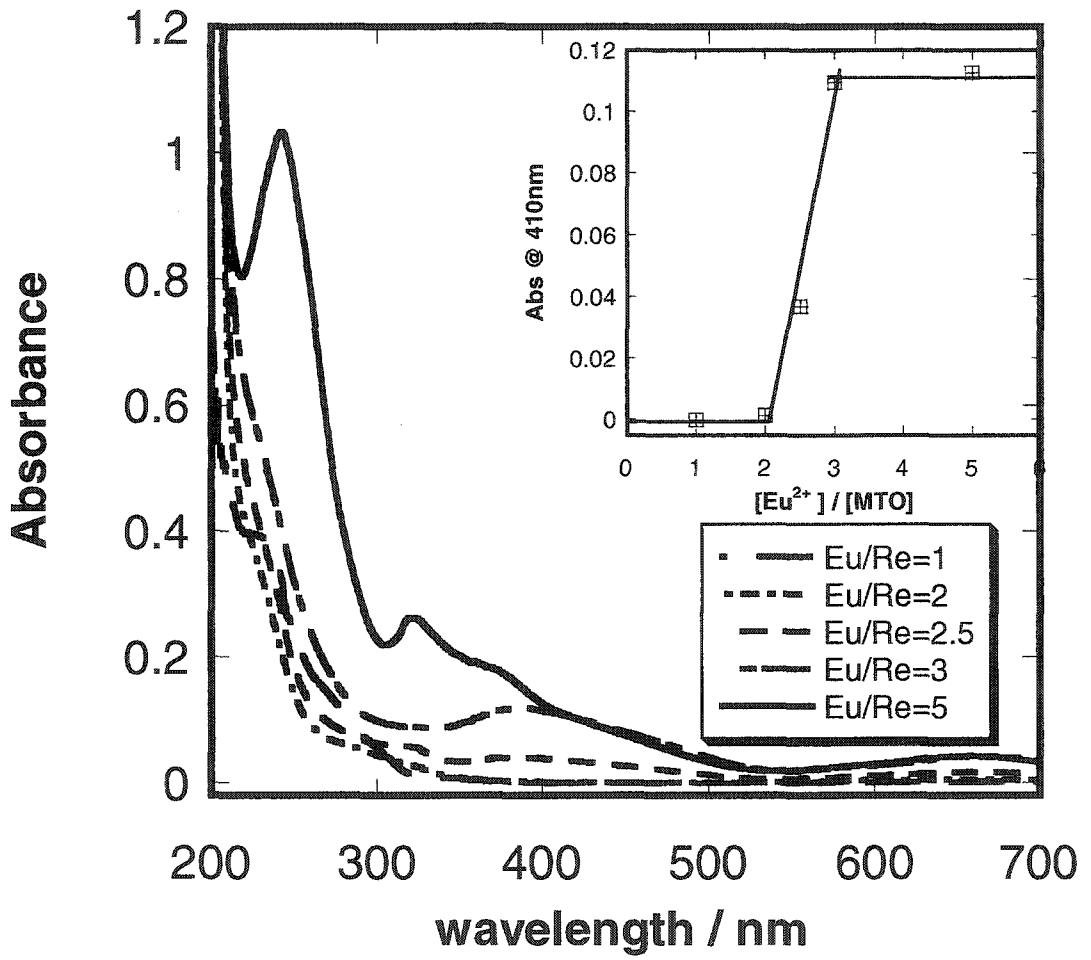

Figure 5. Spectrophotometric titrations of MTO with Eu^{2+}. Conditions: [MTO] = 0.2 mM; $[H^+]$ = 0.6 M, 1-cm cell at 25 °C. Inset: titration plot at 410 nm. The endpoint corresponds to a reactant ratio 3:1 $[Eu^{2+}]$: [MTO].

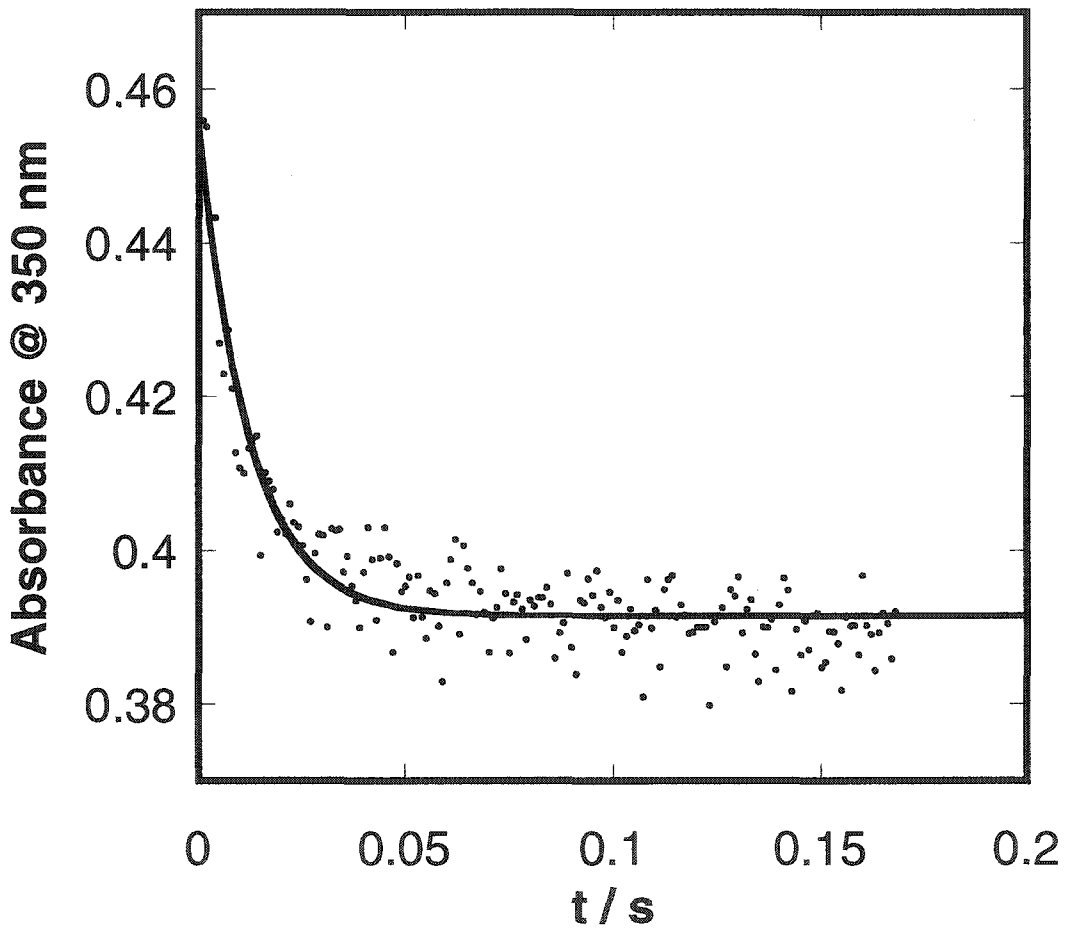

Figure 6a. Absorbance change showing that Eu^{2+} is rapidly oxidized by MTO. Conditions: 3.09 mM MTO, 0.4 mM Eu^{2+} in 0.6 M H^+ at 25 °C. The plot is fitted by pseudo-first-order kinetics to give k_ψ 83.0 s^{-1}.

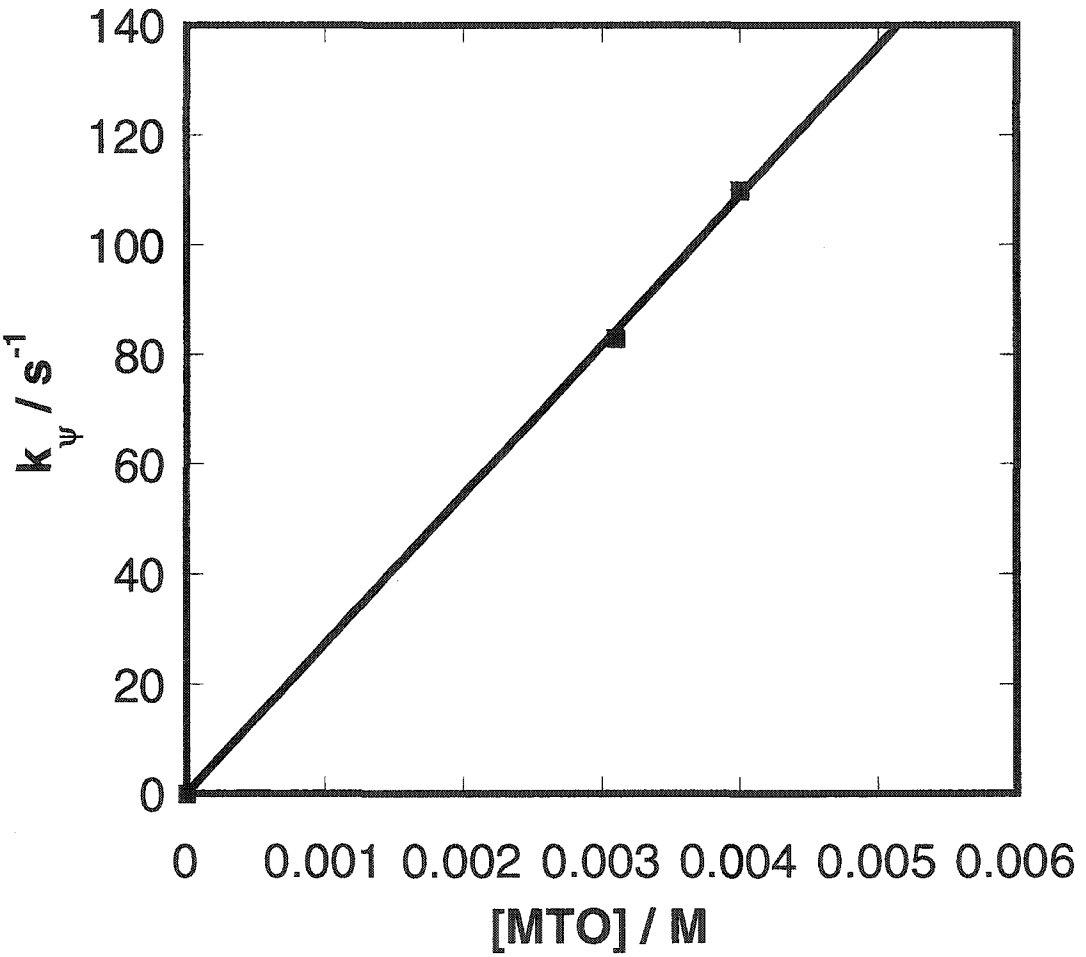

Figure 6b. Plot of k_ψ against the concentration of MTO for reaction 11. The plot is fitted by a linear equation and yields k_1 of eq 11 2.7×10^4 M^{-1} S^{-1} at 25 °C.

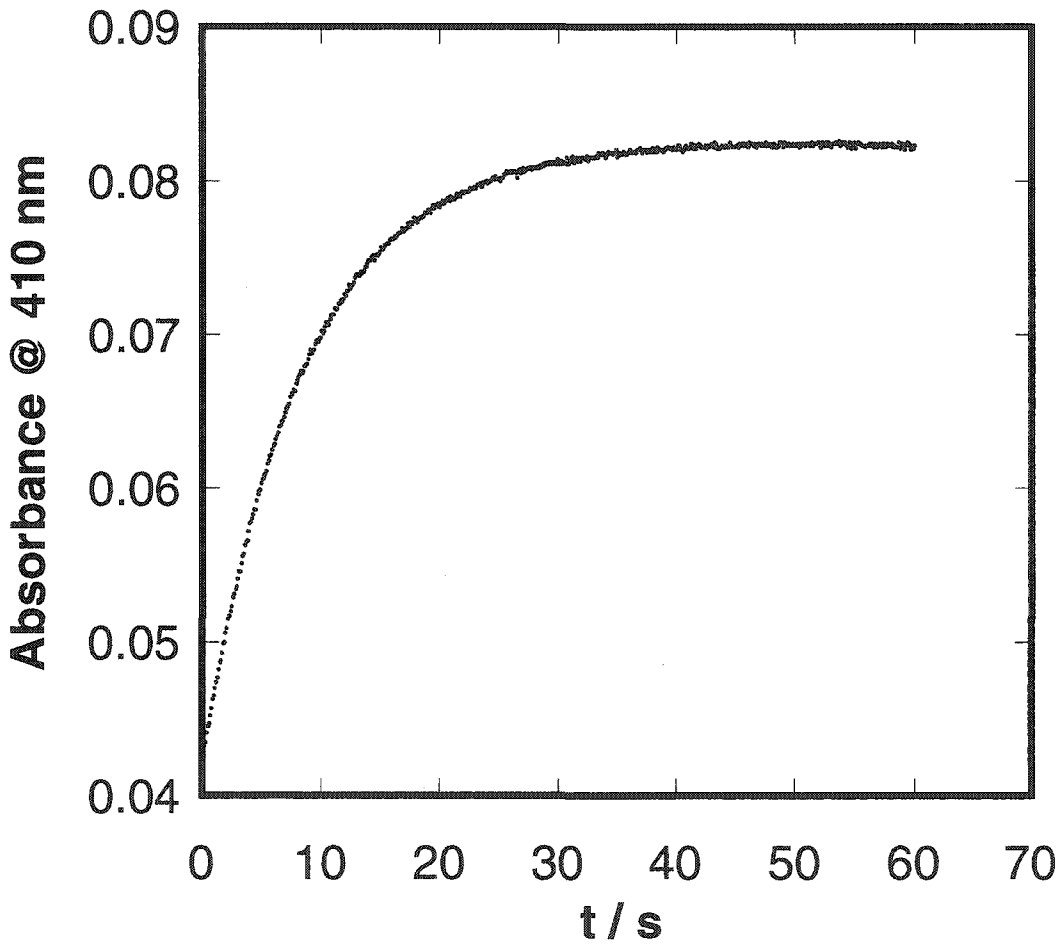

Figure 7. A typical kinetic trace for **L410** formation monitored spectrophotometrically at 410 nm. Conditions: 0.2 mM MTO, 2.12 mM Eu^{2+} in 0.6 M H^+ at 25 °C. The plot is fitted by pseudo-first-order equation to give k_{obs} 0.118 s^{-1}.

Table 4. Kinetic data for the formation of **L410** by MTO with excess acidic Eu^{2+} solution. Conditions: $[H^+] = 0.6$ M, $\mu = 0.62$ M.

$[Eu^{2+}] / 10^{-3}$ M	$[MTO] / 10^{-3}$ M	k_{obs} / s^{-1}
9.76	0.20	0.616
5.08	0.20	0.315
4.87	0.20	0.299
3.81	0.20	0.244
3.53	0.20	0.196
3.25	0.20	0.201
3.25	0.30	0.193
3.25	0.26	0.198
3.25	0.23	0.193
3.25	0.20	0.197[a]
2.83	0.20	0.153
2.53	0.20	0.153
2.19	0.20	0.118
2.12	0.20	0.118

[a] $[H^+] = 0.2$ M

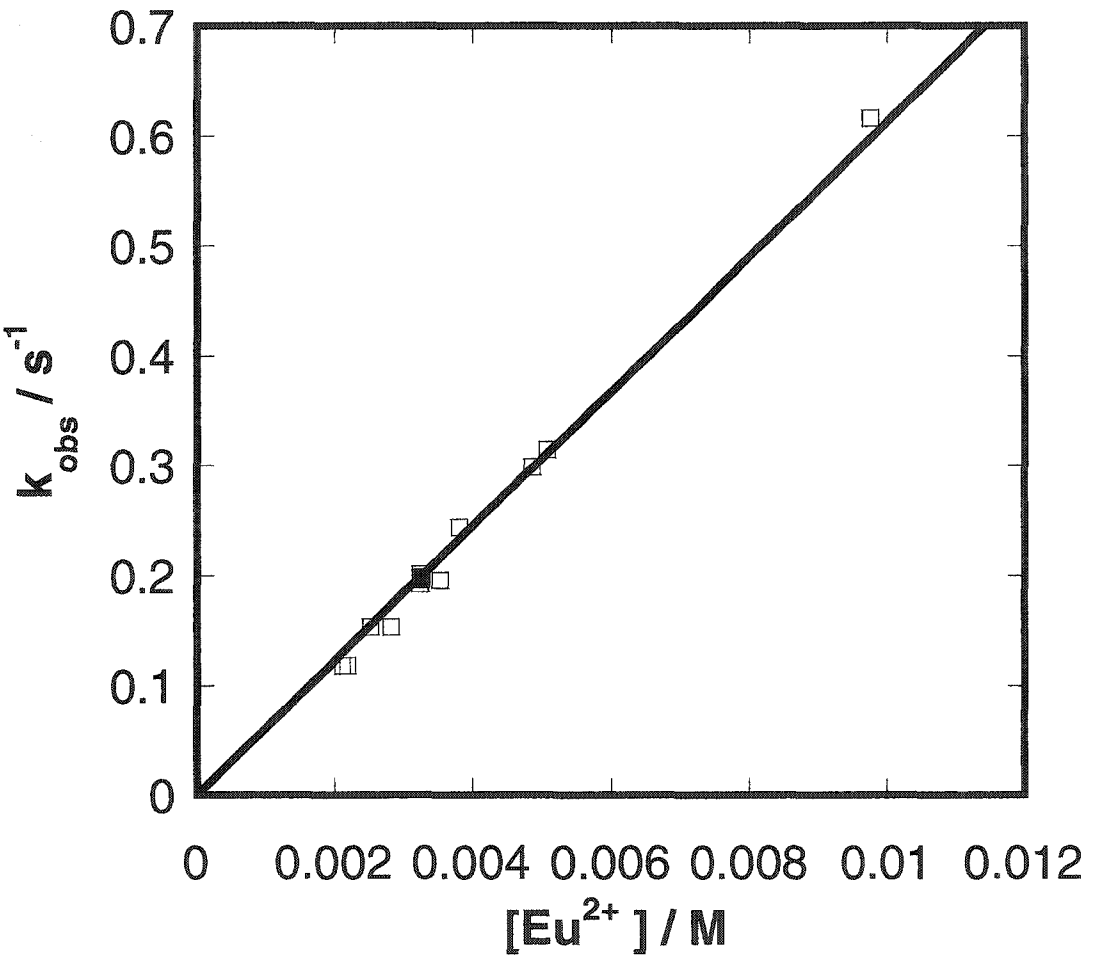

Figure 8. Plot of k_{obs} for eq 13 against the concentration of Eu^{2+}, conditions: [MTO] = 0.2 mM, $[H^+]$ = 0.6 M (□), $[H^+]$ = 0.2M (■) at 25 °C.

Determination of the rate law for hydrogen evolution. The hydrogen gas was collected by microvolumeter apparatus and a full time course kinetic method was used to study the dependence of the rate on the concentrations of the species in the rate law. All the experiments were studied under conditions present excess acid concentration with limit amount of Eu^{2+}. Figure 9 gives a typical kinetic trace of gas buildup with MTO as catalyst. When 0.193 mM MTO reacted with 12.8 mM Eu^{2+} in 0.22 M anaerobic HCl, the reaction followed by a pseudo-first-order kinetics. Pseudo-first-order rate constant k_{obs} was obtained by fitting the data to first-order kinetics. The kinetic data are summarized in Table 5a and 5b. The reaction is first-order with respect to [Re] and first-order dependent on $[Eu^{2+}]$. These dependencies are illustrated in Figure 10 and Figure 11 by plots of k_{obs} vs. one concentration. We can notice that the values of k_{obs} are independent of $[Eu^{2+}]$, which is because the Eu^{2+} is the limiting reagent in the reaction. In addition, we found that, with a constant ionic strength, reactions were retarded by raising the concentration of acid. Figure 12a shows that k_{obs} is inversely dependent on $[H^+]$. From these kinetic results, the rate law can be expressed by eq 14.

$$v = \frac{k[\mathrm{Re}][\mathrm{Eu}^{2+}]}{[\mathrm{H}^+]} \qquad (14)$$

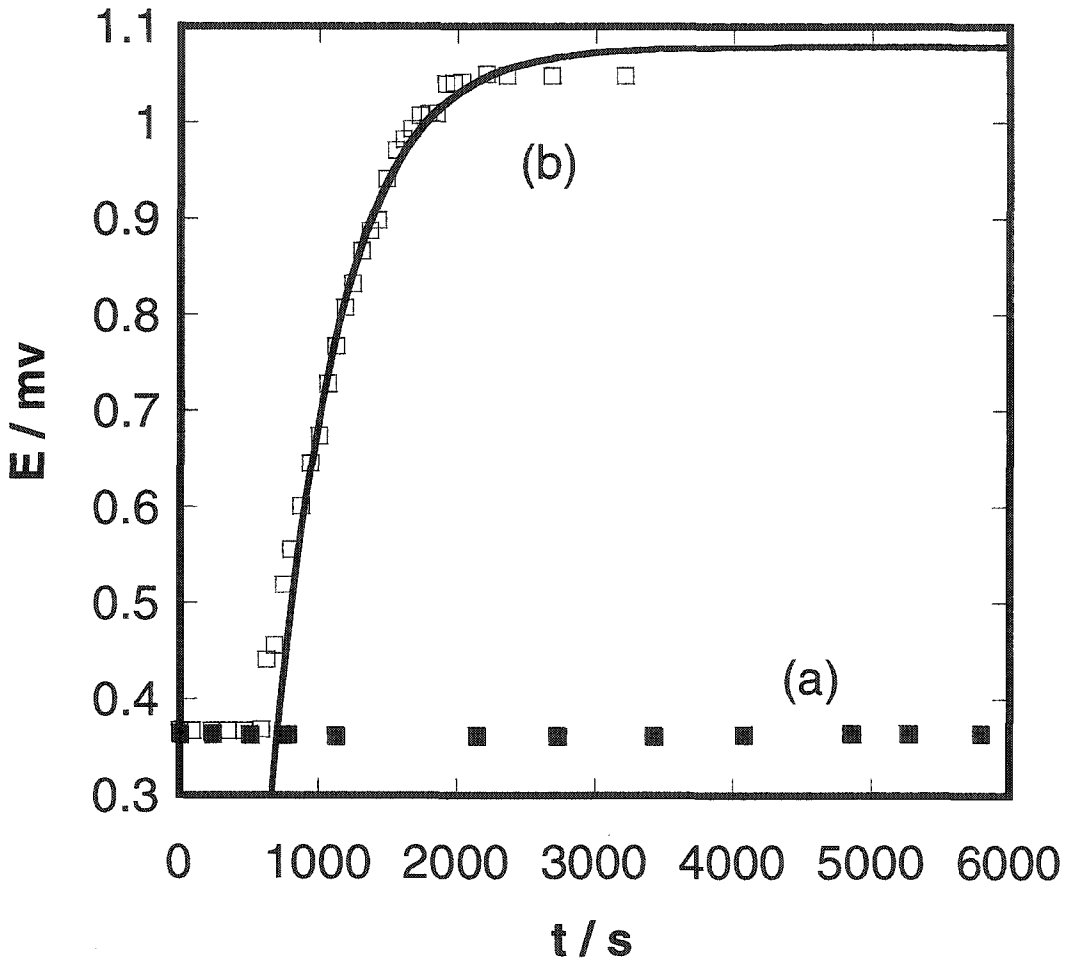

Figure 9. Experiments showing hydrogen evolution from Eu^{2+} acidic solution catalyzed by MTO. Conditions: $[Eu^{2+}]$ = 12.8 mM, $[H^+]$ = 0.22 M and μ = 0.29 M. (a) the control experiment without MTO; (b) MTO = 0.193 mM.

Table 5a. Kinetic data for hydrogen evolution by MTO and Eu^{2+}. Conditions: $[H^+]$ = 0.22 M, $\mu \sim 0.3$ M at 25 °C.

$[Eu^{2+}] / 10^{-3}$ M	MTO / 10^{-3} M	$k_{obs} / 10^{-3}$ s^{-1}
12.8	0.193	2.07
12.4	0.394	4.42
12.4	0.320	3.48
12.3	0.497	5.85
9.9	0.320	3.54
8.77	0.320	3.42
8.03	0.320	2.88
5.85	0.320	3.49
5.07	0.320	3.47
3.2	0.320	3.62

Table 5b. Kinetic data for hydrogen evolution by MTO and Eu^{2+} with variations of acid concentration. Conditions: [MTO] = 0.21 mM, μ = 0.33 M at 25 °C.

$[H^+]$ / M	$[Eu^{2+}]$ / 10^{-3} M	k_{obs} / 10^{-3} s^{-1}
0.114	6.94	4.80
0.127	6.41	4.39
0.150	6.6	3.58
0.170	8.42	3.13
0.194	6.94	2.55
0.222	6.84	2.31
0.246	6.6	2.25
0.298	6.94	1.69

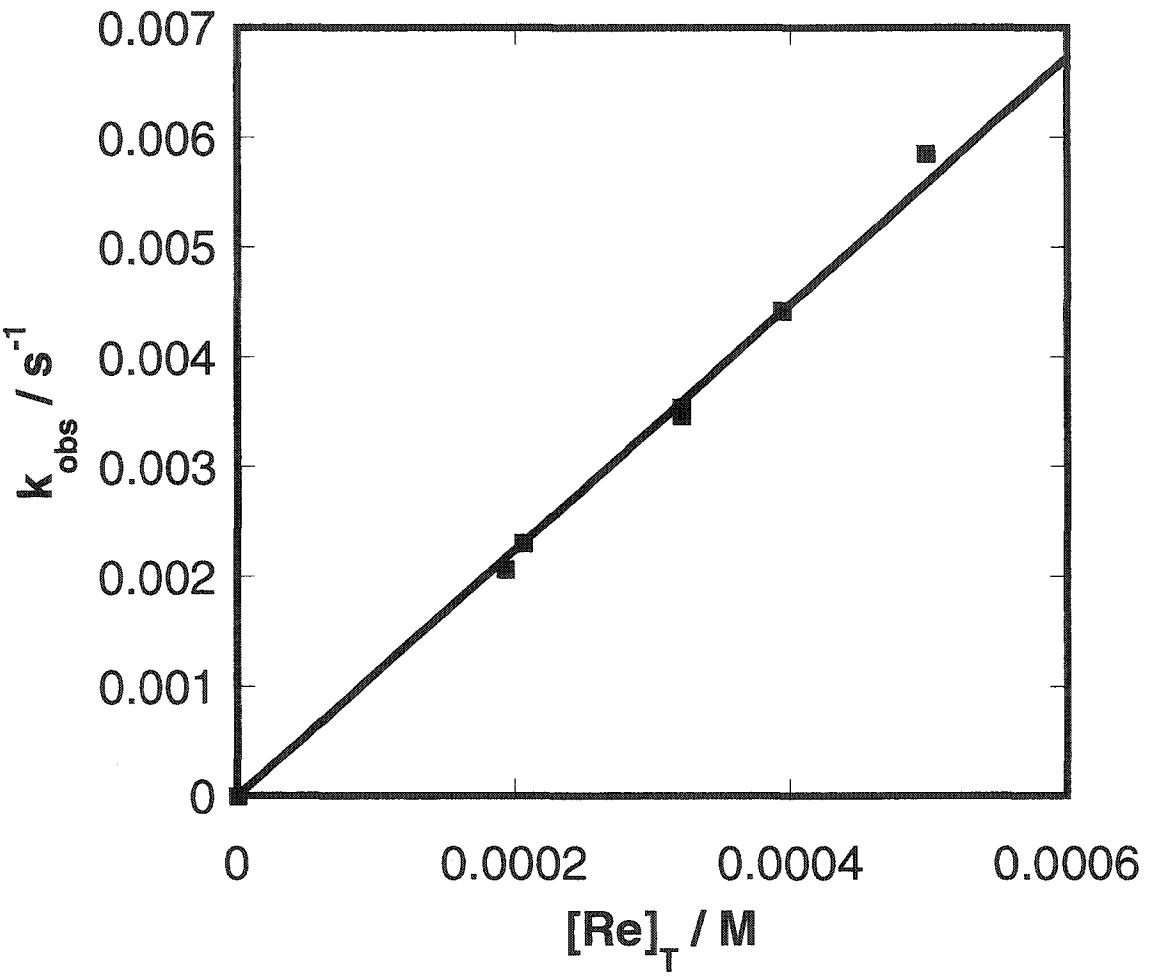

Figure 10. Plot of k_{obs} against rhenium concentration. Conditions: [MTO] = 0 ~ 0.5 mM, $[Eu^{2+}]$ = 6 ~ 12 mM; $[H^+]$ = 0.22 M, and μ = 0.3 M at 25 °C.

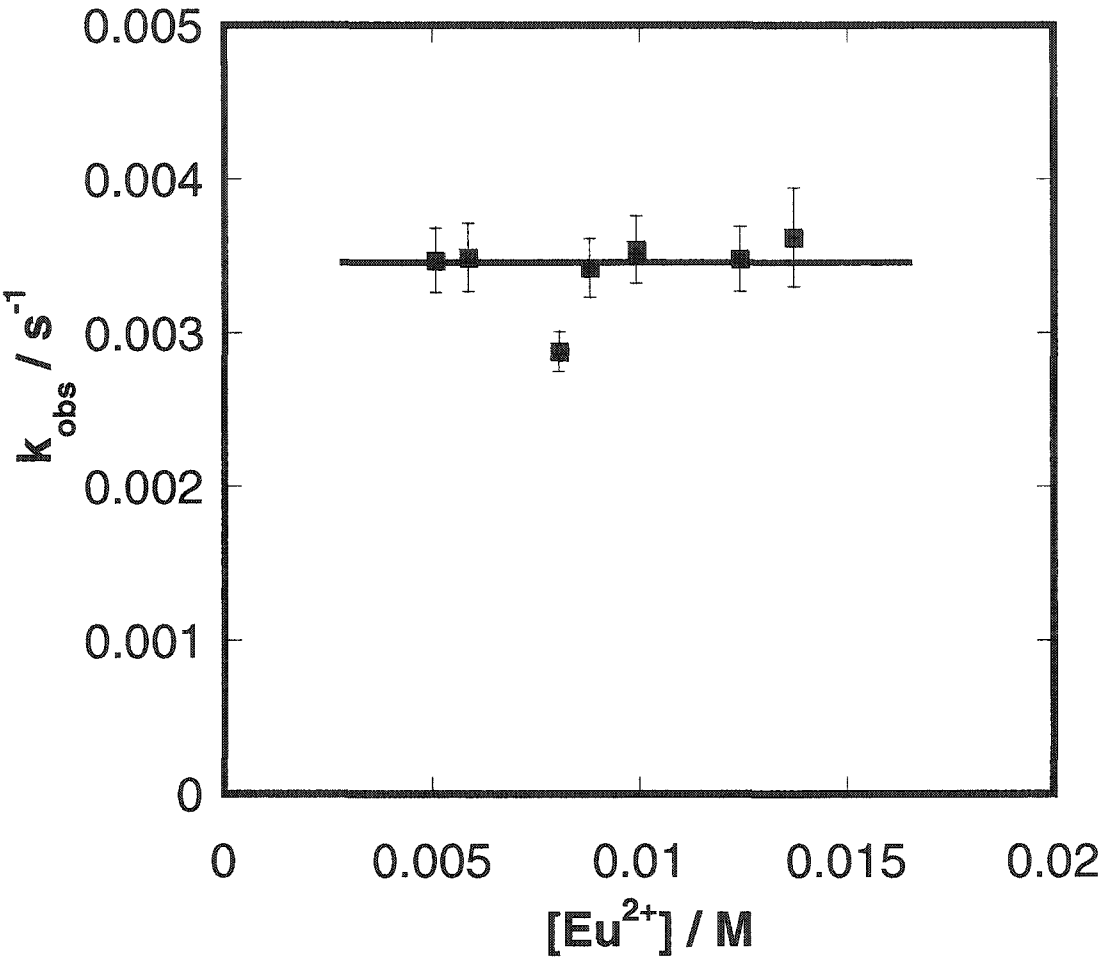

Figure 11. Plot represents the pseudo-first-order rate constant k_{obs} independent of Eu^{2+} concentration. Conditions: [MTO] = 0.32 mM; $[H^+]$ = 0.22 M, μ = 0.3 M and Eu^{2+} is the limiting reagent at 25 °C.

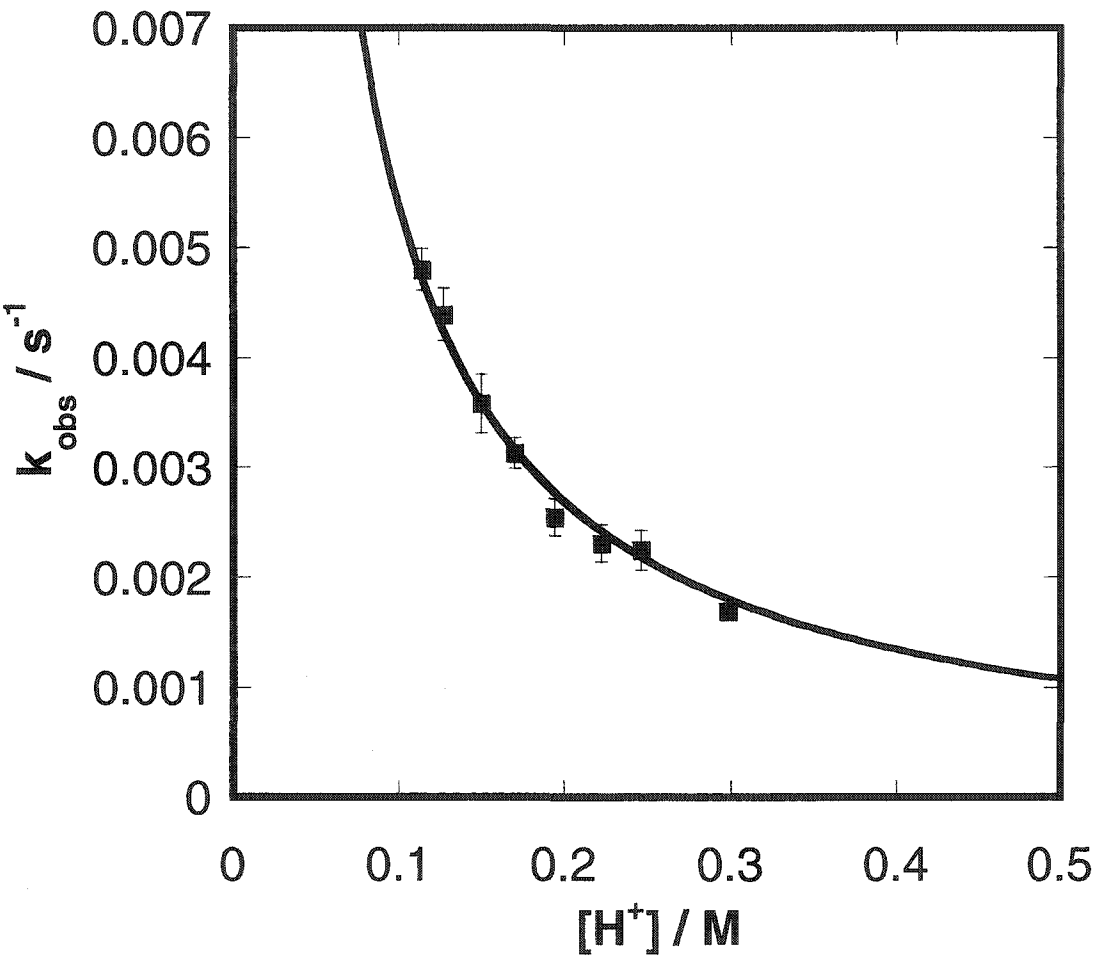

Figure 12a. The variation of k_{obs} with $[H^+]$ for hydrogen evolution from acidic Eu^{2+} solution by MTO as catalyst. Conditions: [MTO] = 0.21 mM, $[Eu^{2+}]$ = 6-9 mM with μ = 0.33 M at 25 °C.

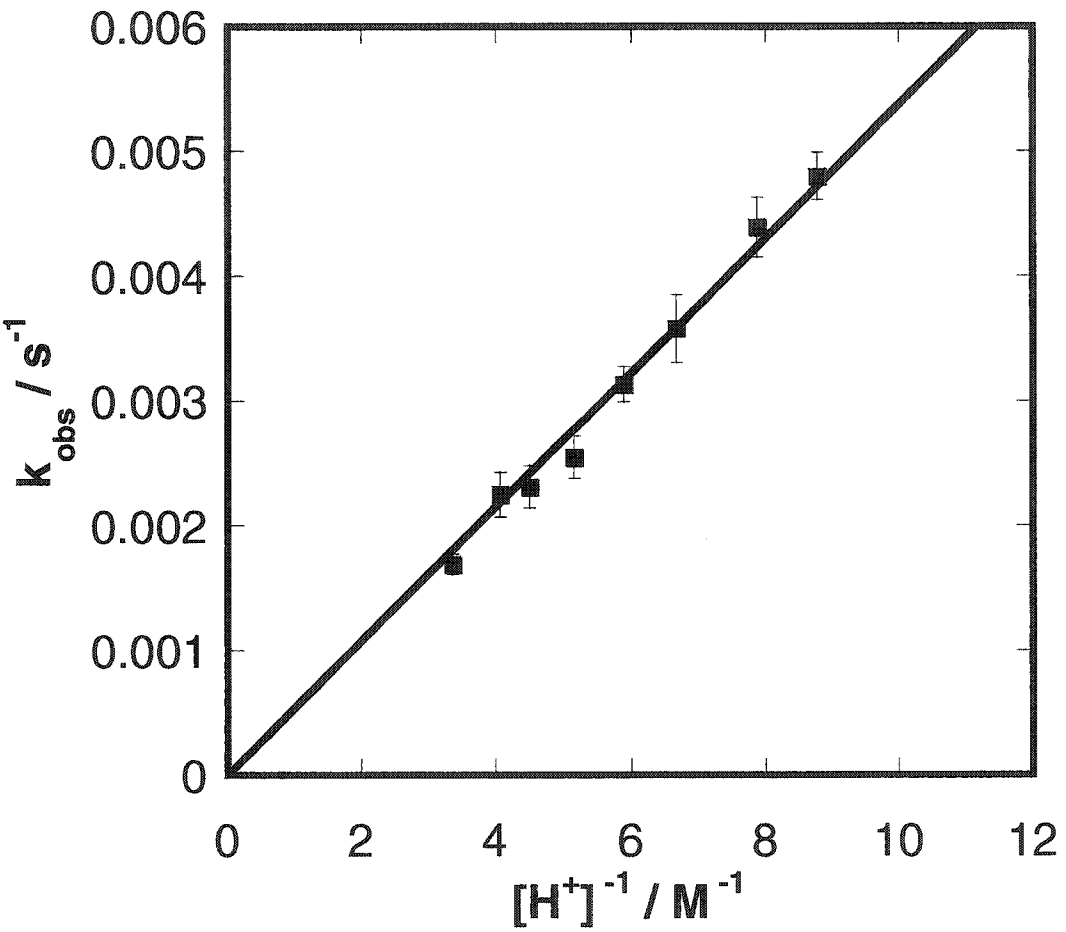

Figure 12b. Plot of k_{obs} *vs.* $1/[H^+]$ for hydrogen evolution.

Investigation of the acid dissociation constant for L410. As described above, the rate of hydrogen formation is inhibited by acid concentration. In addition, we also observed that the UV-vis spectrum for L410 changes with different acid concentration. This indicates that there is a protonation step before the rate controlling hydrogen evolution step. Thus we suggested there are two Re(IV) species absorbing at 410nm and they exist as partners in an acid-base equilibrium. In this equilibrium, the acid form is a neutral Re(IV) hydroxide species, called L410-AH, and its conjugate base is a Re(IV) anion, named as L410-A. The equilibrium can be expressed by eq 17.

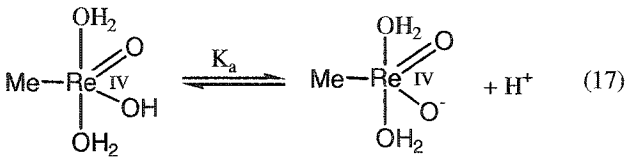

(17)

L410-AH L410-A

Where K_a symbolizes the acid dissociate constant for the reaction as written.

In order to investigate the value of K_a, we studied the acid effect on L410. Figure 13 shows the UV-vis spectra of L410 at different pH. We found that the absorbance at 410 nm decreased with increasing acid concentration. If both L410-AH and L410-A have absorptions at 410 nm and the molar absorptivities are ε_{AH} and ε_A respectively, the average molar absorptivity ε at any time should obey equation 18:

$$\varepsilon = \frac{\varepsilon_{AH}[H^+] + K_a \cdot \varepsilon_A}{K_a + [H^+]} \qquad (18)$$

We can notice that only when $K_a << [H^+]$, ε at 410 is linearly dependent on $1 / [H^+]$, which agrees with the experimental results shown in Figure 14. Thus, Ka is much smaller than 0.1,

and ε_{AH} is about 550 M^{-1} cm^{-1}. Since K_a falls well below the acid concentration examined, rhenium species exists almost completely in its protonated form L410-AH throughout.

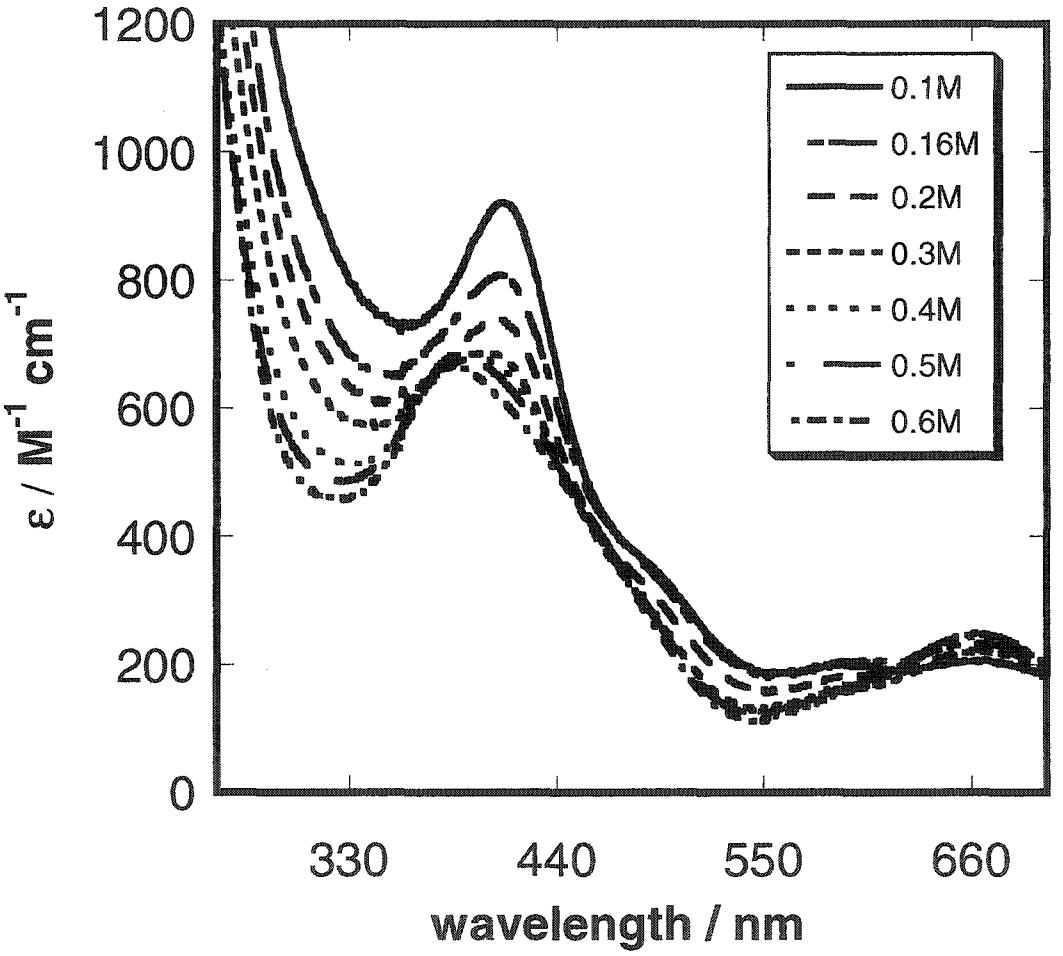

Figure 13. Variations of the average molar absoptivity of L410 with acid concentration.

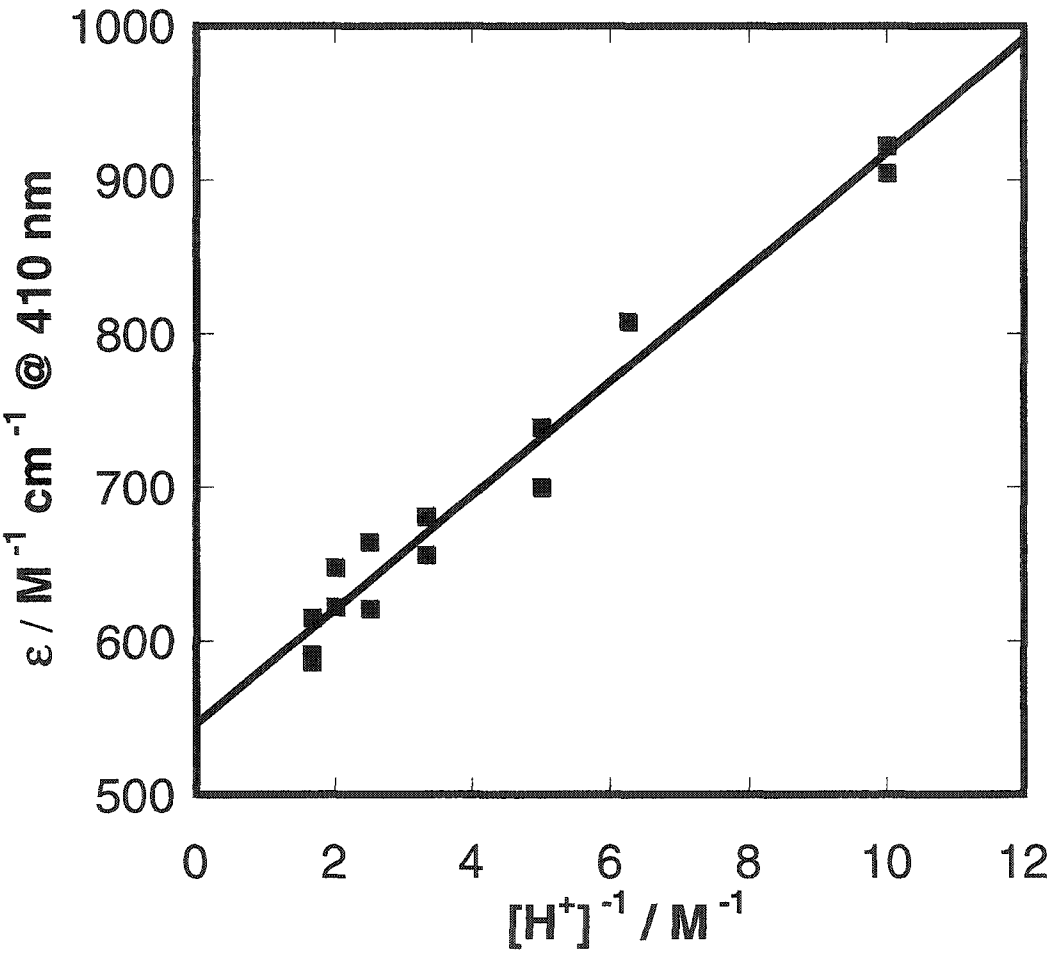

Figure 14. Plot of molar absorptivity ε of L410 at 410 nm against 1 / $[H^+]$.

Variation of ionic strength for hydrogen formation. Salt effects on the hydrogen evolution were examined in the ionic strength range 0.118-0.297 M by adjusting the LiCl concentration. In these experiments the acid concentration was kept constant at 0.1 M with variable concentrations of MTO [(2.16-3.54)×10 $^{-4}$ M] and Eu^{2+} [(5.00-5.66)×10 $^{-3}$ M]. These results are summarized in Table 6. On the basis of the rate dependence studies, the pseudo-first-order rate constant is independent of Eu^{2+} and first order with respect to MTO. Thus, a plot of $k_{obs}/[Re]_T$ against $0.509\mu^{1/2}/(1+\mu^{1/2})$ is presented in Figure 15. From the plot, we found that the reaction slows down at higher ionic strength with the slope of -2.3 ± 0.2.

Table 6. Pseudo-first-order rate constant k_{obs} for hydrogen evolution with varying ionic strength at $[H^+] = 0.1M$.

μ / M	$F_\mu = \mu^{1/2}/(1+\mu^{1/2})$	$[Eu^{2+}] / 10^{-3}$ M	[MTO] / 10^{-3} M	$k_{obs} / 10^{-3}$ s^{-1}
0.118	0.2557	5.66	0.354	13.0
0.118	0.2557	5.66	0.354	13.1
0.121	0.2581	5.00	0.216	7.72
0.142	0.2737	5.08	0.216	7.68
0.161	0.2864	5.00	0.216	7.37
0.19	0.3036	5.66	0.354	11.2
0.246	0.3315	5.08	0.216	6.73
0.297	0.3527	5.00	0.216	5.93

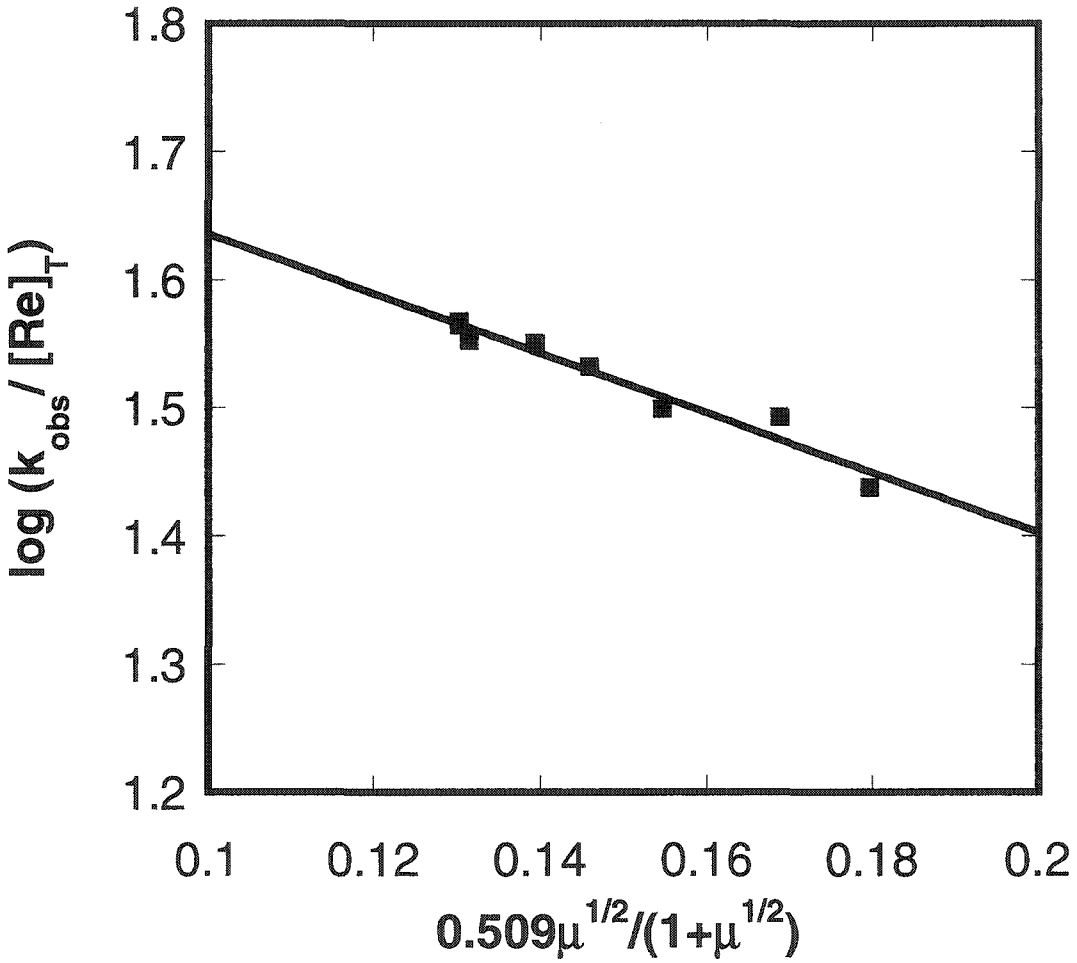

Figure 15. The effect of variable ionic strength on the rate constants for the hydrogen evolution.

Stoichiometry of perchlorate reduction. Measurement of chloride ion concentration in acidic solutions showed that Cl^-_{aq} was formed quantitatively by the reaction of Eu^{2+}, MTO and sodium perchlorate in HOTf (trifluoromethanesulfonic acid). The same results were found for reactions of MTO and Cr^{2+} in perchloric acid solution. These stoichiometric determinations (Table 7) established that the overall stoichiometry to be 8:1 Eu^{2+}(or Cr^{2+})/Cl^- as expected from eq 15.

$$8Eu^{2+}\ (\text{or } 8Cr^{2+}) + ClO_4^- + 8H^+ \xrightarrow{\text{MTO}} 8Eu^{3+}\ (\text{or } 8Cr^{3+}) + Cl^- + 4H_2O \quad (15)$$

Kinetic studies of perchlorate reduction. A single kinetic experiment was carried out with stopped-flow techniques under the following conditions: 1.55 mM Eu^{2+}, 0.1 mM MTO, 0.03 M ClO_4^- and 0.55 M HCl at 25 °C with μ = 0.8 M. Figure 16 shows the repetitive scans for the progress of this reaction, corresponding the consumption of Eu^{2+}. A typical kinetic trace at 321 nm is presented in Figure 17. The trace showed a curve at the beginning of the reaction, which we believe was due to residual oxygen in the instrument system. This will be discussed later in detail. The initial curve was followed by a straight line until all Eu^{2+} was consumed. The data were fitted to a linear equation and the pseudo-zero-order rate constant k_{obs} is 1.10×10^{-4} M s^{-1}. The same method was applied for all the kinetic studies with varying the concentrations of three reactants. All the data are summarized in Table 8. The reaction rates are independent of [Eu^{2+}] and directly proportional to $[Re]_T$ and [ClO_4^-] , as shown in Figures 18 to 20 . This implies the rate law

$$-\frac{d[Eu^{2+}]}{dt} = k[Re]_T[ClO_4^-] \quad (16)$$

with k = 43.2±0.8 at 25 °C.

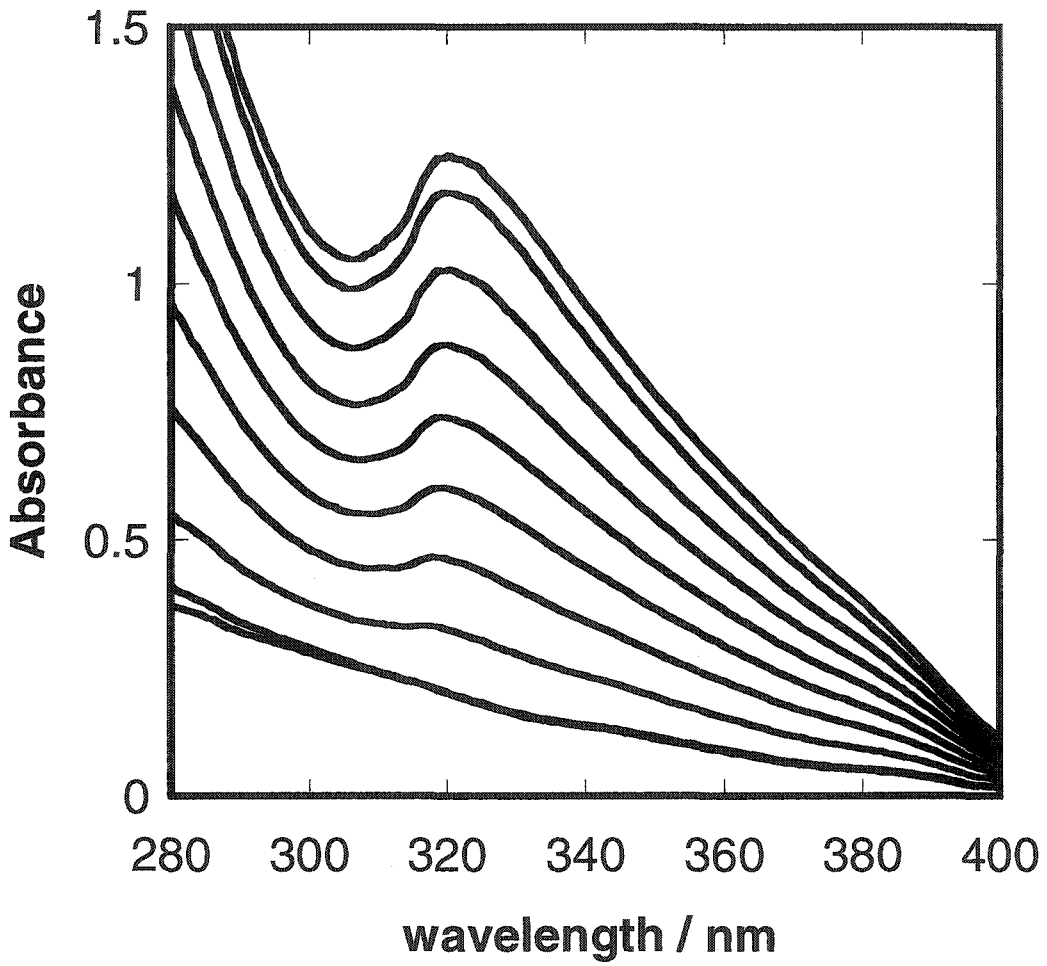

Figure 16. Repetitive scans of UV-vis spectra representing the decrease of Eu^{2+} for perchlorate reduction with 1 s interval. Condition: $[Eu^{2+}]$ = 1.55 mM, [MTO] = 0.1 mM; $[ClO_4^-]$ = 0.05 M and $[H^+]$ = 0.55 M with μ = 0.8 M at 25 °C.

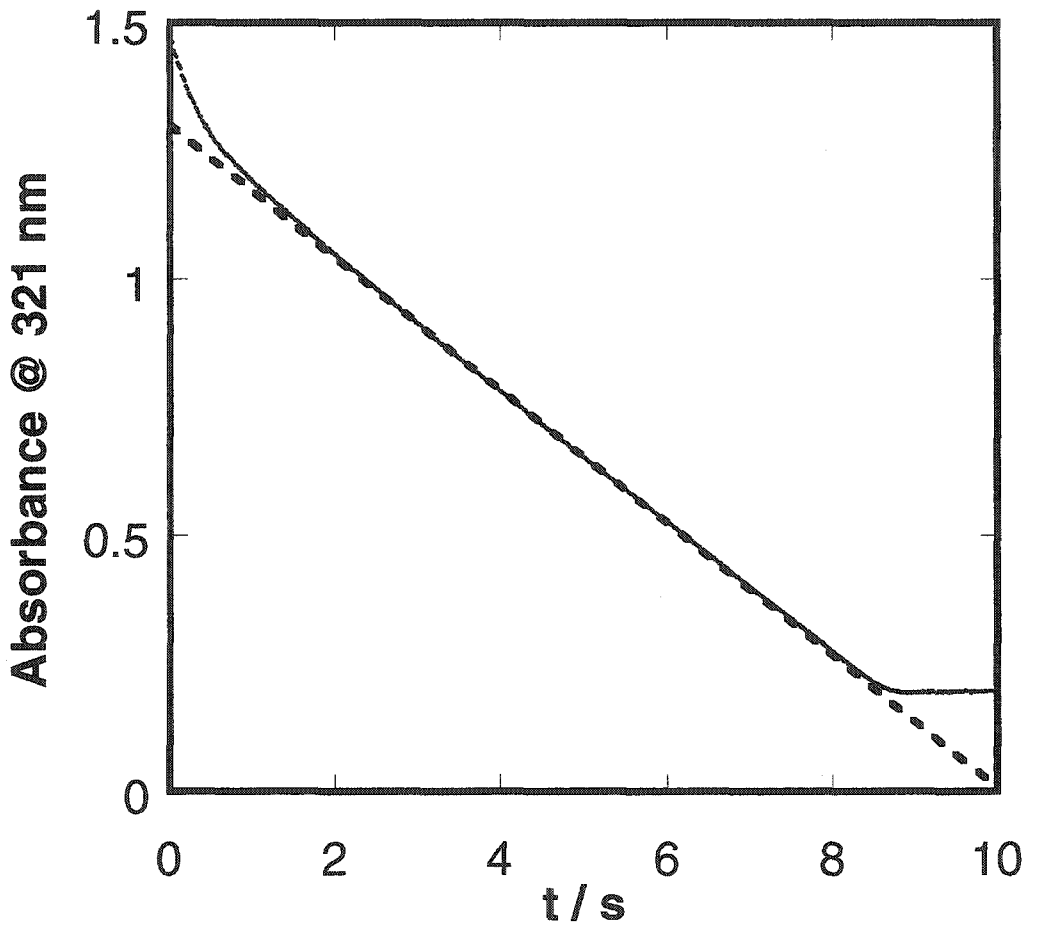

Figure 17. A typical kinetic trace for perchlorate reduction. Condition: $[Eu^{2+}]$ = 1.55 mM, [MTO] = 0.1 mM; $[ClO_4^-]$ = 0.03 M and $[H^+]$ = 0.55 M with μ = 0.8 M at 25 °C.

Table 7. Quantitative measurements of chloride ion concentration for the reaction of perchlorate ion reduction.

$[Eu^{2+}$ (or $Cr^{2+})]$ 10^{-3} M	[MTO] 10^{-3} M	$[Cl^-]_{measured}$ 10^{-3} M	$[Eu^{2+}$ (or $Cr^{2+})]$ / $[Cl^-]$
8.00	0.20	0.958	8.4
4.00	0.08	0.479	8.4
3.00	0.08	0.406	7.4
2.00	0.08	0.228	8.8
1.00	0.08	0.136	7.4

Table 8. Kinetic data for perchlorate ion reduction with $[H^+] = 0.55$ M at $\mu = 0.8$ M.

$[ClO_4^-]$ / M	[MTO] / 10^{-4} M	$[Eu^{2+}]$ / 10^{-3} M	k_{obs} / 10^{-4} M s^{-1}
0.050	0.965	1.55	2.11
0.050	0.965	1.24	2.15
0.050	0.965	1.86	1.93
0.030	1.00	1.55	1.11
0.050	1.00	1.55	2.00
0.070	1.00	1.55	2.97
0.100	1.00	1.55	4.80
0.120	1.00	1.55	5.38
0.050	0.595	1.23	1.21
0.050	0.760	1.23	1.64
0.050	1.21	1.23	2.54
0.050	1.58	1.23	3.38
0.050	1.97	1.23	4.49
0.040	0.98	1.55	1.53
0.100	0.98	1.55	4.50

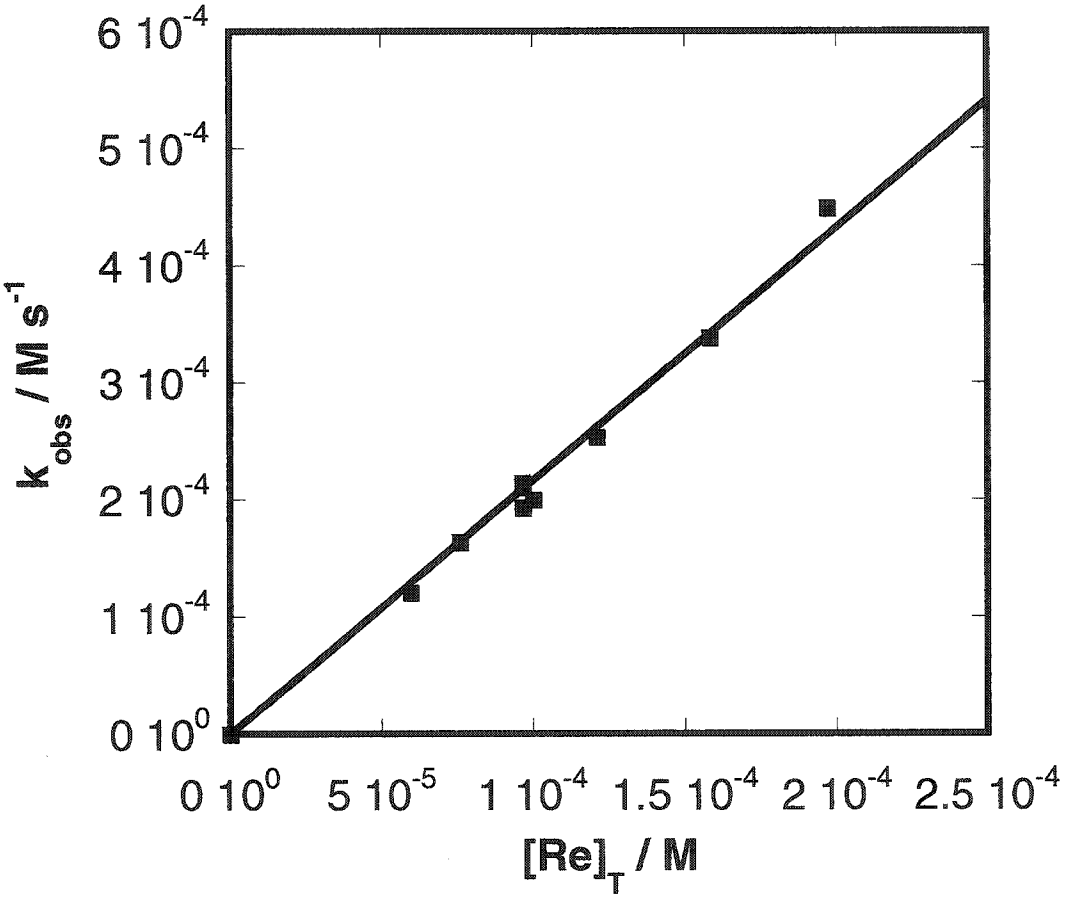

Figure 18. Plot showing the linear variation of the pseudo-zero-order rate constant k_{obs} with the concentration of $[Re]_T$. Condition: $[Eu^{2+}]$ = 1.23 ~ 2.00 mM, [MTO] = 0 ~ 0.2 mM; $[ClO_4^-]$ = 0.05 mM and $[H^+]$ = 0.55 M with μ = 0.8 M at 25 °C.

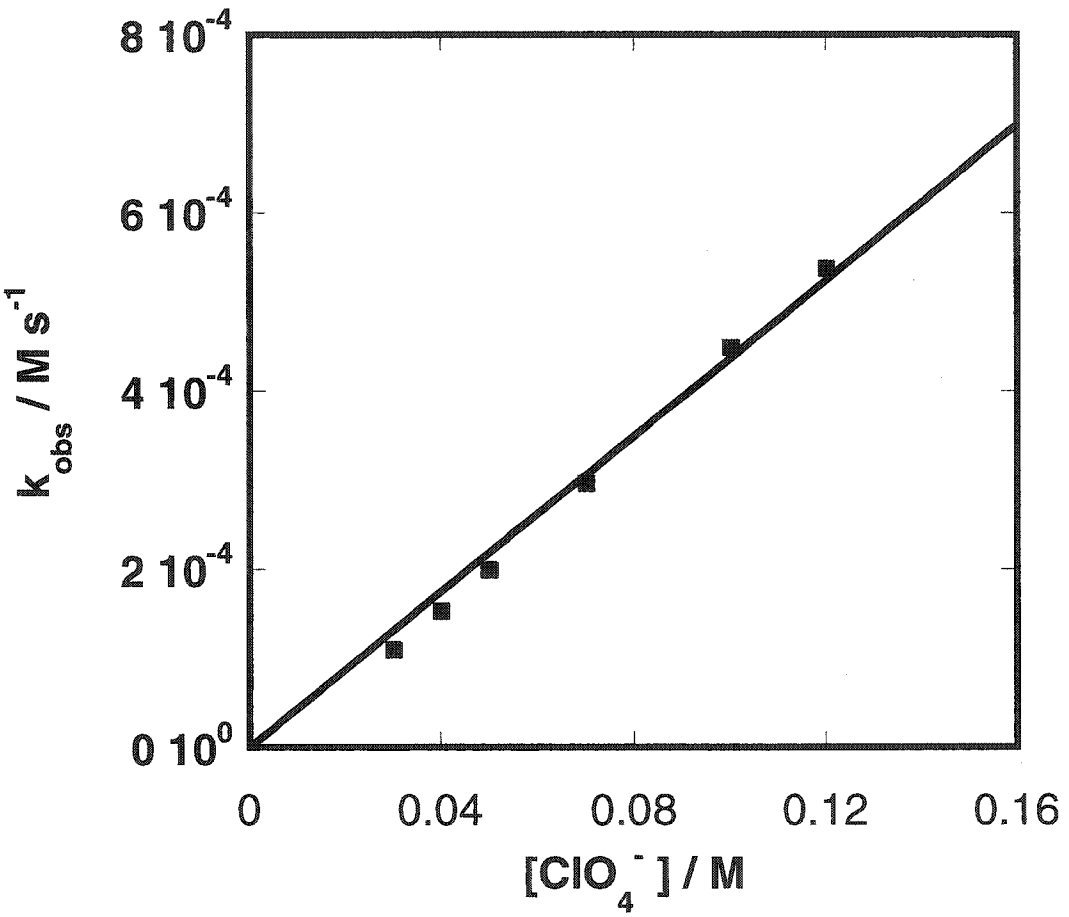

Figure 19. Plot showing the first-order dependence upon $[ClO_4^-]$ for perchlorate reduction. Condition: $[Eu^{2+}]$ = 1.55 mM, [MTO] = 0.1 mM; $[ClO_4^-]$ = 0.03 ~ 0.12 mM and $[H^+]$ = 0.55 M with μ = 0.8 M at 25 °C.

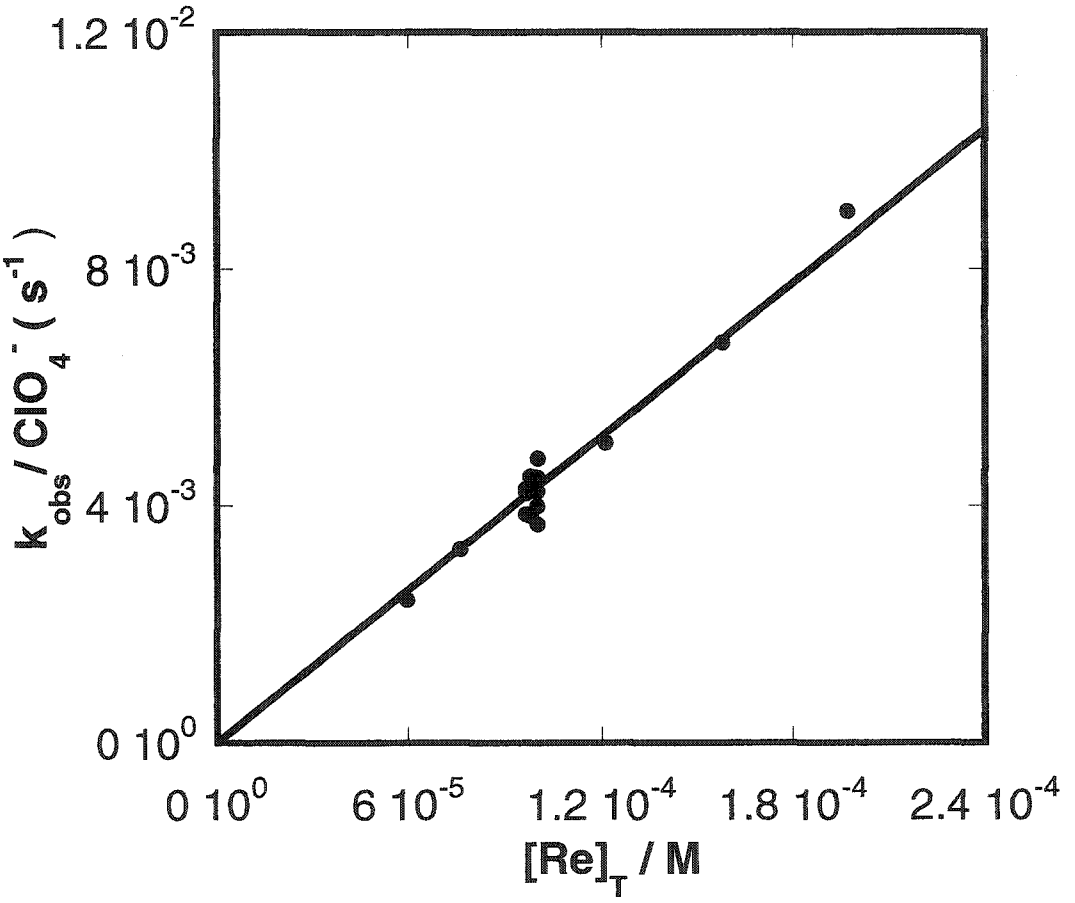

Figure 20. Variations of k_{obs} / $[ClO_4^-]$ with $[Re]_T$ for perchlorate ion reduction.

Discussion

General considerations concerning the reaction scheme for hydrogen evolution reaction. According to experimental results, we have observed the following information: Eu^{2+} reduces MTO to L410 by 3 single-electron steps. The first two steps are very fast and they take only 0.1 second. The third step occurs over 1 min and is fast compared with hydrogen evolution, which usually finishes in one half to one hour. We believe the rate determining step for hydrogen evolution is after the formation of L410. Based on this evidence, we outline a reaction scheme for hydrogen evolution, described in Scheme 1:

$$\text{MTO} \xrightarrow[k_1]{2\,Eu^{2+}} \text{MDO} \xrightarrow[k_3]{Eu^{2+}} \text{L410} \xrightarrow[k]{Eu^{2+}} H_2$$

Scheme 1

In this scheme, the third step is the rate-determining step for H_2 evolution. Thus, the reaction rate is first-order each in Eu^{2+} and in rhenium species. However, it does not account for the inverse-first-order dependence on $[H^+]$, so more experiments were carried out to understand the acid effect on L410 intermediate.

Mechanism of hydrogen evolution. Accounting for our observations, we proposed a reaction mechanism in Scheme 2. It is proposed that Eu^{2+} rapidly reduces MTO from Re(VII) to Re(V), and then Re(V) is further reduced by one more Eu^{2+} to make a Re(IV) anion, L410-A. With acid in solution, the Re(IV) anion rapidly adds a proton to make a neutral Re(IV) hydroxide species, L410-AH. As we discussed previously, K_a is much less than the acid concentration investigated, so the predominant species is L410-AH under experimental conditions. However, the active species for hydrogen evolution is the anionic Re(IV) species, L410-A. So, the rhenium species should be activated by deprotonation from L410-AH to

make L410-A during the process of hydrogen evolution. This leads to the observed acidity dependence for hydrogen evolution. After deprotonation, the anionic Re(IV) is further reduced by Eu^{2+} to produce the Re(III) intermediate, which is formulated as a Re(III) hydroxide complex. We believe it quickly converts to a Re(V) oxo hydride complex, and then this hydride complex picks up a proton and fast eliminates a dihydrogen molecule. The Re(V) hydride is necessary for hydrogen evolution in order to avoid the high-energy intermediate H•, which is the thermodynamic and kinetic barrier for the reaction without MTO.

Scheme 2

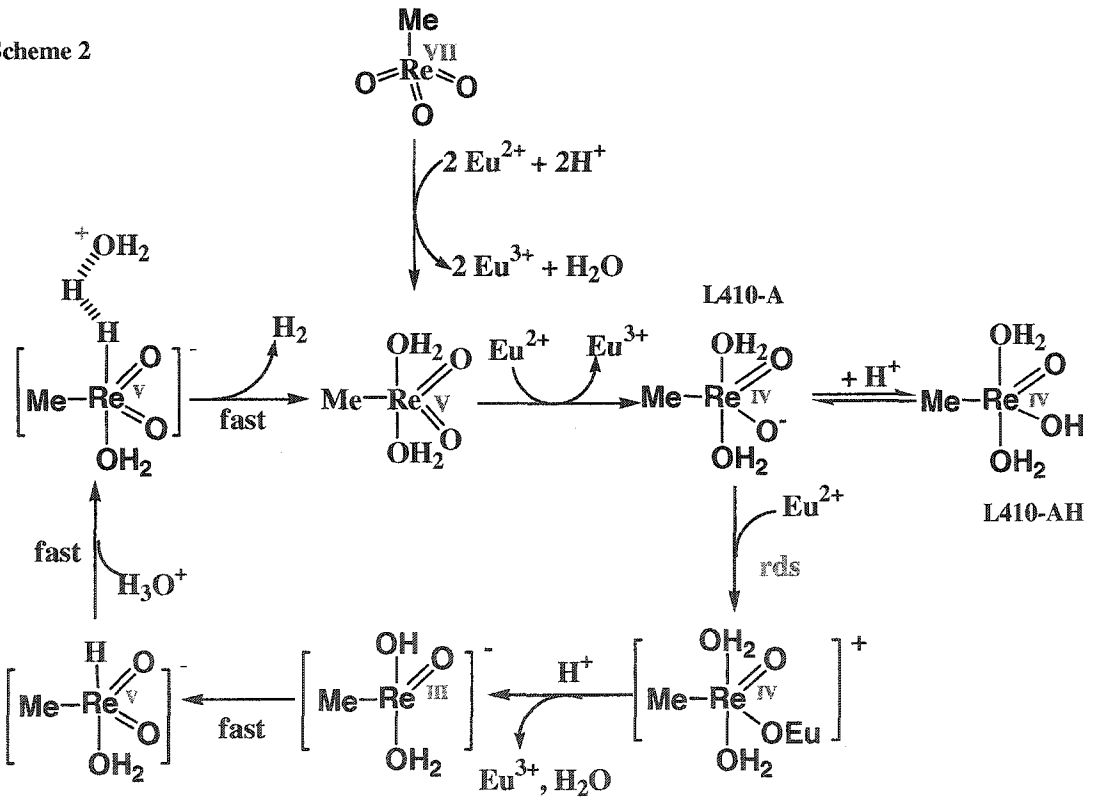

On the basis of Scheme 2, the reaction establishes a prior-equilibrium before the rate-determining step, so the rate expression for the formation of H_2 is given by eq 19.

$$v = \frac{k_4 K_a [Re]_T [Eu^{2+}]}{K_a + [H^+]} \qquad (19)$$

where $[Re]_T$ is the total concentration of added MTO, and K_a is the acidity constant for L410-AH. Since K_a is much less than the acidity range for all the reaction conditions studied, the K_a term in the denominator may be neglected and eq 19 can be simplified to eq 20:

$$v = \frac{k_4 K_a [Re]_T [Eu^{2+}]}{[H^+]} \qquad (20)$$

This is consistent with our experimental results, and yields the product of K_a and k_4 equals 2.56 s^{-1} at $\mu = 0.33$ M.

Mechanistic implication of the effect of ionic strength. Salt effect experiments are carried out to support this mechanism. The values of k_{obs} / $[Re]_T$ will vary with ionic strength and they are expected to obey a Bronsted-Debye-Huckel equation 21,

$$\log(k/\mathrm{Re})_i = \log(k/\mathrm{Re})_i^{\,0} + \frac{A(\Delta Z^2)^{\neq}_i \mu^{1/2}}{1+\mu^{1/2}} \qquad (21)$$

where A is a constant (A = 0.509 in water at 25 °C), and $(\Delta Z^2)^{\neq}$ is the difference in the squares of the ionic charges between the activated complex and the reactants for the net activation process. According to the rate law, the net activation process is given by eq 22.

$$\text{L410-AH} + Eu^{2+} \longrightarrow [\ +\ ]^{\neq} + H^+ \qquad (22)$$

In this case, $(\Delta Z^2)^{\neq} = 1^2+1^2-2^2-(Z_{\text{L410-AH}})^2$. If L410-AH is a neutral compound, and its ionic charge is 0 as we suggested in the reaction scheme, the theoretical value of $(\Delta Z^2)^{\neq}$ equals -2.

Because this value of $(\Delta Z^2)^{\neq}$ matches the experimental value of -2.3, the data confirm that L410AH is uncharged.

Reduction of MTO by Cr^{2+}_{aq}. We turn now to the case that Cr_{aq}^{2+} acts as the reducing agent. It is meaningful to compare Cr_{aq}^{2+} with Eu_{aq}^{2+}, because they have very close reduction potentials, -0.43 and -0.38 V respectively. When 0.3 mM MTO and 12 mM Cr^{2+} solutions were mixed in anaerobic 0.12 M HCl, a yellow-green color was observed, which also had an intense absorbance at 410, named as L410(Cr). However, no H_2 bubbles were produced over 10 hours. The spectrophotometric titration for L410(Cr) showed the ratio of Cr_{aq}^{2+} to MTO was 3 to 1, which was same as Eu^{2+} reaction.. This stoichiometry indicates the yellow-green species L410(Cr) is also a Re(IV) species, but with a different molar absorptivitiy from the Eu^{2+} case. At 0.1M acid concentration, molar aborptivity ε at 410 nm is 910 M^{-1} cm^{-1} for L410(Eu) and 1200 M^{-1} cm^{-1} for L410(Cr).

In order to understand why Cr^{2+} does not make H_2 under similar conditions where Eu^{2+} does, more examinations were carried out. Figure 21 presents the buildup of H_2 in different conditions. First, 3mM Cr^{2+} was added in right after we mixed 3.3mM Eu^{2+} with 0.19mM MTO; Second, 3.3mM Eu^{2+} was added in right after we mixed 3mM Cr^{2+} with 0.19mM MTO; Third, a comparison experiment, 6.6mM Eu^{2+} was divided into two parts and added into 0.19mM MTO separately. In all cases, H_2 evolution was observed. Reactions 1 and 2 were obviously slower and produced much less H_2 than case 3. In addition, delayed hydrogen evolution was observed in case 2. Our explanation for all the observations is the different property of intermediate L410 in Eu^{2+} and Cr^{2+} cases. The reaction is given in eq 24-25.

$$MTO + 2M^{2+} + 2H^{+} \longrightarrow MDO + 2M^{3+} + H_2O \qquad (24)$$

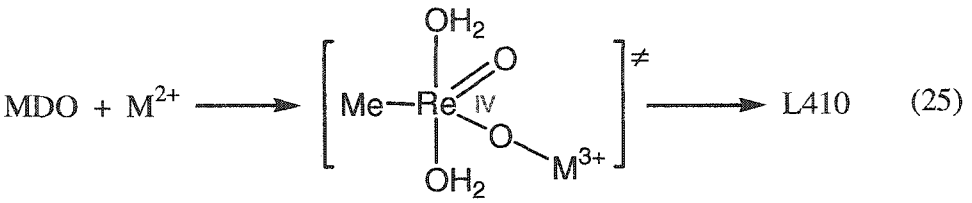

(25)

It is well known that the labilities of the transition metal ions are strongly affected by the electronic occupancy of their d-orbitals. Cr^{3+} has a d^3 configuration and it is the least labile in the first transition species because of its large ligand field activated energy (LFAE). Thus the dissociation of Cr-O bond is very difficult. In addition, Re(IV) also has a d^3 configuration, and because of its inert property, breaking the Re-O bond is also unfavorable. Considering this d^3-d^3 interaction, we proposed that rhenium, oxygen and chromium are binding together and produce a 2+ cation intermediate for L410(Cr). However, Eu^{3+} belongs to f-block category and usually it is very labile because of its large ionic radius. So Eu^{3+} could dissociate from Re-O species and make an anion intermediate, which is the active L410-A species and will be reduced further by one Eu^{2+} to evolve H_2. The reactions and structures proposed for L410 in Eu^{2+} and Cr^{2+} cases are outlined in Scheme 3. When we use Cr^{2+} as the reducing agent, Cr^{3+} is bound to the oxygen on rhenium, so no more reduction can occur. This explains why there is no H_2 bubbles observed in Cr^{2+} reactions. However, when we used 1:1 ratio of Eu^{2+} and Cr^{2+} in the solutions, we observed that Cr^{2+} slowed down the reaction, instead of stopping the reaction completely. This might be due to some dissociation of L410(Cr) to produce tiny amount L410-A, which can be picked up by Eu^{2+} to make H_2. However this dissociation constant K_d should be very small. Because of the competition between Cr^{2+} and Eu^{2+}, and the inert property of L410(Cr), the hydrogen evolution is much slower than that with only Eu^{2+} in solution. This assumption also answers the question as to

why the starting point for hydrogen evolution is different in case 1 and 2. In case 2, the reaction started to evolve H_2 gas at a much delayed time. Because of the different sequence of reagents, the competition occurs at a different point. In case 1, Eu^{2+} reduced MTO to make L410-A first, and then competition for Eu^{2+} and Cr^{2+} starts from the second cycle of MDO. However, in case 2, Cr^{2+} reduced MTO to make L410(Cr), which is very inert. Only when some dissociation of L410(Cr) occurs, Eu^{2+} will pick up L410-A to make H_2. This step is competing with Cr^{2+}. So we believe that the delay of hydrogen evolution is due to the difficulty of dissociation of L410(Cr).

Scheme 3

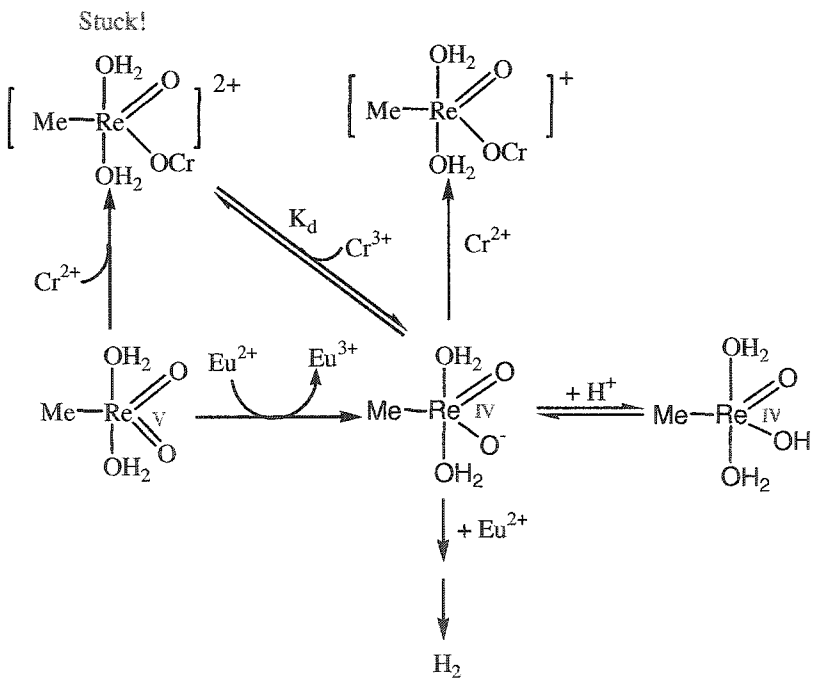

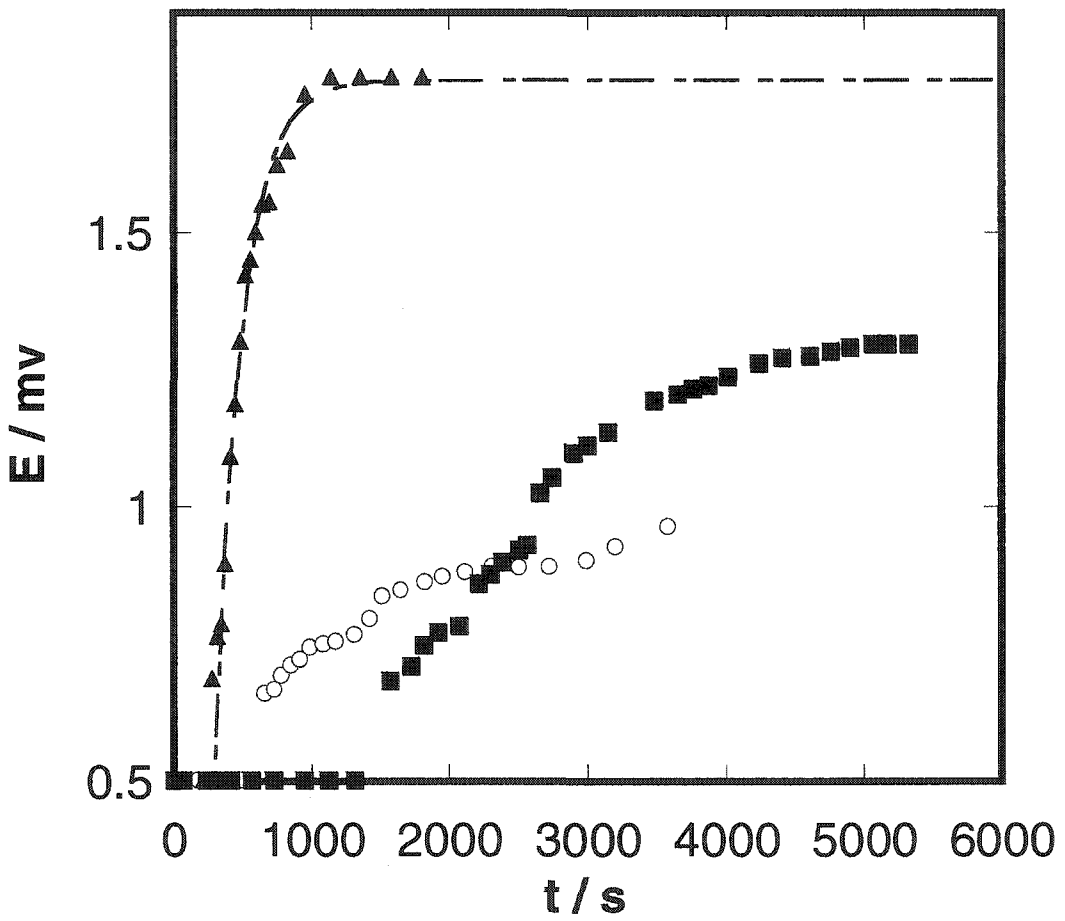

Figure 21. Plots of hydrogen evolution with Cr_{aq}^{2+} in the solution. Conditions: $[H^+]$ = 0.11 M, μ = 0.3 M, 25 °C. **Case 1**(○), 3.3 mM Eu^{2+} mixed with 0.19 mM MTO, then added 3 mM Cr^{2+}; **Case 2**(■), 3 mM Cr^{2+} mixed with 0.19 mM MTO, then added 3.3 mM Eu^{2+}; **Case 3**(▲), a comparison experiment, 3.3 mM Eu^{2+} mixed with 0.19 mM MTO, then added another 3.3 mM Eu^{2+}.

Reaction scheme for perchlorate reduction. Kinetic studies of perchlorate reductions show that this reaction follows a stepwise process, which is similar to Abu-Omar's findings.[14] However, in our case, Eu^{2+} is the reducing agent and MTO serves as the catalyst. So the overall reaction

$$8Eu^{2+} + ClO_4^- + 8H^+ \xrightarrow{MTO} 8Eu^{3+} + Cl^- + 4H_2O \quad (26)$$

can be written into the following reaction equations.

$$MTO + 2Eu^{2+} + 2H^+ \xrightarrow{k_1} 2Eu^{3+} + MDO + 2H_2O \quad (27)$$

$$MDO + ClO_4^- \xrightarrow{k_5} MTO + ClO_3^- \quad (28)$$

$$MDO + ClO_3^- \longrightarrow\longrightarrow\longrightarrow Cl^- \quad (29)$$

Because Eu^{2+} reduces MTO very fast with $k_1 = 2.7\times10^4\ M^{-1}\ s^{-1}$, the perchlorate reduction is the rate controlling step, and the rate expression derived from eq 27-29 can be given as

$$-\frac{d[Eu^{2+}]}{8dt} = -\frac{d[ClO_4^-]}{dt} = k_5[\mathrm{Re}]_T[ClO_4^-] \quad (30)$$

where $k_5 = k / 8 = 5.4\pm0.1\ M^{-1}\ s^{-1}$.

Effect of reagents' sequence for the rate of perchlorate ion reduction. It has been shown in the results of perchlorate ion reduction that the reaction finished in 10 s when MTO solution was mixed with an acidic solution provided Eu^{2+} and ClO_4^- ions. However, a different result was found when we mixed MTO and Eu^{2+} first and added ClO_4^- last. The reaction became much slower and a typical kinetic trace is given in Figure 22. Such a difference is due to L410 formation by Eu^{2+} and MDO in the absence of perchlorate ion, illustrated by the reaction eq 31-37. When we added ClO_4^- first, it reacted with MDO immediately once MTO was reduced by Eu^{2+}, following eq 31-34. Because the reaction

between MDO and ClO_4^- is very fast, the reaction finished in seconds. However, if we added ClO_4^- last, MDO made by Eu^{2+} and MTO was reduced further by Eu^{2+} to make Re(IV) intermediate, taking eq 31, 32, 35 to 37. When ClO_4^- ions entered the system, there was trace MDO in the solution, coming from further reactions of hydrogen evolution. Under experimental conditions, hydrogen evolution took place in a slower time scale. This is the reason why perchlorate ion reduction becomes so slow when ClO_4^- ion is the last reagent put into solution.

$$MTO + Eu^{2+} \xrightarrow{k_1} Re(VI) \qquad (31)$$

$$Re(VI) + Eu^{2+} + 2H^+ \xrightarrow{k_2} 2Eu^{3+} + MDO + 2H_2O \qquad (32)$$

$$MDO + ClO_4^- \xrightarrow{k_5} MTO + ClO_3^- \qquad (33)$$

$$3MDO + ClO_3^- \longrightarrow \longrightarrow \longrightarrow 3MTO + Cl^- \qquad (34)$$

$$MDO + Eu^{2+} \xrightarrow{k_3} L410\text{-}A \qquad (35)$$

$$L410\text{-}A + H^+ \rightleftharpoons L410\text{-}AH \qquad (36)$$

$$L410\text{-}A + Eu^{2+} + 2H^+ \xrightarrow{k_4} H_2 + MDO + 2Eu^{3+} \qquad (37)$$

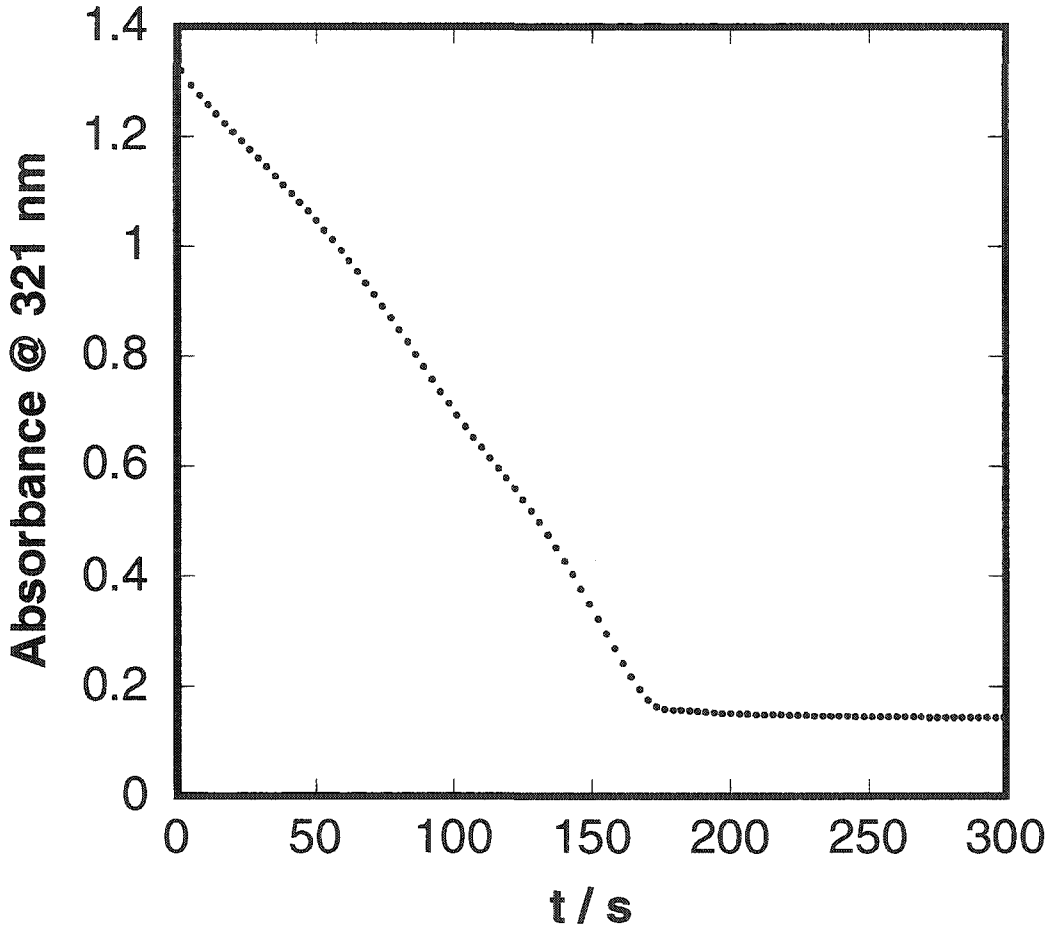

Figure 22. Influence of reagents' sequence on kinetic trace of perchlorate reduction. Condition: $[Eu^{2+}]$ = 2.92 mM, [MTO] = 0.2 mM; $[ClO_4^-]$ = 0.167 M and $[H^+]$ = 0.5 M with μ = 0.8 M at 25 °C, adding ClO_4^- last.

Oxygen effect on kinetic traces for perchlorate ion reduction. All the kinetic traces for perchlorate ion reduction show an initial curvature at the beginning of the reaction. We propose this phenomenon is due to the trace amount of oxygen which can not be completely excluded from the system in the OLIS stopped-flow device and it consumes Eu^{2+} fast. In order to confirm this supposition, an experiment for oxygen effect was examined. An aerobic solution of MTO was mixed with the anaerobic solution of ClO_4^- and Eu^{2+} and recorded the spectrum change by OLIS. Figure 23 presents the kinetic trace for this experiment. It is seen that the initial curvature became bigger and more Eu^{2+} was consumed before the reaction with perchlorate ion. The increase loss of Eu^{2+} before the perchlorate ion reduction was caused by higher oxygen concentration than that with both anaerobic solutions. However, since the reaction of perchlorate ion reduction is independent of Eu^{2+} concentration, the pseudo-zero-order constant k_{obs} does not change, $k_{obs} = 2.13\times10^{-4}$ M s^{-1}, which is 2.04×10^{-4} M s^{-1} under normal conditions.

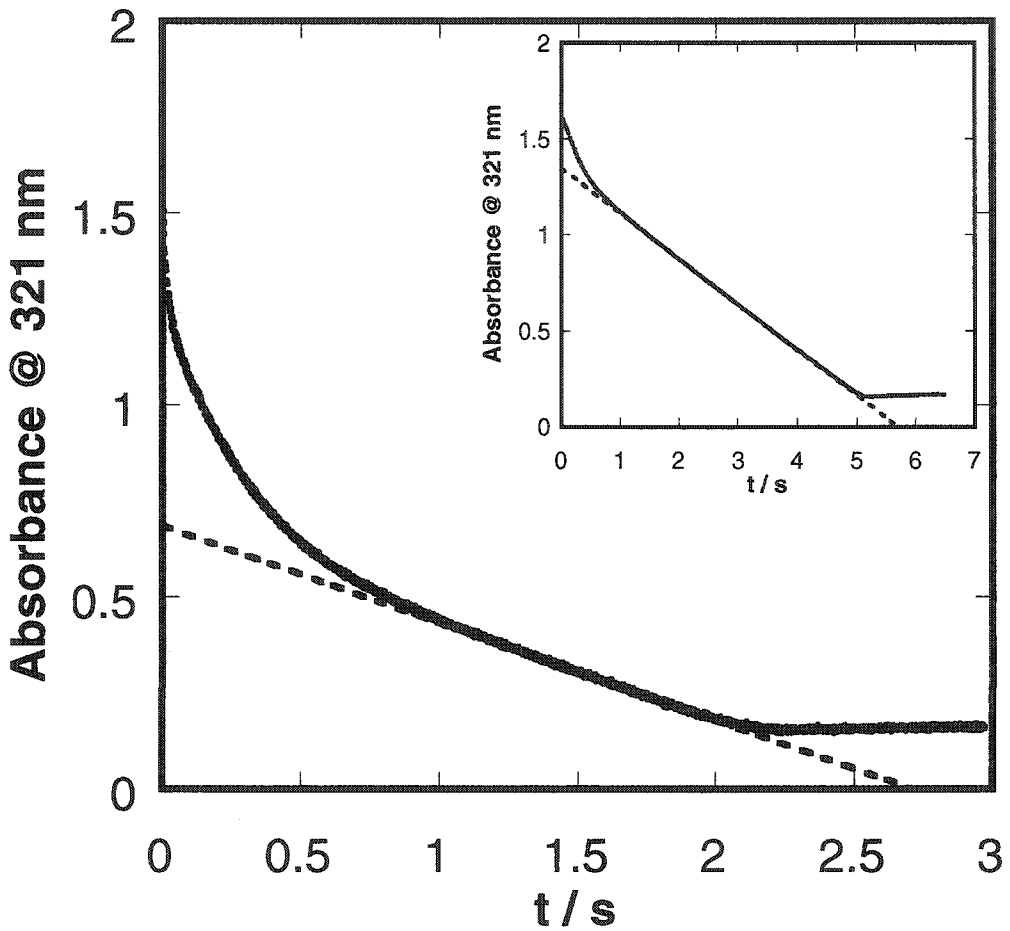

Figure 23. Oxygen effect for kinetic traces of perchlorate ion reduction. Condition: $[Eu^{2+}]$ = 1.62 mM, $[ClO_4^-]$ = 0.05 M, [MTO] = 0.098 mM(aerobic), $[H^+]$ = 0.55 M with μ = 0.8 M, $k_{obs} = 2.13\times10^{-4}$ M s^{-1}; Inset: MTO – anaerobic, $k_{obs} = 2.04\times10^{-4}$ M s^{-1}.

References

(1) Weaver, M. J. *J. Am. Chem. Soc.* **1979**, *101*, 1131-1137.

(2) Weaver, M. J.; Yee, E. L. *Inorg. Chem* **1980**, *19*, 1936-1945.

(3) Evans, J.; Norton, J. R. *J. Am. Chem. Soc.* **1974**, *96*, 7577.

(4) Chao, T.-H.; Espenson, J. H. *J. Am. Chem. Soc.* **1978**, *100*, 129.

(5) Ryan, D. A.; Espenson, J. H. *Inorg. Chem* **1981**, *20*, 4401.

(6) Connolly, P.; Espenson, J. H. *Inorg. Chem* **1986**, *25*, 2684-2688.

(7) Gould, E. S. *Inorg. Chem* **1988**, *27*, 1868-1871.

(8) King, W. R.; Garner, C. S. *Journal of Physical Chemistry* **1954**, *58*, 29-33.

(9) Duke, F. R.; Quinney, P. R. *J. Am. Chem. Soc.* **1954**, *76*, 3800-3803.

(10) Endicott, J. F.; Taube, H. *Inorg. Chem* **1965**, *4*, 437-445.

(11) Earley, J. E.; Kallen, T. W. *Inorg. Chem* **1971**, *10*, 1152-1155.

(12) Kallen, T. W.; Earley, J. E. *J. Chem. Soc. D* **1970**, 851.

(13) Taube, H. *ACS Symposium Series* **1982**, *198*, 151-179.

(14) Abu-Omar, M. M.; Espenson, J. H. *Inorg. Chem* **1995**, *34*, 6239-6240.

(15) Abu-Omar, M. M.; Appelman, E. H.; Espenson, J. H. *Inorg. Chem* **1996**, *35*, 7751-7757.

(16) Felixberger, J. K.; Kuchler, J. G.; Hermann, W. A. *Angew. Chem. Int. Ed. Engl.* **1988**, *27*, 946-948.

(17) Hermann, W. A.; Wang, M. *Angew. Chem. Int. Ed. Engl.* **1991**, *30*, 1641.

(18) Hermann, W. A.; Roesky, P. W. *Organometallics* **1994**, *13*, 4531-4535.

(19) Gable, K. P.; Juliette, J. J. J.; Gartman, M. A. *Organometallics* **1995**, *14*, 3138-3140.

(20) Hermann, W. A.; Kratzer, R. M. *Angew. Chem. Int. Ed. Engl.* **1997**, *36*, 2652.

(21) Leslie, J. P.; Espenson, J. H. *J. Am. Chem. Soc.* **1976**, *98*, 4839.

(22) Davis, D. D.; Stevenson, K. L. *J. Chem. Edu.* **1977**, *54*, 394-395.

(23) Lente, G.; Espenson, J. H. *Internationl Journal of Chemical Kinetics* **2004**, *36*, 449-455.

CHAPTER II. A NEW OXORHENIUM(V) COMPOUND FOR CATALYZED OXYGEN ATOM TRANSGER FROM PICOLINE N-OXIDE TO TRIARYLPHOSPHINES

A manuscript submitted to *Inorganic Chemistry*

Yang Cai, Arkady Ellern and James H. Espenson

Abstract

A new oxorhenium(V) compound, MeReO(edt)(bpym) (**8**), has been synthesized. Its structure was well characterized by NMR spectroscopy and single-crystal X-ray analysis. Compound **8** is a six-coordinate Re(V) compound with a weakly-coordinating bidentate ligand, 2,2'-bipyrimidine, which can be compared to the previously known MeReO(mtp)(bpy) (**4**), MeReO(mtp)(bpy)* (**5**) and MeReO(edt)(bpy) (**6**). Its importance lies in proving that the existence of an open coordination site in rhenium center is necessary for oxygen atom transfer reactions. We found that compound **8** is an active catalyst for the oxygen atom transfer reaction: PicO + $PZ_3 \rightarrow$ Pic + Z_3PO, while compounds **4**, **5**, and **6** are not active catalysts for this reaction. The kinetics of this reaction with catalyst **8** follows the rate law – $d[PicO]/dt = k\,[\mathbf{8}][PicO]/(1 + c[PZ_3])$. With different phosphines, the rate law has the same k value but different c values. For tritolylphosphine, k = 4.17 L mol^{-1} s^{-1} and c = 67.5 L mol^{-1} in benzene at 25 °C. A mechanism has been proposed to account for these findings.

Introduction

Oxygen atom transfer reactions catalyzed by transition metal complexes have received considerable attention from biological and inorganic chemists.[1-3] Extensive studies have been done with molybdenum and tungsten compounds.[3-11] We previously found that certain oxorhenium (V) complexes in Chart 1, such as **1**, are active catalysts for the following reaction.[12-14]

$$PyO + PZ_3 \rightarrow Py + Z_3PO \qquad (1)$$

Chart 1. Structural Formulas of Five-Coordinate Oxorhenium(V) Compounds

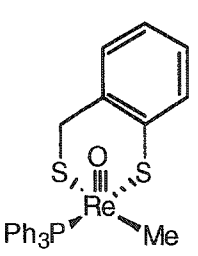

MeReO(mtp)PPh$_3$ 1

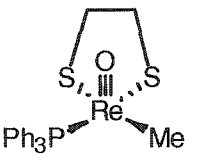

MeReO(edt)PPh$_3$ 2

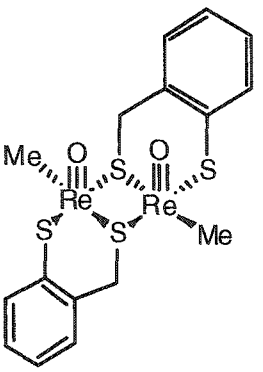

{MeReO(mtp)}$_2$ 3

Until now, the active catalysts have been five-coordinate oxorhenium complexes. In contrast, the six-coordinate rhenium (V) complexes **4**-**7**, Chart 2, do not function as catalysts. [15] We have thus postulated that, not surprisingly, the existence of an open coordination site is needed to allow entry of the oxygen atom of the substrate.

Chart 2. *Structural formulas of Six-Coordinate Oxorhenium(V) Complexes*

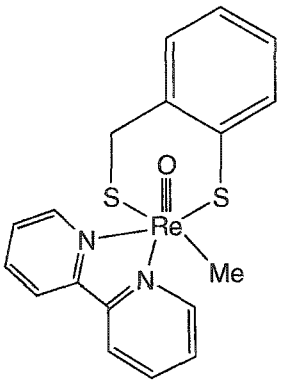

[MeReO(mtp)(bpy)] **4**

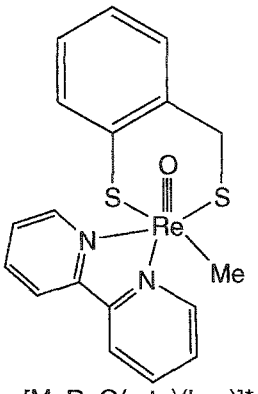

[MeReO(mtp)(bpy)]* **5**

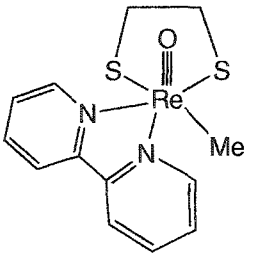

[MeReO(edt)(bpy)] **6**

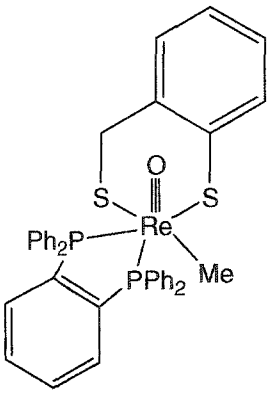

[MeReO(mtp)(dppb)] **7**

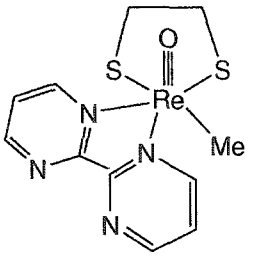

[MeReO(edt)(bpym)] **8**

To test this hypothesis, we designed a potential new catalyst, MeReO(edt)(bpym), **8**, where edt represents 1,2-ethanedithiolate and bpym 2,2'-bipyrimidine. The product is a six-coordinate complex with a weakly-coordinating bidentate ligand, which may be expected to protect the sixth position for the oxygen donor yet still make that position available by way of chelate ring opening. We report here the synthesis and characterization of **8**, and studies of the kinetics and mechanism of its catalysis of reaction 1.

Experimental Section

Reagents and Instrumentation. Methyltrioxorhenium(VII) and the dimer $\{CH_3ReO(edt)\}_2$ were prepared according to literature procedures.[16,17] Other reagents were purchased from commercial sources and used as received. Benzene was the solvent for all the studies.

A Bruker DRX-400MHz spectrometer was used to record ^1H and ^{31}P NMR spectra. The ^1H chemical shifts were referenced internally using the residual proton resonance of the solvent, C_6D_6, and ^{31}P chemical shifts to 85% H_3PO_4. The elemental analysis of compound **8** was performed by Desert Analytics Laboratory.

Synthesis and Characterization of 8. $\{MeReO(edt)\}_2$ (30 mg, 0.049 mmol) was dissolved in toluene (10 mL) followed by 2 equiv of 2,2'-bipyrimidine (bpym). The color changed from brown to deep red in 1 hour. After stirring for about 6 h, the solution was concentrated to ca. 3 mL by rotary evaporation and the product was precipitated by addition of hexanes. Compound **8**, MeReO(edt)(bpym), was obtained as a dark red solid in 54% yield. ^1H NMR (C_6D_6, 25 °C, Figure 1): δ (ppm) 2.83 (s, 3H CH_3), 3.07 (m, H, CH_2), 3.15 (m, H, CH_2), 3.33 (m, H, CH_2), 3.79 (m, H, CH_2), 5.52 (t, H, CH), 5.80 (t, H, CH), 7.77 (dd, 2H, CH), 8.25 (d, H, CH), 9.09 (d, H, CH). Elemental analysis: $C_{11}H_{12}N_4ORe S_2$: C, Found, 29.04, (calcd 28.26); H, 2.88, (2.80); N, 11.79, (11.98); S, 13.15, (13.72).

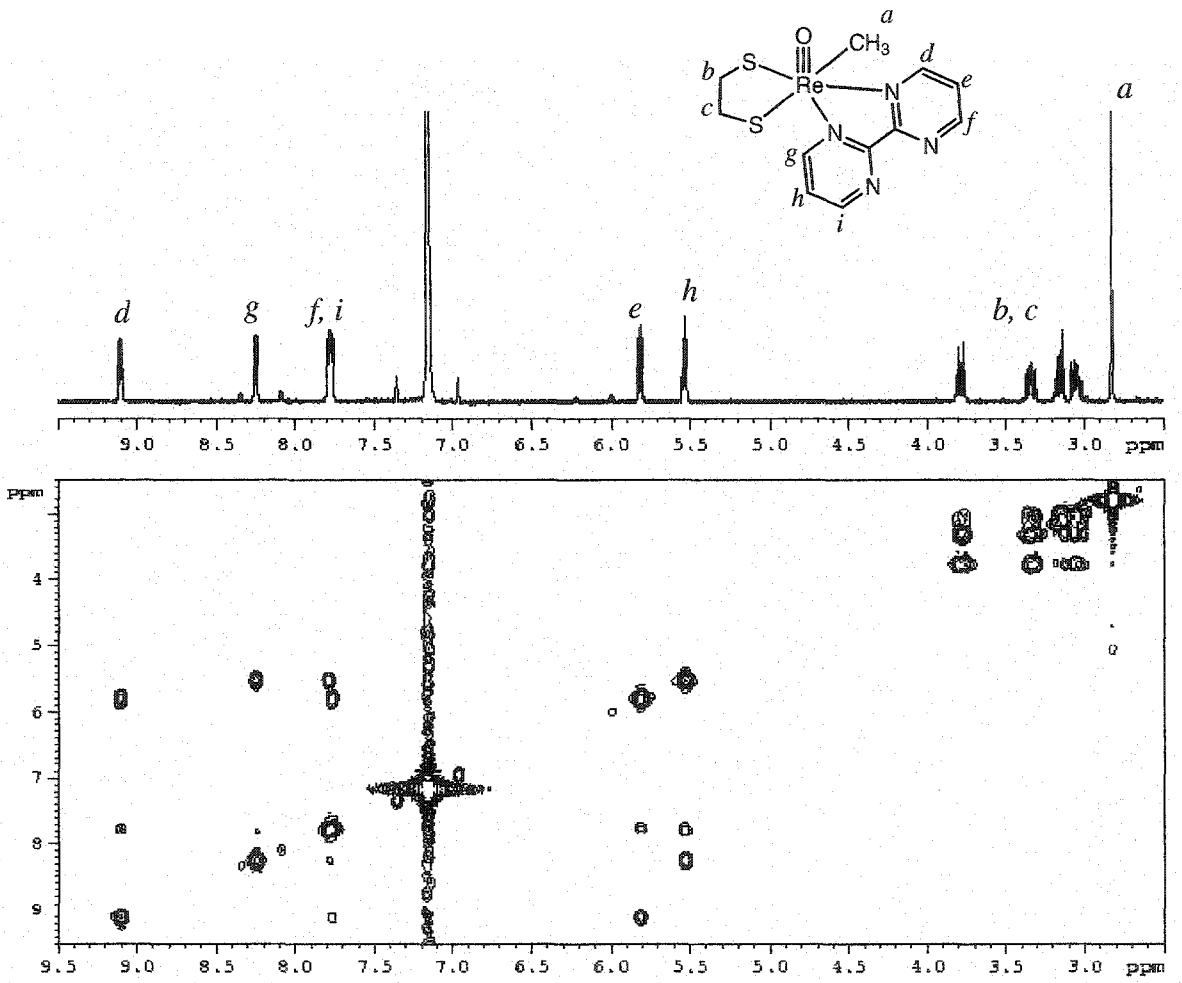

Figure 1. The ^{1}H and COSY NMR spectra of compound **8** in C_6D_6 at 25 °C. δ (ppm) 2.83 (s, 3H CH_3), 3.07 (m, H, CH_2), 3.15 (m, H, CH_2), 3.33 (m, H, CH_2), 3.79 (m, H, CH_2), 5.52 (t, H, CH), 5.80 (t, H, CH), 7.77 (dd, 2H, CH), 8.25 (d, H, CH), 9.09 (d, H, CH).

Crystal Structure of 8. A black prismatic crystal with approximate dimensions 0.23 × 0.15 × 0.1 mm^3 was selected under ambient conditions. The crystal was mounted and centered in the X-ray beam by using a video camera. The crystal evaluation and data collection were performed at 173 K on a Bruker CCD-1000 diffractometer with Mo K_α (λ = 0.71073 Å) radiation and a detector-to-crystal distance of 5.03 cm. The initial cell constants were obtained from three series of ω scans at different starting angles. Each series consisted of 30 frames collected at intervals of 0.3° in a 10° range about ω with the exposure time of 10 s per frame. A total of 189 reflections was obtained. The reflections were successfully indexed by an automated indexing routine built in the SMART program. The final cell constants were calculated from a set of 1428 strong reflections from the actual data collection. The data were collected using the full sphere routine. A total of 4208 data were harvested by collecting four sets of frames with 0.3° scans in ω with an exposure time 10 sec per frame. This dataset was corrected for Lorenz and polarization effects. The absorption correction was based on fitting a function to the empirical transmission surface as sampled by multiple equivalent measurements[18] using SADABS software.[19]

The systematic absences in the diffraction data were consistent with the space group $P2_1/c$, which yielded chemically reasonable and computationally stable results of refinement. The position of heavy atom was found by the Patterson method. The remaining atoms were located in an alternating series of least-squares cycles and difference Fourier maps. All non-hydrogen atoms were refined in full-matrix anisotropic approximation. All hydrogen atoms were found objectively and were allowed to ride on the neighboring atoms with relative isotropic displacement coefficients. Final least-squares refinement of 172 parameter against

1988 independent reflections converged to R (based on F^2 for $I \geq 2\sigma$) and wR (based on F^2 for $I \geq 2\sigma$) of 0.016 and 0.039, respectively.

Kinetics. The reactions of 4-picoline *N*-oxide (PicO) and triarylphosphines (PZ_3) were monitored by the integration of the methyl peaks of PicO and 4-picoline (Pic). The phosphine was added in greater than 10-fold excess, allowing the concentration-time data to be fitted by pseudo-first-order kinetics eq 2.

$$[\mathrm{PicO}]_t = [\mathrm{PicO}]_0 \times e^{-k_{obs}t} \qquad (2)$$

Table 1. Crystal data and structure refinement for MeReO(edt)(bpym) **8**.

Identification code	MeReO(edt)(bpym)	
Empirical formula	$C_{11}\ H_{13}\ N_4\ O\ Re\ S_2$	
Formula weight	467.57	
Temperature	173(2) K	
Wavelength	0.71073 Å	
Crystal system	Monoclinic	
Space group	P2(1)/c	
Unit cell dimensions	a = 13.547(3) Å	α= 90°.
	b = 8.056(2) Å	β= 103.227(4)°.
	c = 12.984(3) Å	γ = 90°.
Volume	1379.4(6) $Å^3$	
Z	4	
Density (calculated)	2.251 Mg/m^3	
Absorption coefficient	9.108 mm^{-1}	
F(000)	888	
Crystal size	0.23 x 0.15 x 0.10 mm^3	
Theta range for data collection	2.96 to 23.32°.	
Index ranges	-10<=h<=15, -8<=k<=8, -14<=l<=14	
Reflections collected	5904	
Independent reflections	1988 [R(int) = 0.0194]	
Completeness to theta = 23.32°	99.4 %	
Absorption correction	Empirical	
Max. and min. transmission	0.70 and 0.39	
Refinement method	Full-matrix least-squares on F^2	
Data / restraints / parameters	1988 / 0 / 172	
Goodness-of-fit on F^2	1.042	
Final R indices [I>2sigma(I)]	R_1 = 0.0156, wR_2 = 0.0392	
R indices (all data)	R_1 = 0.0163, wR_2 = 0.0395	
Largest diff. peak and hole	0.792 and -0.806 e.$Å^{-3}$	

$R_1 = \Sigma \, | \, |F_o| - |F_c| \, | \, / \, \Sigma \, |F_o|$ and $wR_2 = \{ \, \Sigma \, [\, w(F_o^2 - F_c^2)^2 \,] \, / \, \Sigma \, [\, w(F_o^2)^2 \,] \, \}^{1/2}$

Results and Discussion

Structure of 8. Figure 2 shows the molecular structure of compound **8**. The rhenium atom is six-coordinate, located in the center of a distorted octahedron. Table 2 lists selected bond distances and angles. The Re-O bond length is 169.2(3) pm, which is quite similar to most well characterized Re(V) oxo compounds.[20-22] As reported in the literature, the distances for ideallized $Re^{V}\equiv O$ and $Re^{V}=O$ bonds were estimated to be approximately 160 and 176 pm, respectively.[20-25] The Re–N(1) bond distance of 226.4 pm for the N which lies trans to the oxo group is longer than that of Re–N(3), 218.6 pm, for N trans to a sulfur atom. This is due to the *trans* influence of the terminal oxo group on rhenium.

Table 2. Selected Bond Lengths (pm) and Angles (deg) in **8**.

Re(1)–O(1)	169.2(3)	O(1)–Re(1)–C(9)	102.48(14)
Re(1)–C(9)	217.5(4)	O(1)–Re(1)–N(3)	85.16(11)
Re(1)–N(3)	218.6(3)	C(9)–Re(1)–N(3)	85.13(13)
Re(1)–N(1)	226.4(3)	O(1)–Re(1)–N(1)	155.90(11)
Re(1)–S(2)	227.33(11)	C(9)–Re(1)–N(1)	77.62(13)
Re(1)–S(1)	236.75(11)	N(3)–Re(1)–N(1)	70.78(11)
N(1)–Re(1)–S(2)	96.90(8)	O(1)–Re(1)–S(2)	107.08(9)
O(1)–Re(1)–S(1)	105.09(10)	C(9)–Re(1)–S(2)	83.12(11)
C(9)–Re(1)–S(1)	152.17(11)	N(3)–Re(1)–S(2)	164.59(8)

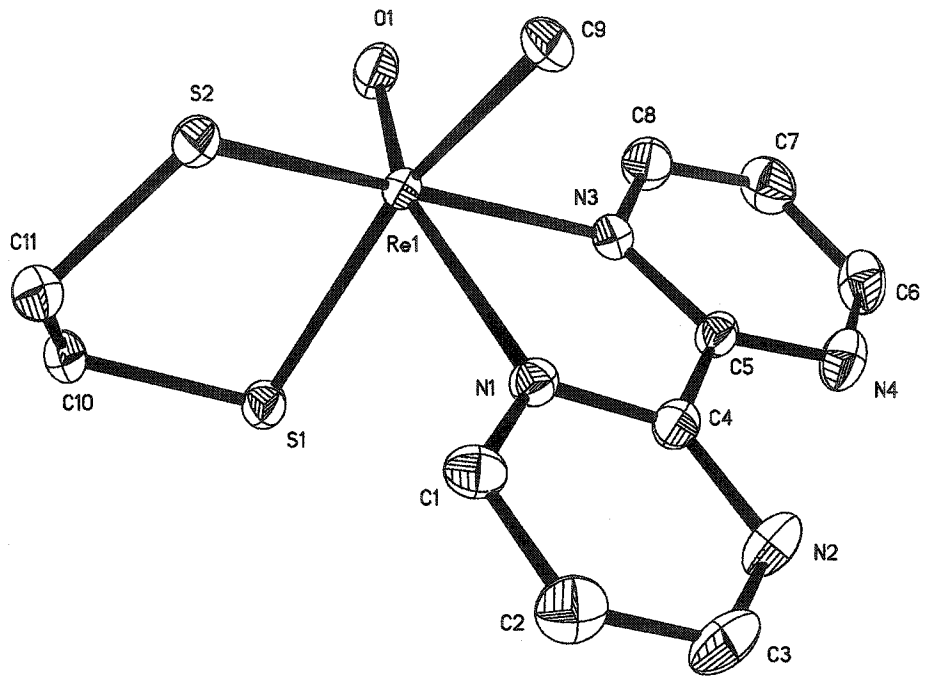

Figure 2. Molecular structure of MeReO(edt)(bpym) **8** with ellipsoids drawn at the 50% probability level.

Kinetics: An Induction Period. The first system studied was the reaction between 4-picoline N-oxide (PicO) and tri-*p*-tolylphosphine ($PTol_3$) in benzene. As reported previously, no reaction occurred over 10 h in the absence of the catalyst. When 4.17 mM PicO and 50.0 mM $PTol_3$ were mixed, followed by 0.56 mM compound **8**, we found that the reaction went to completion in 3 h as monitored by ^1H NMR spectroscopy. A kinetic plot of PicO concentration against time is shown in Figure 3. As one can see, there is an induction period at the beginning of the reaction. However, when we changed the mixing sequence, different kinetic traces were found. Mixing either PicO and **8** first and adding $PTol_3$, or mixing $PTol_3$ with **8** and then PicO, gave data that did not show an induction period and gave concentration-time data that followed first-order kinetics throughout. The kinetic traces are presented in Figure 4 and 5. The results showed that the pseudo-first-order rate constant k_{obs}, obtained by first-order kinetics fittings, were different in these two cases. The k_{obs} value is 5.4×10^{-4} s^{-1} with $PTol_3$ as the last reagent, and k_{obs} equals 4.3×10^{-4} s^{-1} instead, when PicO was added last. The reason for this difference will be discussed in detail.

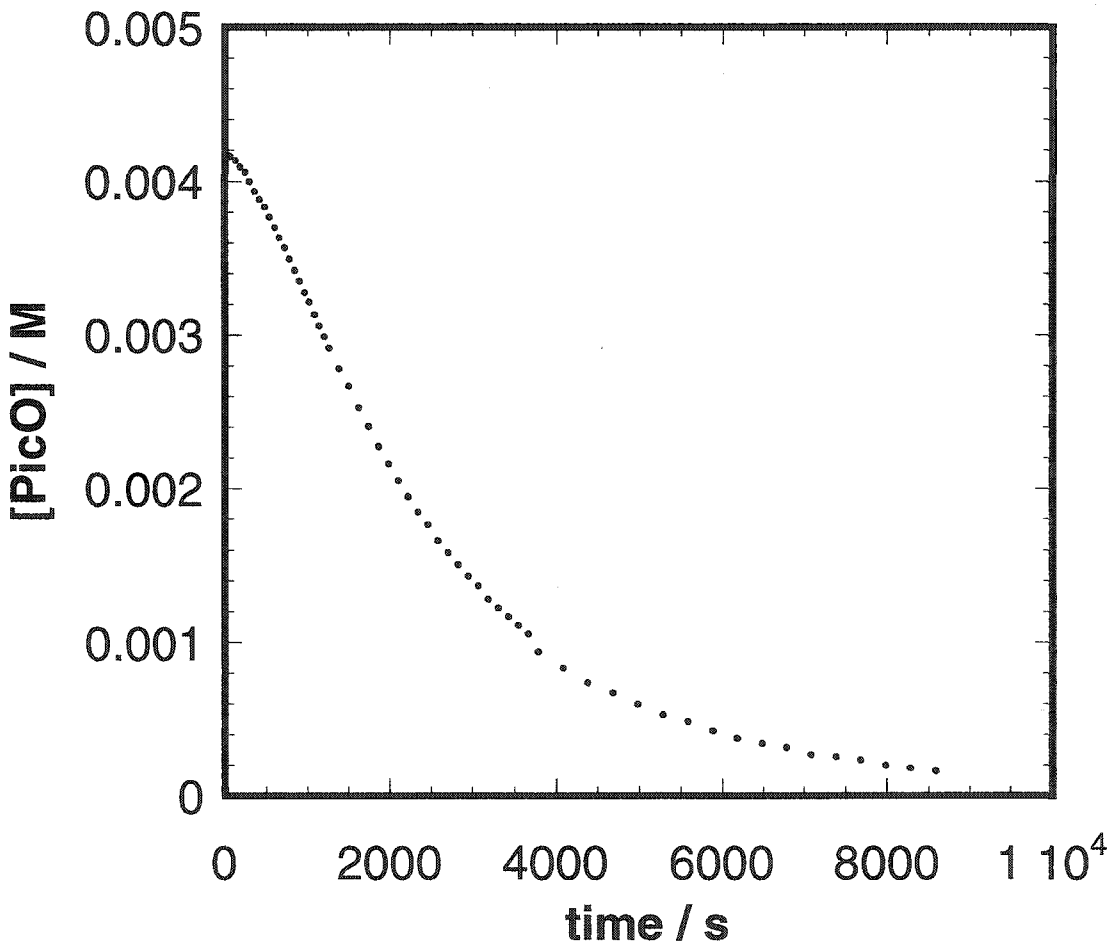

Figure 3. Induction period observed for the reaction of picoline N-oxide, tritolyphosphine and rhenium species **8** when **8** is the last reagent put into system. Conditions: 4.17 mM PicO, 50.0 mM $PTol_3$ and 0.56 mM **8** in benzene at 25 °C.

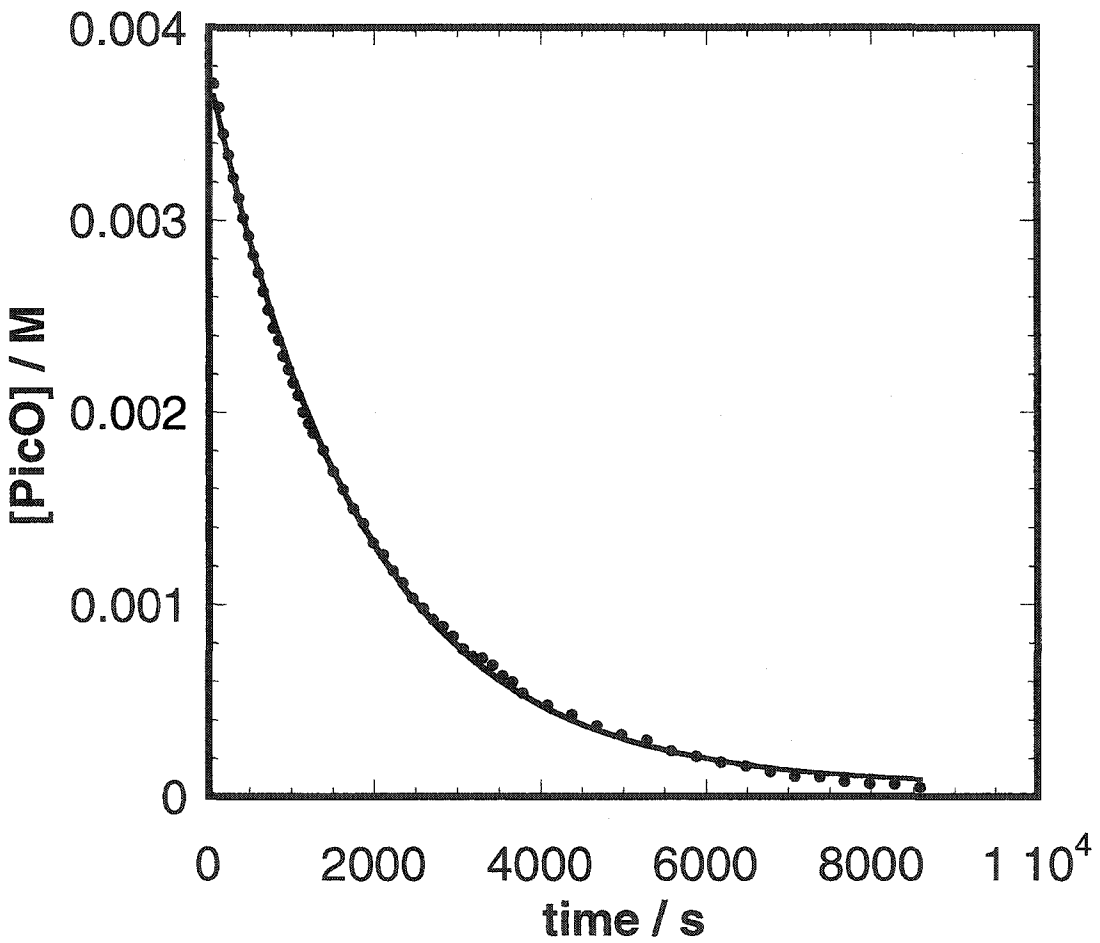

Figure 4. A kinetic trace for the reaction of PicO, $PTol_3$ and **8** when $PTol_3$ was the last reagent added. Conditions: 4.17 mM PicO, 50.0 mM $PTol_3$ and 0.56 mM **8** in benzene at 25 °C. The data were fitted by first-order kinetics and yielded k_{obs} 5.4×10^{-4} s^{-1}.

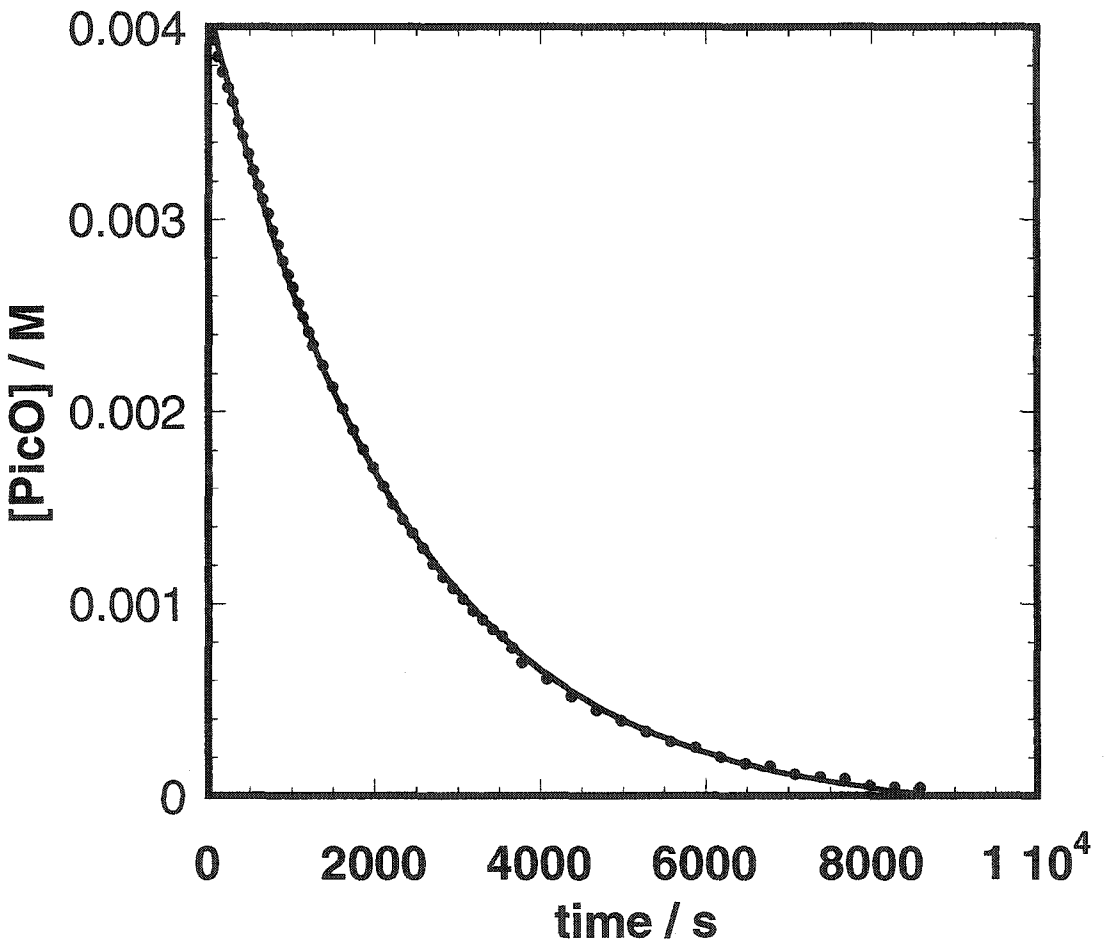

Figure 5. A plot of the disappearance of PicO in the reaction of PicO, $PTol_3$ and **8** when PicO was added last. Conditions: 4.17 mM PicO, 50.0 mM $PTol_3$ and 0.56 mM **8** in benzene at 25 °C. The data were fitted by first-order kinetics giving k_{obs} 4.3×10^{-4} s^{-1}.

Determination of the Rate Law. Time-course kinetic analysis was used to determine the dependence of the rate on the concentration of the participating species. All the experiments were done under conditions where triarylphosphine was greater than 10-fold excess over picoline N-oxide and was the last reagent added. Generally, the experiments were performed with added 4-picoline and bipyrimidine to avoid any effect from product or complete dissociation of the chelate ligand. In each run, the kinetic data conformed to a first-order rate kinetics yielding the pseudo-first-order rate constant k_{obs}. An example is shown in Figure 6. The summary of all the kinetic data is given in Table 3, which lists the concentrations used in each set of measurements. Figure 7 presents the plot of k_{obs} vs. [**8**]. The linear fitting establishes that the rate of reaction shows a simple first-order dependence on catalyst **8**. As for tritolylphosphine, the values of k_{obs} / [**8**] show a nonlinear dependence on the concentration of $PTol_3$, as depicted in Figure 8. The relation is adequately described by eq 3.

$$\frac{k_{obs}}{[\mathbf{8}]} = \frac{m_1}{1 + m_2[PTol_3]} \qquad (3)$$

These data allow the rate expression for the disappearance of 4-Picoline N-oxide to be

$$-\frac{d[PicO]}{dt} = \frac{k[\mathbf{8}][PicO]}{1 + c[PTol_3]} \qquad (4)$$

$$\text{where } k_{obs} = \frac{k[\mathbf{8}]}{1 + c[PTol_3]} \qquad (5)$$

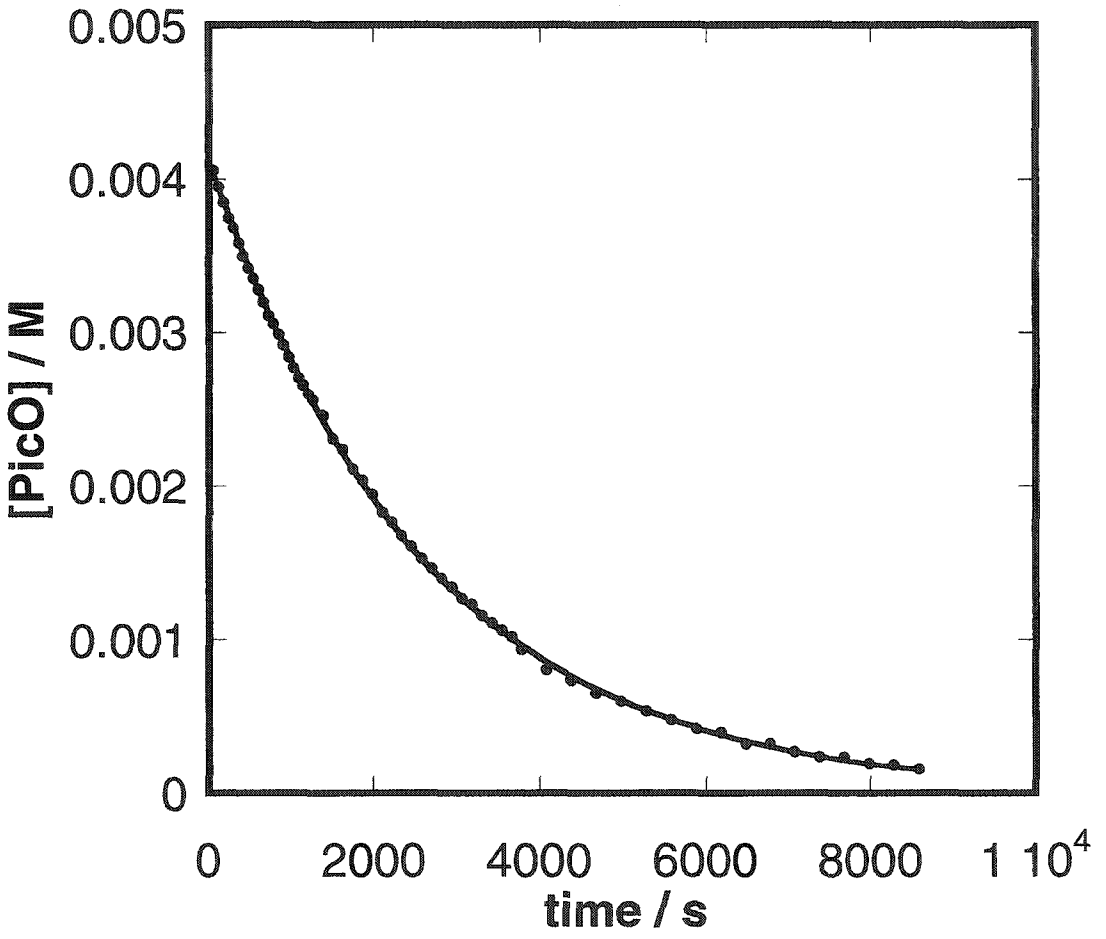

Figure 6. A typical kinetic trace of the reaction of PicO, $PTol_3$ and **8.** Condition: 4.17 mM PicO, 50.0 mM $PTol_3$, 0.420 mM **8**, 44.1 mM Pic and 10.0 mM bpym in benzene at 25 °C. The data were fitted by first-order kinetics giving k_{obs} 3.85×10^{-4} s^{-1}.

Table 3. Pseudo-first-order rate constants k_{obs} for the oxidation of $PTol_3$ by 4-picoline N-oxide with **8** as catalyst at 25 °C in benzene. Condition: [4-picoline] = 0.044 M, [bpym] = 0.010 M.

[PicO] / 10^{-3} M	[**8**] / 10^{-3} M	[$PTol_3$] / 10^{-3} M	k_{obs} / 10^{-4} s^{-1}
4.17	0.322	50.0	3.12
4.17	0.420	50.0	3.85
4.17	0.630	50.0	5.99
4.17	0.770	50.0	7.22
4.17	0.910	50.0	9.17
4.20	0.490	49.4	4.76
4.20	0.490	71.4	3.67
4.20	0.490	91.7	2.77
4.20	0.490	109.8	2.46
4.20	0.490	130.4	2.17

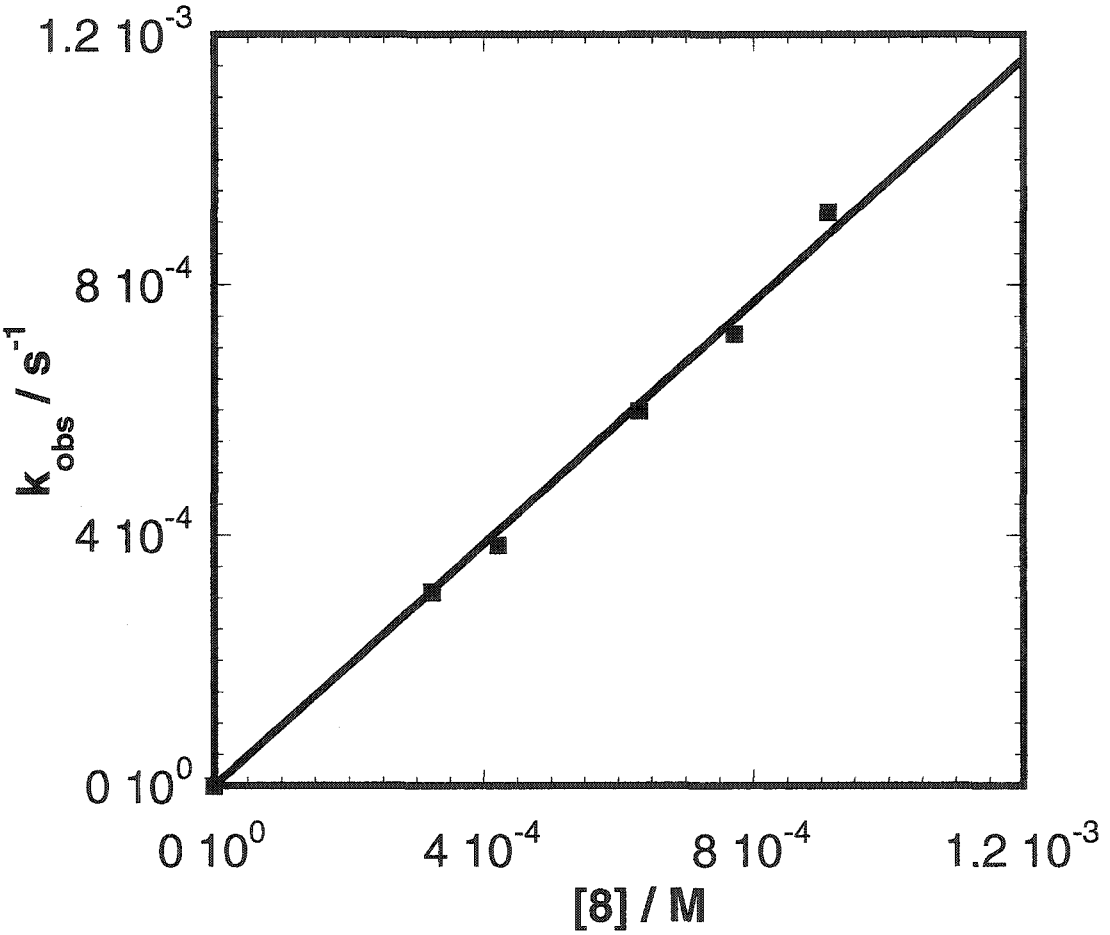

Figure 7. A plot of pseudo-first-order rate constants k_{obs} vs. concentration of catalyst **8**.

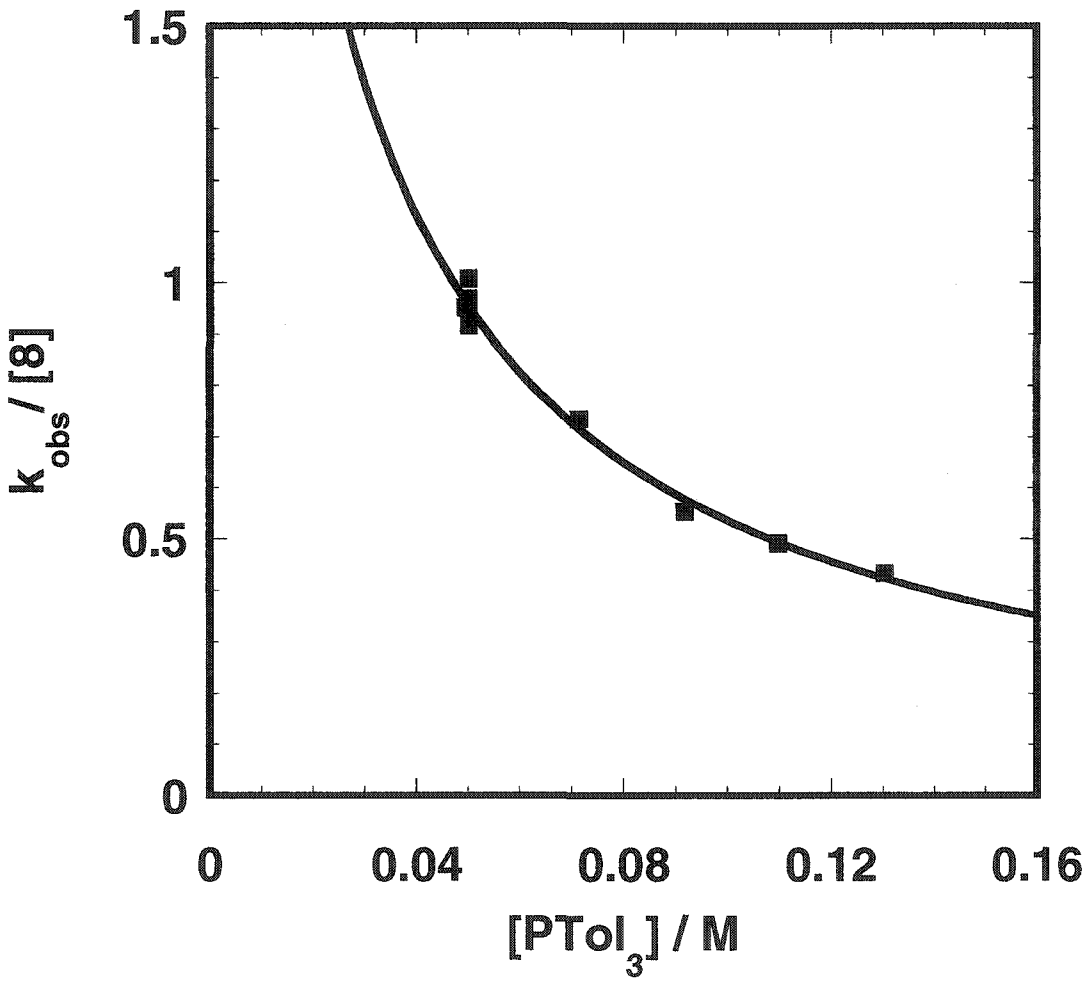

Figure 8. The variation of k_{obs} / [8] with [$PTol_3$] does not follow a linear dependence.

Para-Substituted Phosphines. Kinetic studies for different $(4\text{-}XC_6H_4)_3P$ reagents were carried out with PicO and catalyst **8**, to which eq 5 still applies. The values of k_{obs} for each reaction were obtained by the same method previously described. The resulting pseudo-first-order rate constants for the reactions under investigations are summarized in Table 4.

It is useful to consider the same set of data from a graphical point of view, to display the effect of phosphine for each term. For that purpose the expression for k_{obs} eq 5

$$k_{obs} = \frac{k[\mathbf{8}]}{1 + c[PAr_3]} \quad (5)$$

can be rearranged to the following form:

$$\frac{[\mathbf{8}]}{k_{obs}} = \frac{1}{k} + \frac{c}{k}[PAr_3] \quad (6)$$

Based on this relation, the value of $[\mathbf{8}] / k_{obs}$ should vary linearly with the concentration of triarylphosphine. Such plots for all of para-substituted phosphine complexes investigated are shown in Figure 9. As one can see, they have a common intercept, k^{-1}, but have slopes that differ from one phosphine to another. Table 5 gives the values of k and c for these phosphines. The fastest reactions are those with the most-electron-withdrawing substituent, X = Cl, and vice versa. Further analysis will be discussed later.

Table 4. Pseudo-first-order rate constant k_{obs} for the reaction between 4-picoline N-oxide and $(4\text{-}XC_6H_4)_3P$ catalyzed by **8** at 25 °C in benzene. Condition: [4-picoline] = 0.044 M, [bpym] = 0.010 M.

$(4\text{-}XC_6H_4)_3P$	$[PAr_3]$ / 10^{-3}M	[8] / 10^{-3} M	k_{obs} / 10^{-4} s^{-1}
X = Cl	49.5	0.500	15.0
	68.2	0.143	4.19
	70.2	0.286	7.32
	95.5	0.286	7.05
	143.2	0.143	3.06
X = F	55.6	0.778	21.6
	80.4	0.778	21.0
	102.2	0.215	4.55
	146.3	0.518	8.87
X = H	50.7	0.572	15.3
	71.2	0.714	13.5
	99.7	0.714	11.6
	101.3	0.572	10.0
	128.2	0.572	11.2
X = OMe	49.0	0.500	2.89
	77.1	0.500	1.66
	108.6	0.500	1.35

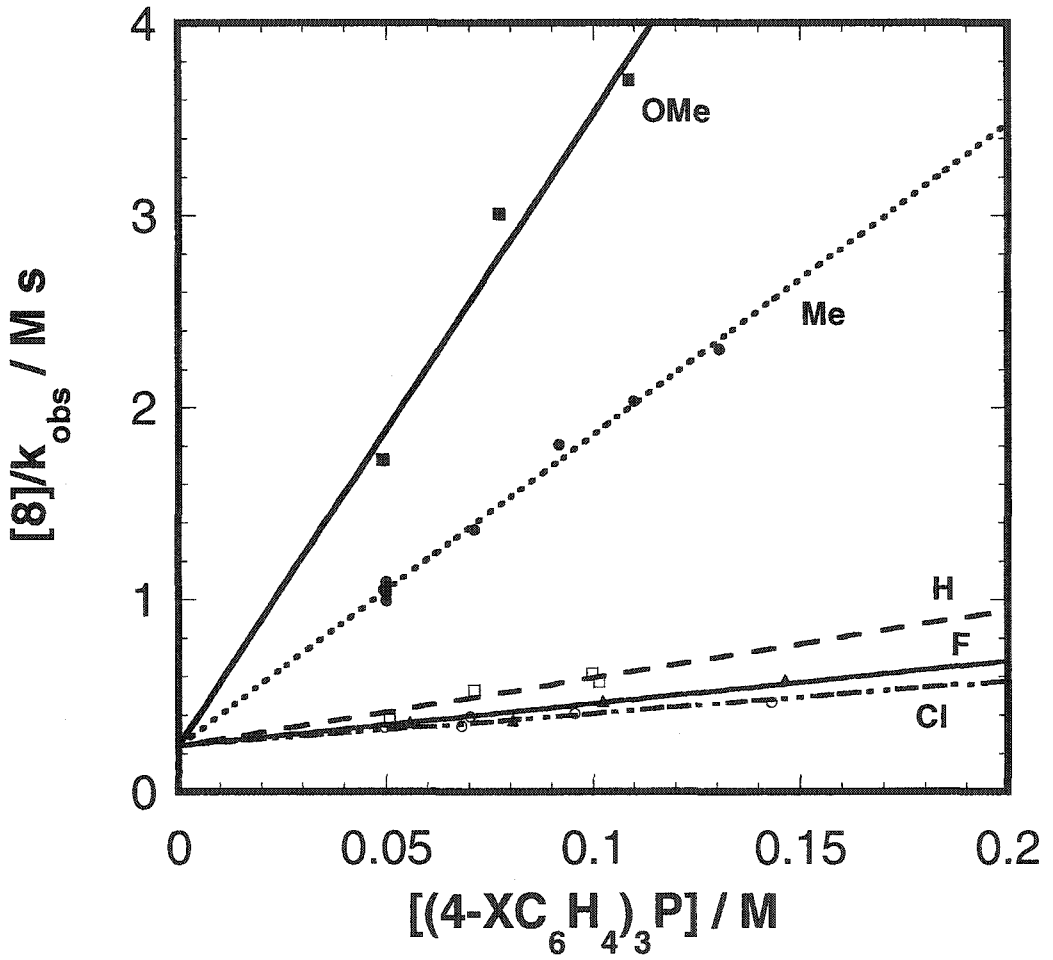

Figure 9. A plot of [**8**] / k_{obs} against concentration of $(4\text{-}XC_6H_4)_3P$ for the reaction between $(4\text{-}XC_6H_4)_3P$ and 4-picoline N-oxide catalyzed by **8** at 25 °C in benzene. X = OMe(■); X = Me(●); X = H(▫); X = F(▲); X = Cl(○).

Table 5. Values of k and c in eq 6 for the reaction between 4-picoline N-oxide and (4-$XC_6H_4)_3P$ catalyzed by **8** at 25 °C in benzene.

$(4\text{-}XC_6H_4)_3P$	$k / M^{-1} s^{-1}$	c / M^{-1}
X = Cl	4.17	7.04
X = F	4.17	9.17
X = H	4.17	14.8
X = Me	4.17	67.5
X = OMe	4.17	137.2

Reaction Scheme and Chemical Mechanism. On the basis of the kinetic data and the rate law, a possible reaction mechanism was proposed in Scheme 1.

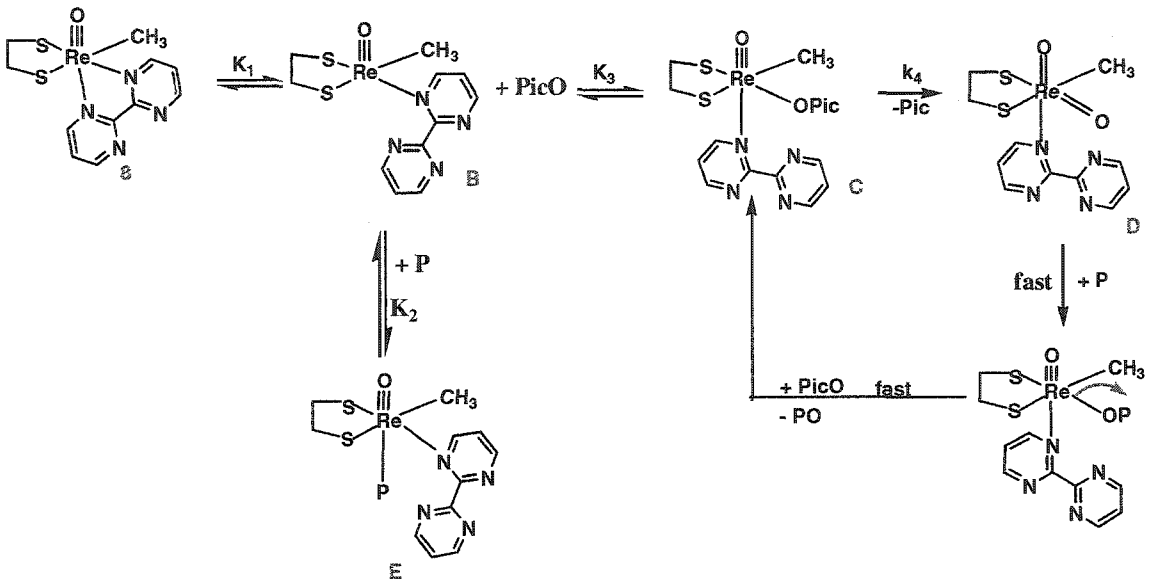

Scheme 1

In this scheme, we believe, in solution, there is an equilibrium between **8** and the half-open-chelate species B. From crystal data, we know that the Re-N bond which trans to oxo group is weaker, it is reasonable to postulate there is a chelate-ring-opening step during the process to start the reaction. Although this step is fairly thermodynamically unfavorable, very small amount of B would exist in solution. After that, the rhenium species offers a vacant axial position for ligands, such as picoline N-oxide or phosphine to attack and produce a six-coordinate rhenium complex. This ring-opening step also accounts for the induction period observed when we mixed picoline oxide and phosphine first and added catalyst last, because those species need time to reach equilibrium. However, when we first mixed picoline oxide with catalyst or added phosphine and catalyst first, we did not observe any induction period in the reaction. We attribute this phenomenon to ligand substitution, which would help to dissociate the sixth ligand and start the reaction. Compared with the five-coordinate

rhenium(V) monodentate phosphine catalyst, compound **8** is less active by 1 or 2 orders of magnitude. In addition, as we recall the previously reported cases, rhenium(V) compounds with strongly-coordinating chelates are completely inactive for OAT reactions, which includes 2,2'-bipyridine coordinated compounds **4** and **6**, and rhenium(V) compound **7** with ligand of 1,2-bis(diphenylphosphino)benzene. Thus we can say it is very important to have an open site for the rhenium center to be a potential catalyst for OAT reactions. For the latter compounds, the chelate effect is so strong and it is difficult to provide a coordination position for the substrate. The difference in Lewis basicity between bipyrimidine and bipyridine is also manifest in the large difference Bronsted basicities.r The value of pK_a of LLH^+ for bipyrimidine is around 0.6, whereas for bipyridine it is about 4.4. [26,27]

Once the half-opening chelate species B is produced in the solution, both of picoline N-oxide and phosphine ligands could coordinate with rhenium center to make sixth-coordinate rhenium compounds. If B adds the picoline N-oxide, the catalytic intermediate C is formed and followed by the rate-controlling step to release picoline and produce a dioxo Re(VII) intermediate D. Finally, D transfers an oxygen atom to phosphine in a much more rapid step that gives phosphine oxide, regenerates catalytic intermediate C, and continues the catalytic cycle. So the reaction shows a first order dependence on picoline N-oxide. But if phosphine coordinates with rhenium, it will make a dead end species E, which accounts for the inverse dependence on phosphine. In addition, with different interactions of picoline oxides or phospines to rhenium species, we also can explain the reason why we got two different rate constants (5.4×10^{-4} s^{-1} *vs.* 4.3×10^{-4} s^{-1}) when we used different adding sequences. We believe this result is due to the relative different concentration of active species in the solution. Adding either picoline oxide or phosphine could push the rhenium

compound **8** to open the chelate and start the catalytic reaction, but they would do so to different degrees. If mixing phosphine and compound **8** first, although it would help produce the active species B in the solution, it will also deactive the catalyst by coordinating phosphine to rhenium center. However this would not happen for adding picoline oxide first. So the rate constant we got when phosphine and **8** reacted first is smaller than that when we added picoline oxide and **8** first. Comparing with the mechanism for same reaction but with another catalyst, $MeReO(mtp)PPh_3$,[14] the reaction is second order dependence on picoline N-oxide, because in that system the catalytic intermediate needs a second PicO as nucleophilic assistance. But in our case, the chelate ligand bipyrimidine itself plays the role of a nucleophile because it has free N atom, which is illustrated in the following scheme.[14,28]

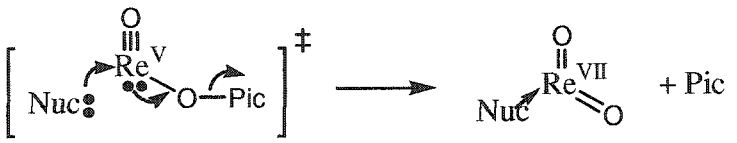

Scheme 2. Nucleophilic assistance

On the basis of this scheme, a rate expression is derived by using equilibrium constants. It is given by eq 7.

$$v = \frac{K_1K_3k_4[PicO][Re]_T}{1+K_1+K_1K_3[PicO]+K_1K_2[P]} \quad (7)$$

As we mentioned before, the ring-opening step for **8** is thermodynamically unfavorable, it is reasonable to assume that K_1 is much less than 1. In addition, larger excess of phosphines over 4-picoline N-oxides were used for all experiments examined, combining with $K_2 >> K_3$, which is due to the stronger coordination ability of triarylphosphine than picoline oxide, so $K_1K_3[PicO]$ should be much smaller than $K_1K_2[P]$ and it can be dropped from the

denominator in the rate law. Under these assumptions, the rate law is simplified to eq 8, which is exactly the form that we obtained from the kinetic data.

$$v = \frac{K_1K_3k_4[PicO][Re]_T}{1+K_1K_2[P]} = \frac{k[PicO][\mathbf{8}]}{1+c[P]} \quad (8)$$

and with excess phosphine,

$$k_{obs} = \frac{K_1K_3k_4[\mathbf{8}]}{1+K_1K_2[P]} \quad (9)$$

where $k = K_1K_3k_4$ and $c = K_1K_2$.

Reactivity Trends and Hammett Analysis. The phosphine substrate inhibits the oxygen transfer reaction between picoline N-oxide and phosphine catalyzed by **8**. This phenomenon can be explained by the equilibrium step K_2 in the scheme where phosphine takes up the sixth position to make six-coordinate rhenium species E and thus make a dead end of the catalytic cycle. From Table 3 and 4, we found that the rate increases with electron-withdrawing group on the para position of the phenyl rings in triarylphosphine. The reason is that triarylphosphine, which has electron-donating group on the para position, has better coordination ability. It coordinates to Re center and slows down the reaction. According to the rate law, we know c in eq 8 represents the combination of the equilibrium constants K_1K_2, which refers the interaction between phosphine and rhenium compound **8**. To illustrate this effect, a plot of $\log(K_1K_2)$ for eq 8 vs. the Hammett substituent constant 3σ is shown in Figure 10, yielding $\rho = -0.93$. The negative ρ value suggests the phosphine coordination ability: the strongest Lewis base gives the greatest equilibrium constant to coordinate with Re species.

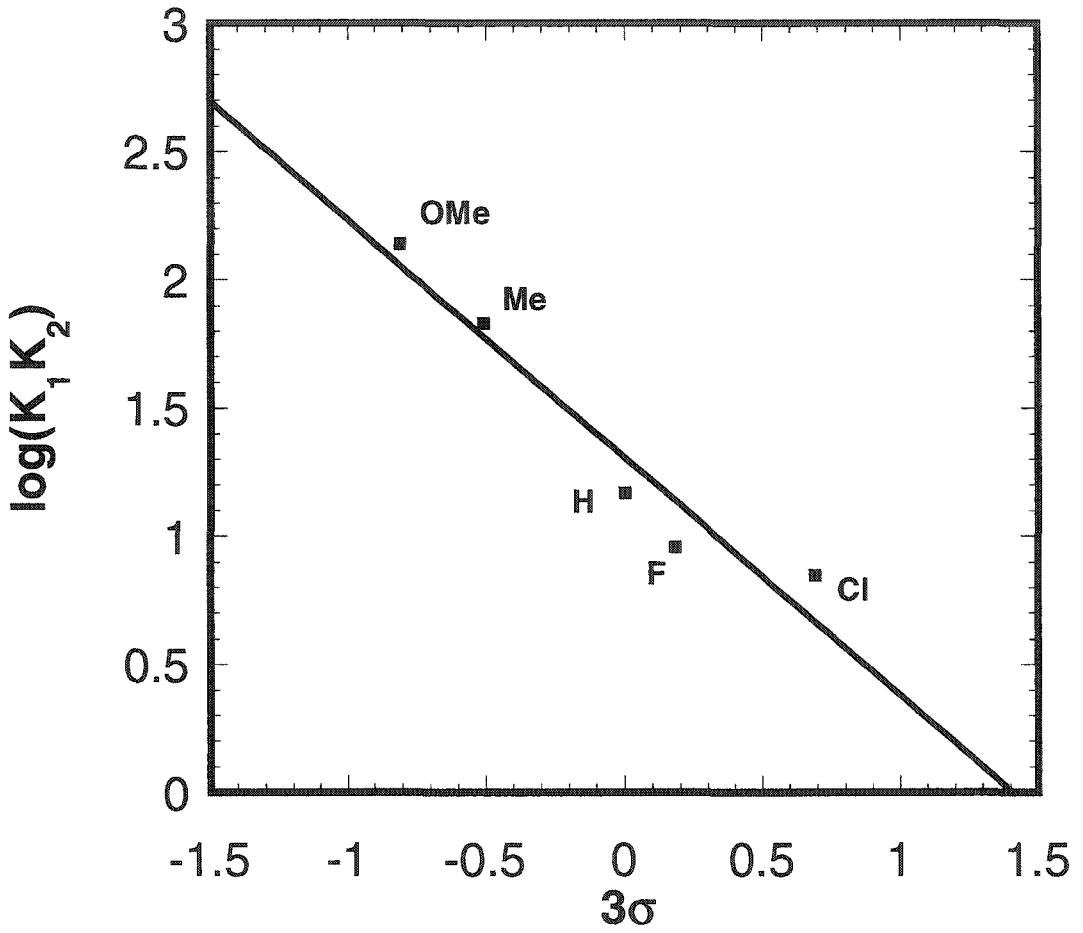

Figure 10. The analysis of the substituent effects in terms of $\log K_1K_2$ *vs.* the Hammett substituent constant 3σ for the given group X in $(4\text{-}XC_6H_4)_3P$.

References

(1) Martiny, L.; Jorgensen, K. A. *J. Chem. Soc., Perkin Trans. 1* **1995**, 699-704.

(2) Deubel, D. V.; Sundermeyer, J.; Frenking, G. *Eur. J. Inorg. Chem.* **2001**, 1819-1827.

(3) Holm, R. H. *Chem. Rev. (Washington, D. C.)* **1987**, *87*, 1401-1449.

(4) Lorber, C.; Donahue, J. P.; Goddard, C. A.; Nordlander, E.; Holm, R. H. *J. Am. Chem. Soc.* **1998**, *120*, 8102-8112.

(5) Donahue, J. P.; Lorber, C.; Nordlander, E.; Holm, R. H. *J. Am. Chem. Soc.* **1998**, *120*, 3259-3260.

(6) Donahue, J. P.; Goldsmith, C. R.; Nadiminti, U.; Holm, R. H. *J. Am. Chem. Soc.* **1998**, *120*, 12869-12881.

(7) Baird, D. M.; Aburri, C.; Barron, L. S.; Rodriguez, S. A. *Inorg. Chim. Acta.* **1995**, *237*, 117-122.

(8) Over, D. E.; Critchlow, S. C.; Mayer, J. M. *Inorg. Chem.* **1992**, *31*, 4643-4648.

(9) Hall, K. A.; Mayer, J. M. *J. Am. Chem. Soc.* **1992**, *114*, 10402-10411.

(10) Shi, Y. L.; Gao, Y. C.; Shi, Q. Z.; Kershner, D. L.; Basolo, F. *Organometallics* **1987**, *6*, 1528-1531.

(11) Harlan, E. W.; Berg, J. M.; Holm, R. H. *J. Am. Chem. Soc.* **1986**, *108*, 6992-7000.

(12) Lente, G.; Espenson, J. H. *Inorg. Chem.* **2000**, *39*, 4809-4814.

(13) Wang, Y.; Espenson, J. H. *Org. Lett.* **2000**, *2*, 3525-3526.

(14) Wang, Y.; Espenson, J. H. *Inorg. Chem.* **2002**, *41*, 2266-2274.

(15) Espenson, J. H.; Shan, X.; Lahti, D. W.; Rockey, T. M.; Saha, B.; Ellern, A. *Inorg. Chem.* **2001**, *40*, 6717-6724.

(16) Herrmann, W. A.; Kratzer, R. M.; Fischer, R. W. *Angew. Chem., Int. Ed. Engl.* **1997**, *36*, 2652-2654.

(17) Espenson, J. H.; Shan, X.; Wang, Y.; Huang, R.; Lahti, D. W.; Dixon, J.; Lente, G.; Ellern, A.; Guzei, I. A. *Inorg. Chem.* **2002**, *41*, 2583-2591.

(18) Blessing, R. H. *Acta Cryst* **1995**, *A51*, 33-38.

(19) All software and sources of the scattering factors are contained in the SHELXTL (version 5.1) program library (G. Sheldrick, B. A. X.-R. S., Madison, WI).

(20) Banerjee, S.; Bhattacharyya, S.; Dirghangi, B. K.; Menon, M.; Chakravorty, A. *Inorg. Chem.* **2000**, *39*, 6.

(21) Edwards, C. F.; Griffith, W. P.; White, A. J. P.; Williams, D. J. *J. Chem. Soc., Dalton Trans.* **1992**, 957.

(22) Mayer, J. M. *Inorg. Chem.* **1988**, *27*, 3899.

(23) Berning, D. E.; Katti, K. V.; Barbour, L. J.; Volkert, W. A. *Inorg. Chem.* **1998**, *37*, 334.

(24) Smith, C. J.; Katti, K. V.; Volkert, W. A.; Barbour, L. J. *Inorg. Chem.* **1997**, *36*, 3928.

(25) Wang, Y. P.; Che, C. M.; Wang, K. Y.; Peng, S. M. *Inorg. Chem.* **1993**, *32*, 5827.

(26) Martell, A. E.; Smith, R. M. *Critical Stability Constants, Vol. 3: Other Organic Ligands*, 1974.

(27) Bly, D. D.; Mellon, M. G. *Anal. Chem.* **1963**, *35*, 1386-1392.

(28) Vasbinder, M. J.; H.;, E. J. *Organometallics* **2004**, *23*, 3355.

CHAPTER III. KINETICS OF SELF-DECOMPOSITION AND HYDROGEN ATOM TRANSFER REACTIONS OF SUBSTITUTED PHTHALIMIDE N-OXYL RADICALS IN ACETIC ACID

A manuscript accepted by the *Journal of Organic Chemistry*

Yang Cai, Nobuyoshi Koshino, Basudeb Saha, and James H. Espenson

Introduction

N-Hydroxyphthalimide (NHPI, X = Y = H in Chart 1) has gained considerable attention in several fields such as organic and catalytic chemistry. [1-4] Since fascinating catalysis of NHPI with Co(II) has been found by Ishii,[1] a number of studies of its reactivity and applications have been reported.[2-4] It is proposed that NHPI is oxidized to phthalimide *N*-oxyl radical (PINO•), which is a key species in the catalytic cycles.[2] We have previously studied the kinetics for hydrogen abstraction reactions by PINO• from methyl arenes and other organic substrates.[5,6]

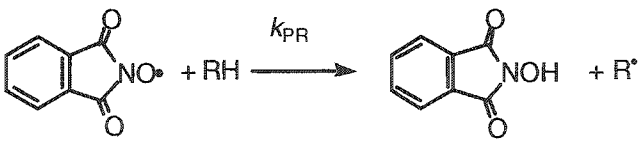

PINO• NHPI (1)

These reactions are characterized by large kinetic isotope effects, and we proposed that quantum tunneling plays an important role there. This is not without further qualification, however, as will be taken up at the end of the Discussion.

In this study, we present new kinetic data using ring-substituted NHPI derivatives (Chart 1), and discuss self-decomposition reactions, hydrogen atom self-exchange reactions, and hydrogen abstraction reactions from *para*-xylene and toluene.

Chart 1

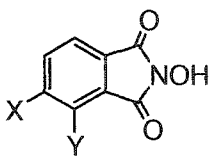

	X	Y
4-Me-NHPI	Me	H
4-Cl-NHPI	Cl	H
4-F-NHPI	F	H
3-F-NHPI	H	F

Experimental Section

Materials. *N*-hydroxyphthalimide (NHPI) was purchased from Aldrich and used as received. 3-Fluoro and 4-methyl substituted NHPI derivatives were synthesized as previously reported.[7] 4-Fluoro-NHPI, whose synthesis had not been reported, was prepared from 4-fluorophthalic anhydride and hydroxylamine hydrochloride by the same method,[7] and obtained in 25% yield. It was characterized by ^{1}H NMR spectroscopy in DMSO-d_6: δ 7.62-7.67 (m, 1H), 7.74-7.76 (m,1H), 7.89-7.92 (m, 1H), 10.89 (s, 1H). Glacial acetic acid (Fischer) and acetic acid-d_4 (99.5% D, CIL) were used as received. Each PINO radical was generated by the oxidation of its NHPI with Co(III) acetate or lead tetraacetate. Cobalt(III) solutions were prepared by passing ozone through a solution of $Co(OAc)_2$ in acetic acid.[8] The Co(III) solutions were then bubbled with a vigorous stream of argon to remove excess ozone. Lead tetraacetate (Aldrich) was also used to produce the PINO radicals for hydrogen abstraction reactions with *para*-xylene and toluene.[9] To study kinetic isotope effects for hydrogen abstraction reactions, *para*-xylene-d_{10} (99+% D, Aldrich) and toluene-d_8 (99+% D,

Aldrich) were used as received. Other chemical reagents were obtained commercially, and used without purification.

General. The UV/Vis spectra of the PINO radicals were recorded by a Shimadzu UV-3101 spectrophotometer. The kinetics of self-decomposition of the PINO radicals was monitored by using a UV/Vis spectrophotometer equipped with a temperature-controlled cell holder. The rate constants for reactions between X-PINO• and Y-NHPI were measured in glacial acetic acid and acetic acid-d_4 by a stopped-flow spectrophotometer (OLIS RSM 1000) with a temperature-controlled water circulation bath. The rate constants for reactions of the PINO radicals with *para*-xylene and toluene were measured spectrophotometrically in HOAc at 25.0 ± 0.1 °C under an argon atmosphere.

Results and Discussion

Molar Absorptivities of the Substituted PINO Radicals. The substituted PINO radicals were generated by the oxidation of the parent NHPI compounds with Co(III) in HOAc. Although the PINO radicals decompose slowly, they persist long enough for accurate UV/Vis spectra to be recorded (Figure S1). Table 1 shows the wavelengths of the absorption maxima and the molar absorptivities of the PINO radicals, which differ relatively little from one another. It seems that there is no obvious correlation between substitutents on NHPI and maximum absorption wavelengths or molar absorptivities.

Self-Decomposition of the Substituted PINO Radicals. We previously studied self-decomposition reaction of the unsubstituted PINO radical and found that the reaction obeys second-order kinetics in glacial acetic acid.[5] The products of this reaction have been identified as some oligomers (primarily a trimer) formed by subsequent reactions of the initial disproportionation.[10]

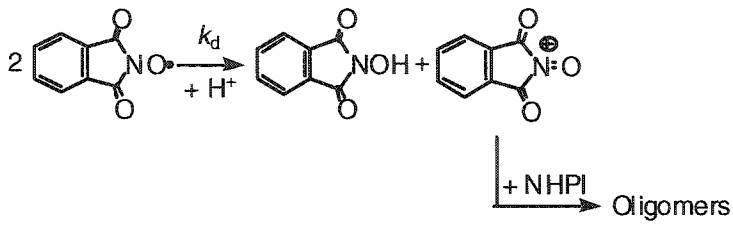

(2)

The second-order rate constant, k_d, was obtained by using eq 3, where Y represents absorbance, [X-PINO•]$_0$ the initial concentration of the X-PINO radical, and [X-PINO]$_0$ is expressed by $(Y_0 - Y_\infty)/\varepsilon$. [5,11] The decomposition rate constants (k_d) are summarized in Table 2.

$$Y_t = Y_\infty + \frac{(Y_0 - Y_\infty)}{1 + [\text{X-PINO}]_0 k_d t} = Y_\infty + \frac{(Y_0 - Y_\infty)}{1 + (Y_0 - Y_\infty) k_d t / \varepsilon} \tag{3}$$

We have previously reported that the reactivity of substituted NHPI compounds in the autoxidation of *p*-xylene follows the order of 4-Me-NHPI < 3-F-NHPI < NHPI,[12] and proposed that the reactivity order could be explained by the kinetic stability of the corresponding radical species. As shown in Table 2, the unsubstituted PINO• (4-H-PINO•) is much more stable than 4-Me-PINO•. The comparison of the stability of 3-F-PINO• with those of 4-substituted PINO radicals cannot be straightforward because of the temperature differences. However, the self-decomposition of 4-Me-PINO• would be faster than 1.7 s^{-1} in practical conditions because hydrogen abstraction from methyl group also takes place (see

below). Therefore, the stability of the three PINO radicals would be in the order of 4-Me-PINO• < 3-F-PINO• < NHPI, which is consistent with the reactivity of the NHPIs in the catalytic cycle.

The self-decomposition reactions of nitroxyl radicals are usually observed to follow second-order kinetics.[13,14] However, Amorati et al. reported that the self-decomposition of PINO• obeyed first-order kinetics in benzene containing 10% CH_3CN,[3] which is inconsistent with our data in HOAc and those of Masui in CH_3CN.[10] According to their experimental data, the decomposition of the PINO radical in benzene obeys the first-order kinetics, and they proposed a fragmentation at one of the carbonyl carbon-nitrogen bonds.[3,15]

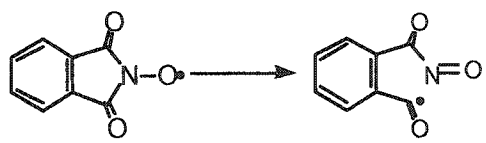

PINO• (4)

We generated the PINO radical in benzene containing 10% CH_3CN by the oxidation of NHPI with AgO (Aldrich), and monitored the self-decomposition. The result is shown in Figures S2(a) and 2(b). It seems that the decomposition of the PINO radical is more likely to follow second-order kinetics. We have not obtained the accurate molar absorptivity of PINO• in benzene, however, if we suppose ε_{382} in benzene/CH_3CN is equal to ε_{382} in HOAc, k_d in benzene/CH_3CN is calculated as 31 L mol^{-1} s^{-1}, which is fairly close to the value of k_d in CH_3CN, 24.1 L mol^{-1} s^{-1}.[10] Even if we hypothesize that the reaction follows the first-order kinetics, the pseudo-first-order rate constant is given as 1.2×10^{-3} s^{-1}. This rate constant is much smaller than that reported (0.1 s^{-1}).[3] The discrepancy may arise from the procedures to generate the PINO radical.[3,5] Amorati et al. used dicumyl peroxide to generate the PINO radical.

$$\{PhC(CH_3)_2O\}_2 \xrightarrow{h\nu} 2PhC(CH_3)_2O\bullet \quad (5)$$

The PINO radical is then generated in the following step,

$$PhC(CH_3)_2O\bullet + NHPI \rightarrow PhC(CH_3)_2OH + PINO\bullet \quad (6)$$

However, the cumyloxyl radical might produce other species such as acetophenone by β-scission,[16]

$$PhC(CH_3)_2O\bullet \rightarrow PhCOCH_3 + CH_3\bullet \quad (7)$$

It is well known that acetophenone is also photoactive.[17,18] Therefore, we assume that during the irradiation in their experiments, the resulting acetophenone could produce some by-products with which PINO• may react.

Table 1. Maximum Absorption Wavelengths and Molar Absorptivities of Substituted PINO Radicals [a]

X-PINO•	λ_{max} / nm	ε_{max} / 10^3 L mol^{-1} cm^{-1}
4-Cl	394	1.38
4-F	382	1.21
4-H	382 [b]	1.36 [b]
4-Me	397 [c]	1.39 [d]
3-F	367 [c]	1.32 [d]

[a] In HOAc at 25 °C; [b] Ref 5; [c] Ref [12]. [d] Re-examined more accurately.

Table 2. Rate Constants for Self-decomposition of Substituted PINO Radicals in HOAc at 25 °C

X-PINO•	k_d / L mol^{-1} s^{-1}
4-Cl	0.4
4-F	0.7
4-H	0.6 [a]
4-Me	1.7 [b]
3-F	0.8 [c]

[a] Ref 5; [b] Net self-decomposition (see text); [c] At 15 °C, Ref. [19]

Self-Decomposition of 4-Me-PINO Radical. An exception to the general pattern of second-order kinetics was found for 4-Me-PINO•, which follows second-order kinetics only at lower concentrations of 4-Me-NHPI (< 0.83 mmol L^{-1}). Deviations from second-order kinetics were noted at higher concentrations of 4-Me-NHPI. As the concentration of 4-Me-NHPI increased, the absorbance-time data approached first-order kinetics, but both first- and second-order terms were needed for precise fitting. Considering the fairly high H-atom abstraction ability of PINO radicals, we concluded that the 4-Me-PINO radical decomposes in two parallel reactions: one is the self-decomposition as expressed by eq 2, and the other is hydrogen abstraction of 4-Me-PINO• from the methyl group on 4-Me-NHPI, eq 8.

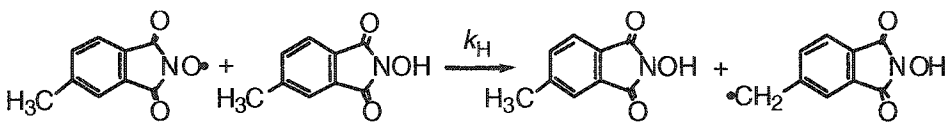

(8)

In that case, the differential rate law and its integrated form are[11]

$$-\frac{d[\text{4-Me-PINO}]}{dt} = k_d[\text{4-Me-PINO•}]^2 + k_H[\text{4-Me-NHPI}][\text{4-MePINO•}] \tag{9}$$

$$Y_t = Y_\infty + \frac{k_{H(obs)}(Y_0 - Y_\infty)_0[\text{4-Me-PINO•}]e^{-k_{H(obs)}t}}{k_{H(obs)} + k_d \cdot [\text{4-Me-PINO•}]_0(1 - e^{-k_{H(obs)}t})} \tag{10}$$

where k_H is the rate constant for reaction 8 and $k_{H(obs)}$ is the related pseudo-first-order rate constant in the presence of excess 4-Me-NHPI ($k_{H(obs)} = k_H$[4-Me-NHPI]). The value of [4-Me-PINO]$_0$ is calculated from the absorbance at 397 nm and its molar absorptivity. We determined the rate constant for the self-decomposition (eq 2) of 4-Me-PINO• using

experimental data at the lowest 4-Me-NHPI concentrations. Figure S3(a) shows the resulting fitting, which gave k_d = 1.7 L mol^{-1} s^{-1}. On the other hand, at higher concentrations of 4-Me-NHPI (> 2 mmol L^{-1}), eq 11 was used to obtain $k_{H(obs)}$ by fixing k_d (1.7 L mol^{-1} s^{-1}). The values of $k_{H(obs)}$ so obtained were plotted against [4-Me-NHPI]$_0$ as illustrated in Figure 1. This procedure gave k_H = 0.080 L mol^{-1} s^{-1} at 25.0 °C as the rate constant of H-atom abstraction from 4-methyl group (reaction 8). We previously reported the rate constants of H-atom abstraction by PINO• from toluic acids as k_{PR}= 0.20 (*meta*-toluic acid) and 0.28 (*para*-toluic acid) L mol^{-1} s^{-1} under an argon atmosphere.[5] The difference of the rate constants between k_H and k_{PR} of the two toluic acids can be attributed to two factors. Firstly, 4-Me-NHPI has two carbonyl groups on the benzene ring which withdraw more electron density, making hydrogen abstraction from methyl group more difficult. Secondly, the BDE of the O-H group of 4-Me-NHPI is smaller than that of unsubstituted NHPI, which is reflected in the equilibrium constant of reaction 11 (see below). Therefore, it is reasonable that the rate constant of H-atom abstraction from 4-methyl group on 4-Me-NHPI by 4-Me-PINO (k_H) is smaller than those from methyl group on *meta*- or *para*-toluic acids by the unsubstituted PINO•.

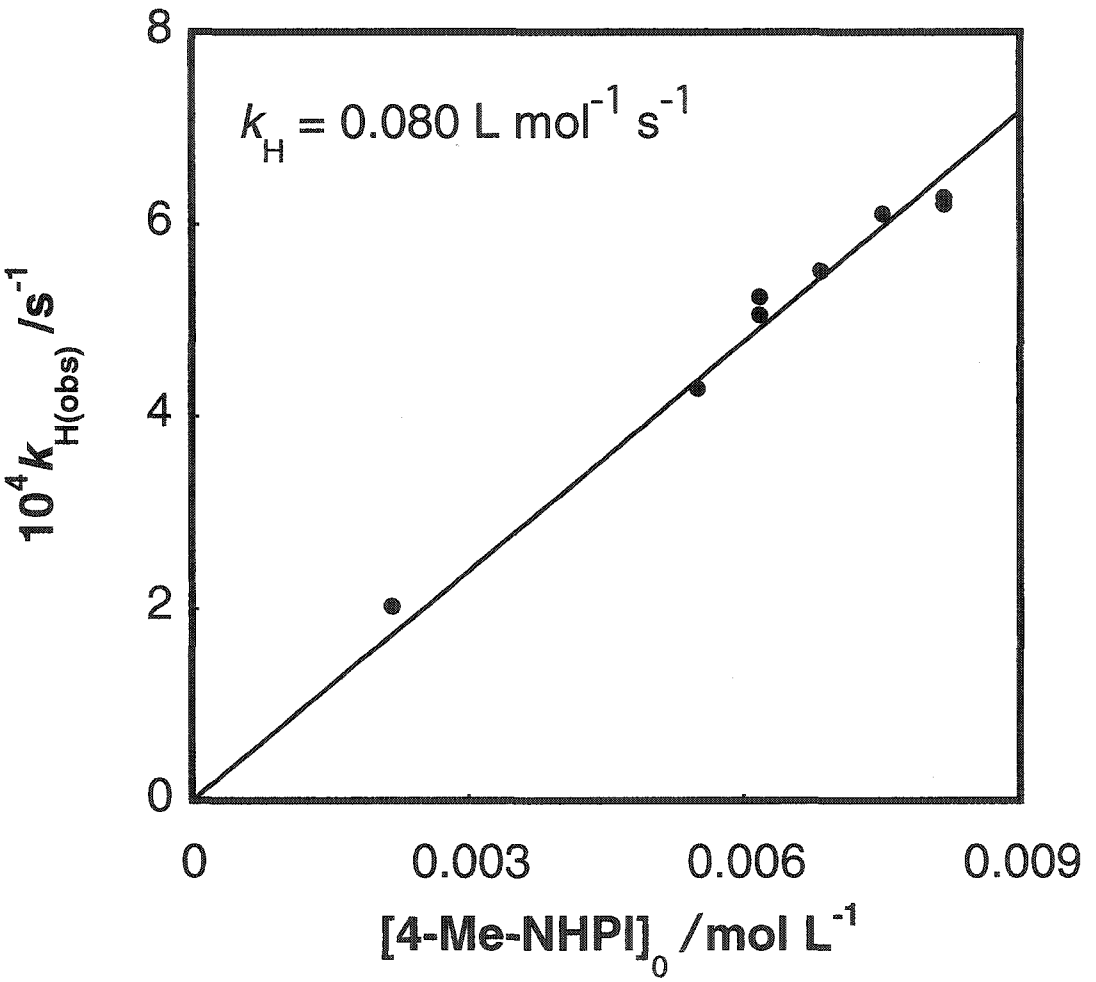

Figure 1. Plot of $k_{H(obs)}$ against [4-Me-NHPI]$_0$. $k_{H(obs)}$ was obtained from eq 10 with k_d fixed (1.7 L mol^{-1} s^{-1}) in HOAc at 25.0 °C.

Hydrogen Atom Transfer Reaction. The combination of NHPI with $Co(OAc)_2$ is known to provide an excellent catalyst for autoxidation of hydrocarbons.[2] This feature is interpreted by the high H-atom abstraction ability of the PINO radical, and we found that quantum mechanical tunneling plays a role in the hydrogen abstraction.[5] We also proposed that the kinetic isotope effect would be maximum when the reaction is thermoneutral.[6] On the basis of this interpretation, we were interested in a pseudo self-exchange reaction between PINO• and substituted NHPI as shown in eq 11.

$$\text{PINO•} + \text{4-Me-NHPI} \underset{k_r}{\overset{k_f}{\rightleftharpoons}} \text{NHPI} + \text{4-Me-PINO•} \qquad (11)$$

Reaction 11 is nearly thermoneutral considering the difference in bond dissociation energies.[20] Although reaction 11 represents hydrogen atom transfer in a stoichiometric sense, there are two possible mechanisms for it: one is hydrogen atom transfer itself (or proton coupled electron transfer), and the other is stepwise transfer of an electron and a proton.[21] We measured rate constants for the reaction 11 with excess 4-Me-NHPI and NHPI in HOAc at 25 °C. Reaction 11 takes place quite rapidly, therefore hydrogen abstraction from the 4-Me group observed in self-decomposition of 4-Me-PINO• is negligible. The reaction was safely monitored by the growth of the absorbance at 397 nm, which is λ_{max} for 4-Me-PINO•. The rate constant for the reaction 11 is given by eq 12 in the presence of excess 4-Me-NHPI and NHPI.

$$k_{obs} = k_f[\text{4-Me-NHPI}] + k_r[\text{NHPI}] \qquad (12)$$

This equation can be rearranged to the following form,

$$\frac{k_{obs}}{[NHPI]} = \frac{k_f[4\text{-Me-PINO}\bullet]}{[NHPI]} + k_r \quad (13)$$

From a series of experiments with varied concentrations (Figure 2), each rate constant was obtained at 25.0 °C: $k_f = 677 \pm 24$ L mol^{-1} s^{-1} and $k_r = 354 \pm 23$ L mol^{-1} s^{-1}, which means that the equilibrium constant, K_{eq} (= k_f/ k_r), for reaction 11 is 1.91 ± 0.10 at 25 °C. Therefore, it is calculated by using equation 14 that the O-H bond dissociation energy of 4-Me-NHPI is 1.6 kJ mol^{-1} lower than that of NHPI.[20]

$$\text{BDE (X-NHPI)} = \text{BDE(NHPI)} - RT \ln K_{eq} \quad (14)$$

We also measured rate constants for the following pseudo-self-exchange reaction.

$$\text{4-F-PINO}\bullet + \text{NHPI} \underset{k_r}{\overset{k_f}{\rightleftharpoons}} \text{4-F-NHPI} + \text{PINO}\bullet \quad (15)$$

The rate constants k_f and k_r, for reaction 15 are 651 L mol^{-1} s^{-1} and 241 L mol^{-1} s^{-1} in HOAc at 25.0 °C, which means the equilibrium constant of the reaction 15 is 2.70. Therefore, the O-H bond dissociation energy of 4-F-PINO• is calculated to be 2.46 kJ mol^{-1} higher than that of NHPI. Thus it is confirmed that electron withdrawing groups on NHPI strengthen the O-H bond and electron donating groups weaken it.

For the reaction 11, rate constants were also measured in acetic acid-d_4 to evaluate the KIE, noting the rapid exchange of protons (deuterons) between R_2NOH and acetic acid-d_4. The rate constants of the reaction 11 in acetic acid-d_4 are $k_f = 61.3 \pm 2.1$ L mol^{-1} s^{-1} and k_r = 31.8 ± 2.0 L mol^{-1} s^{-1}. Therefore, the values of KIE for k_f and k_r are 11.0 and 11.1, respectively This indicates that the reaction 11 takes place through H-atom transfer, not

electron transfer (Scheme 1). This conclusion is also supported by the finding that the rate constants for reaction 11 are not affected by addition of CF_3COOH (Table S1).[22]

Scheme 1. Reaction scheme for pseudo-sef-exchange reaction of PINO• and 4-Me-NHPI

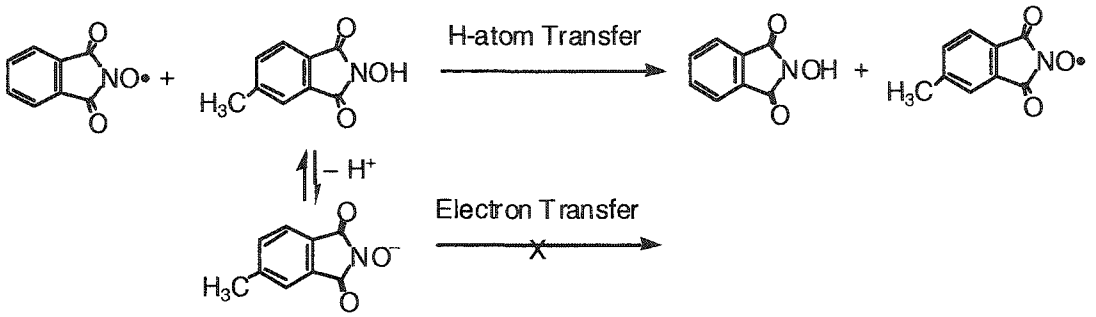

As described above, the reaction 11 takes place through direct H-atom transfer, and the KIEs (11.0 and 11.1) of the rate constants in both directions are larger than the theoretical maximum value from ground-state energy differences (7.8).[11] In previous reports, quantum mechanical tunneling has been proposed to play an important role in PINO radical reactions,[5] such as those with *para*-xylene and toluene, for which remarkably small pre-exponential factors were found, log $A \approx 5$-6. This also implies that tunneling participates in the reactions. Therefore, we predicted that the reaction 11 also has a small pre-exponential factor (in other words, a large negative activation entropy). The rate constant for the reaction 11 were measured at various temperatures, and were in turn analyzed by using the following equation with Scientist 2.0.[23]

$$k_{obs} = \frac{k_B T}{h} \exp\left(\frac{\Delta S^{\ddagger}_{f,r}}{R}\right) \exp\left(-\frac{\Delta H^{\ddagger}_{f}}{RT}\right) [\text{4-Me-NHPI}] + \frac{k_B T}{h} \exp\left(\frac{\Delta S^{\ddagger}_{f,r}}{R}\right) \exp\left(-\frac{\Delta H^{\ddagger}_{r}}{RT}\right) [\text{NHPI}] \quad (16)$$

In this treatment, we set the activation entropies for k_f and k_r equal to one another because each direction should have almost the same activation entropy considering its structural symmetry. As a result, the obtained activation parameters are $\Delta H^{\ddagger}_{f} = 40.8 \pm 1.0$ kJ mol^{-1}, $\Delta H^{\ddagger}_{r} = 41.9 \pm 1.0$ kJ mol^{-1}, $\Delta S^{\ddagger}_{f,r} = -55 \pm 3$ J K^{-1} mol^{-1}; an Arrhenius plot of the same data gave log A = 9.5. This value of log A along with the KIE indicates that tunneling occurs but not to the extent it does in certain other reactions of PINO•.[5,6] Using the obtained activation enthalpies and activation entropy, we compared the experimental data with the calculated values. The result is illustrated in Figure 3, in which the points are experimental data and each line comes from the calculated values.

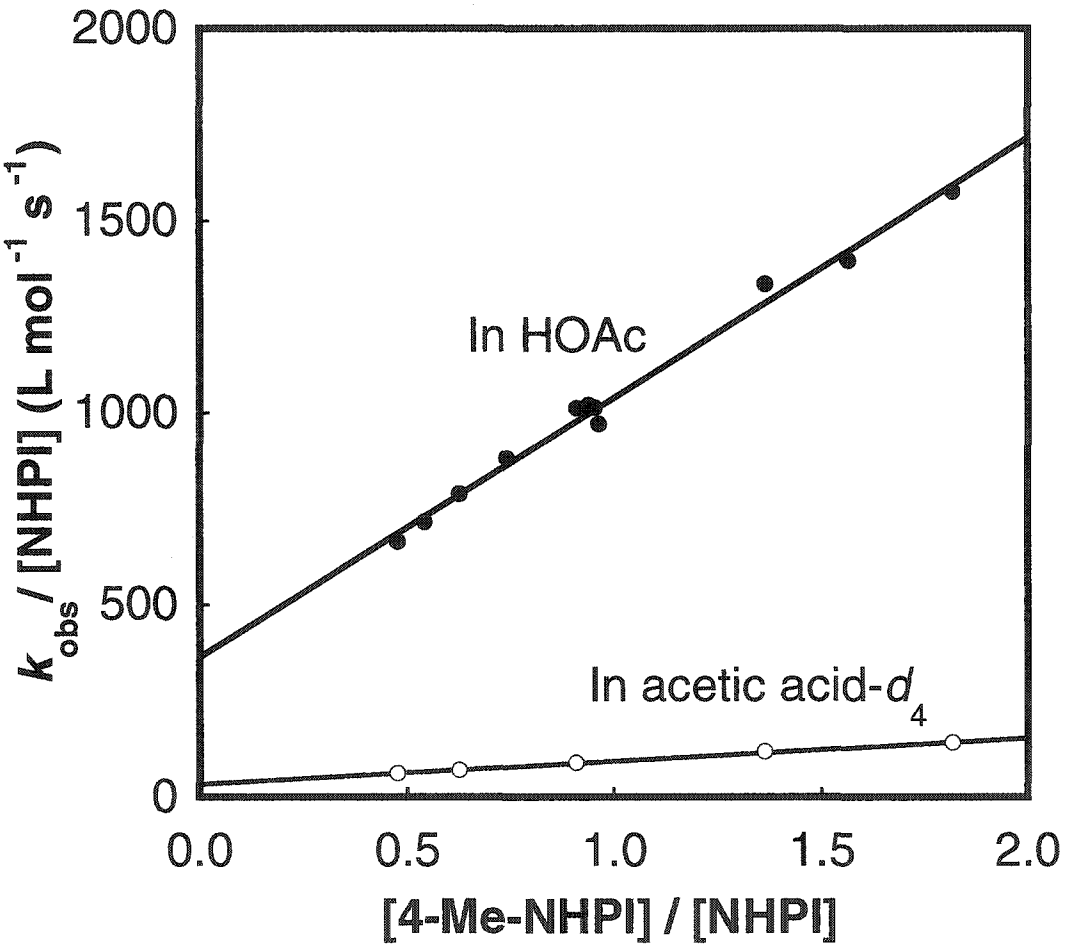

Figure 2. Plot of the kinetic data according to eq 13 to evaluate k_f and k_r of the reaction 11.

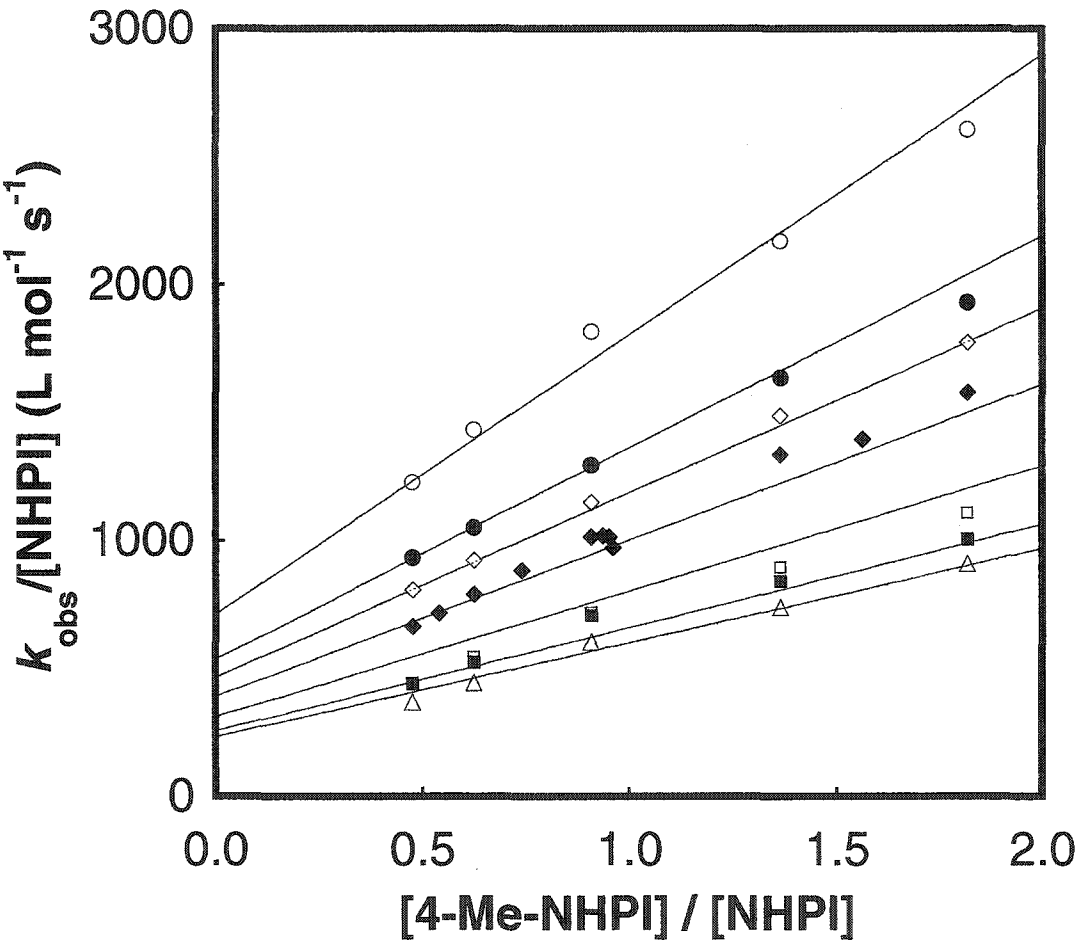

Figure 3. Comparison of experimental data with the calculated values (solid lines) according to eq 16 for H-atom transfer of the reaction 12 in HOAc at various temperatures. 308.45 K (○); 303.45 K (●); 301.05 K (◇); 298.15 K (◆); 294.45 K (□); 291.25 K (■); 289.75 K (△).

Application of the Marcus Cross Relation to Hydrogen Atom Transfer Reaction between PINO• and NHPI. This study has shown that reaction 12 takes place through H-atom transfer with rate constants, k_f = 677 L mol^{-1} s^{-1} and k_r = 354 L mol^{-1} s^{-1}. Therefore, it is estimated that the rate constant of self-exchange reaction between PINO• and NHPI is ca. 500 L mol^{-1} s^{-1}.

$$\text{PINO•} + \text{*NHPI} \xrightarrow{k_{ex}\ (=k_{AA})} \text{NHPI} + \text{*PINO•} \qquad (17)$$

A second approach to estimating k_{AA} is based on applying the Marcus cross relation to H-atom transfer reactions, as has been established.[21,24] There is enough uncertainty in BDE (NHPI)(365-375 kJ mol-1) as to make this approach unreliable.[21,24]

Hydrogen Abstraction by PINO Radicals from *para*-Xylene. As described previously, the O-H bonds of substituted NHPI derivatives are strengthened by electron withdrawing groups. Therefore, the H-atom abstraction ability of PINO• substituted by electron withdrawing groups would be higher than those of PINO• substituted by electron donating groups. To confirm this issue, we measured rate constants for H-atom abstraction by substituted PINO radicals from *para*-xylene and toluene. The obtained rate constants are shown in Table 3 and Table S2.

Table 3. Rate Constants and Kinetic Isotope Effect for the Reaction of PINO Radicals with *para*-Xylene in HOAc at 25 °C

4-X-PINO•	*p*ara-Xylene		
X =	k_H / s^{-1}	k_D / s^{-1}	k_H/k_D
Cl	10.6 ± 0.07	0.426 ± 0.002	24.9
F	8.40 ± 0.18	0.338 ± 0.002	24.9
H [a]	5.95 ± 0.07	0.240 ± 0.001	24.8
CH_3	3.90 ± 0.04	0.166 ± 0.002	23.5

[a] Ref. 5

In the both reactions, the reactivity of substituted PINO• follows the order 4-Me < 4-H < 4-F < 4-Cl, which corresponds to the order of the O-H bond dissociation energies. Alternatively, the acceleration of the rate constants by electron withdrawing groups might be explained by the polar effect at the transition state.

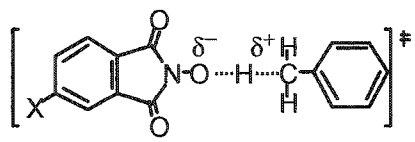

A correlation between redox potentials of the 4-substituted NHPI derivatives and σ_p Hammett constants has been reported.[25] We constructed plots against σ_p, and obtained the reaction constants, $\rho = 1.1$ for *para*-xylene and 1.8 for toluene, Figures S4(a) and S4(b).

We also evaluated the KIE for the reactions with *para*-xylene and toluene. It is noted that the values of KIE for the reaction in the series of the PINO radicals lie in the narrow range of 23.5-25.7. This finding further supports that quantum mechanical tunneling plays a role in the hydrogen abstraction of the PINO radicals. We have reported that H-atom abstraction reaction by PINO• has a maximum with toluene (27.1) or benzaldehyde (27.5).[6] It is expected that a maximum value for H-atom abstraction reaction can be obtained when the reaction is symmetric.[26,27] Therefore, we expected that the maximum of KIE would shift in the reaction of 4-substituted NHPI derivatives which have different O-H BDEs. However, the difference of BDE of NHPI derivatives is not large enough to see the shift. Recently, Annunziatini et al. investigated that aerobic oxidation of benzyl alcohol by substituted NHPIs, and found that 3,6-$(CH_3O)_2$-NHPI has the largest KIE (19.5).[20] The O-H BDE of 3,6-$(CH_3O)_2$-NHPI is 1 kcal mol^{-1} smaller than that of NHPI because of the two electron donating methoxy groups. And it is well known that the C-H BDE of benzyl alcohol is fairly

low (340 kJ mol^{-1}). Therefore, it is understandable that the largest KIE was obtained with 3,6-$(CH_3O)_2$-NHPI which has the lowest O-H BDE in the series of Annunziatini's experiments, where the reaction with 3,6-$(CH_3O)_2$-NHPI is more symmetric than others with substituted NHPIs.

Further comments on tunneling are in order. In an earlier publication the large KIE values were attributed to tunneling as the major or exclusive factor.[5,6] Actually, there is now cause to reassess that view. After allowance for a secondary KIE of 1.15 per D atom in going from sp^3 to sp^2 hybridization,[28,29] the primary KIE is reduced to 19.2 at 25 °C and only 5.23 at 55 °C, the latter being a normal isotope effect. On that basis the tunneling effect is ca. 27% at 17 °C and 7.2% at 55 °C.

Acknowledgement. This research was supported by a grant from the National Science Foundation under grant CHE-020409. Some experiments were conducted with the use of the facilities of the Ames Laboratory of the U.S. Department of Energy, which is operated by Iowa State University of Science and Technology under contract W-7405-Eng-82.

Supporting Information. UV/Vis spectra of the substituted PINO radical in HOAc, plots of kinetic data to illustrate agreement to selected mathematical forms and to evaluate numerical parameters. This material is available free of charge on the Internet at http://pubs.acs.org.

References and Notes

(1) Ishii, Y.; Iwahama, T.; Sakaguchi, S.; Nakayama, K.; Nishiyama, Y. *J. Org. Chem.* **1996**, 61, 4520-4526.

(2) Ishii, Y.; Sakaguchi, S.; Iwahama, T. *Adv. Synth. Catal.* **2001**, 343, 393-427.

(3) Amorati, R.; Lucarini, M.; Mugnaini, V.; Pedulli, G. F.; Minisci, F.; Recupero, F.; Fontana, F.; Astolfi, P.; Greci, L. *J. Org. Chem.* **2003**, 68, 1747-1754.

(4) Arends, I. W. C. E.; Sasidharan, M.; Kühnle, A.; Duda, M.; Jost, C.; Sheldon, R. A. *Tetrahedron* **2002**, 58, 9055-9061.

(5) Koshino, N.; Saha, B.; Espenson, J. H. *J. Org. Chem.* **2003**, 68, 9364-9370.

(6) Koshino, N.; Cai, Y.; Espenson, J. H. *J. Phys. Chem. A.* **2003**, 107, 4262-4267.

(7) Wentzel, B. B.; Donners, M. P. J.; Alsters, P. L.; Feiters, M. C.; Nolte, R. J. M. *Tetrahedron* **2000**, 56, 7797-7803.

(8) Lande, S. S.; Falk, C. D.; Kochi, J. K. *J. Inorg. Nucl. Chem.* **1971**, 33, 4101-4109.

(9) When Co(III) was used to generate PINO•, we obtained slightly different rate constants of hydrogen abstraction reactions even under an argon atmosphere. Probably, Co(II) takes part in the subsequent reactions.

(10) Saha, B.; Koshino, N.; Espenson, J. H. *J. Phys. Chem. A.* **2004**, 108, 425-431.

(11) Ueda, C.; Noyama, M.; Ohmori, H.; Masui, M. *Chem. Pharm. Bull.* **1987**, 35, 1372-1377.

(12) Espenson, J. H. *Chemical Kinetics and Reaction Mechanisms*; 2nd ed.; McGraw-Hill, Inc: New York, **1995**.

(13) The rate constant was measured at 15 °C, because the formation and decomposition steps of 3-F-PINO• were comparable at 25 °C and thus the kinetic trace could not be separated into its components.

(14) Blackley, W. D.; Reinhard, R. R. *J. Am. Chem. Soc.* **1965**, 87, 802-805.

(15) Bowman, D. F.; Gillan, T.; Ingold, K. U. *J. Am. Chem. Soc.* **1971**, 93, 6555-6561.

(16) Minisci, F.; Recupero, F.; Cecchetto, A.; Gambarotti, C.; Punta, C.; Paganelli, R. *Org. Process Res. Dev.* **2004**, 8, 163-168.

(17) Baciocchi, E.; Bietti, M.; Salamone, M.; Steenken, S. *J. Org. Chem.* **2002**, 67, 2266-2270.

(18) Wagner, P. J.; Truman, R. J.; Puchalski, A. E.; Wake, R. *J. Am. Chem. Soc.* **1986**, 108, 7727-7738.

(19) Wagner, P. J.; Zhang, Y.; Puchalski, A. E. *J. Phys. Chem.* **1993**, 97, 13368-13374.

(20) Annunziatini, C.; Gerini, M. F.; Lanzalunga, O.; Lucarini, M. *J. Org. Chem.* **2004**, 69, 3431-3438.

(21) Roth, J. P.; Lovell, S.; Mayer, J. M. *J. Am. Chem. Soc.* **2000**, 122, 5486-5498.

(22) We assumed that if the reaction 12 takes place through electron transfer via pre-equilibrium of proton dissociation, the rate constants would be affected by addition of strong acid; pK_a = 0.52 (CF3COOH) and 4.76 (CH3COOH).

(23) Micro-Math Scientific Software, Inc., Salt Lake City, Utah

(24) Roth, J. P.; Yoder, J. C.; Won, T.-J.; Mayer, J. M. *Science* **2001**, 294, 2524-2526.

(25) Jackson, R. A.; O'Neill, D. W. J. Chem. Soc., *Chem. Commun.* **1969**, 1210-1211.

(26) Lide, D. R. CRC *Handbook of Chemistry and Physics*; 81st ed.; CRC Press: Boca Raton, **2000.**

(27) This value contains some error which comes from the uncertainty of BDE.

(28) Gorgy, K.; Lepretre, J.-C.; Saint-Aman, E.; Einhorn, C.; Einhorn, J.; Marcadal, C.; Pierre, J.-L. *Electrochim. Acta* **1998**, 44, 385-393.

(29) Bell, R. P. *The Tunnel Effect in Chemistry*; Chapman and Hall: London, **1980**.

(30) Cleland, W. W.; O'Leary, M. H.; Northrop, D. B. *Isotope Effects on Enzyme-Catalyzed Reactions*; University Park Press: Baltimore, **1977**.

(31) We are grateful to Prof. A. A. Zavitsas for calling our attention to these issues.

(32) Zavitsas, A. A.; Seltzer, S. *J. Am. Chem. Soc.* **1964**, 86, 3836-3840; See also: Zavitsas, A. A. *J. Phys. Chem. A* **2002**, 106, 5041-5042; Zavitsas, A. A. *J. Chem. Soc., Perkin Trans. 2* **1998**, 499-502; Zavitsas, A. A. *J. Am. Chem. Soc.* **1998**, 120, 6578-6586; Zavitsas, A. A. *J. Chem. Soc., Perkin Trans. 2* **1996**, 391-393; Zavitsas, A. A.; Chatgilialoglu, C. *J. Am. Chem. Soc.* **1995**, 117, 10645-10654.

Supporting Information

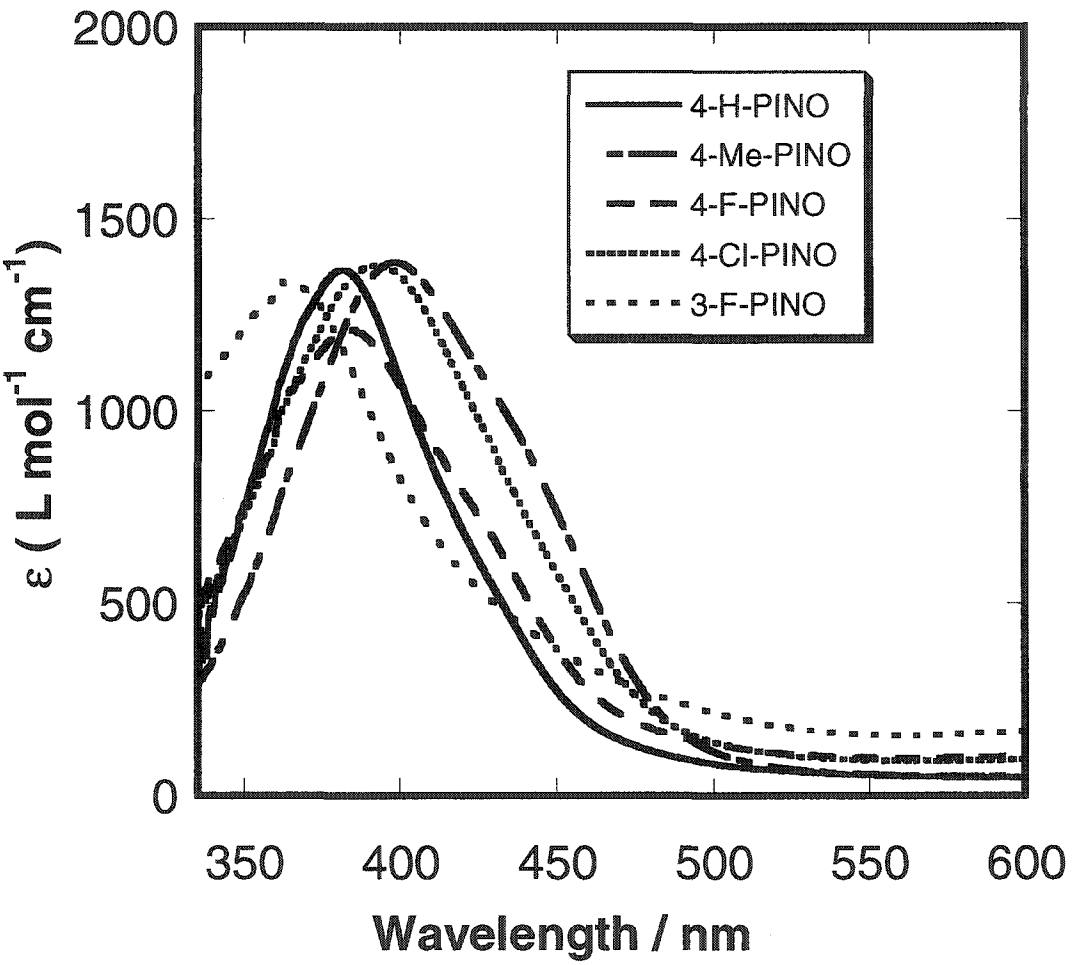

Figure S1. Superimposed spectra of substituted PINO radicals in HOAc.

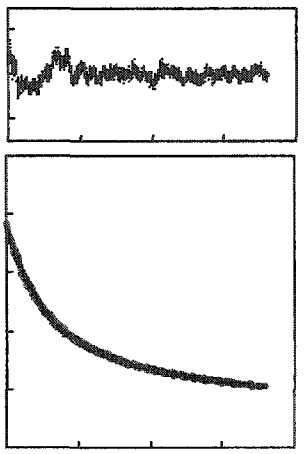

Figure S2(a). Second-order curve fitting for the decomposition of PINO• in benzene containing 10% of acetonitrile at 25 °C. $k_d = 31$ L mol^{-1} s^{-1}.

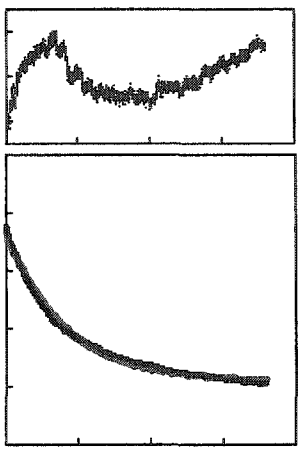

Figure S2(b). First-order curve fitting for the decomposition of PINO• in benzene containing 10% of acetonitrile at 25 °C. The pseudo-first-order rate constant is 1.2×10^{-3} s^{-1}.

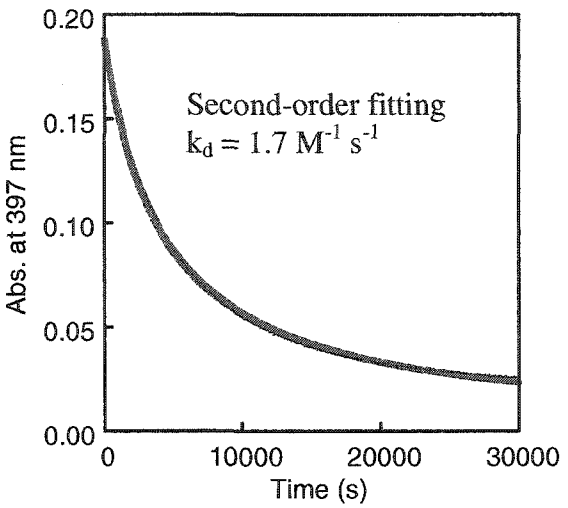

Figure S3(a). Decomposition of 4-Me-PINO radical in HOAc at 25 °C. $[Co(III)]_0$ = 0.500 mM and [4-Me-NHPI] = 0.833 mM.

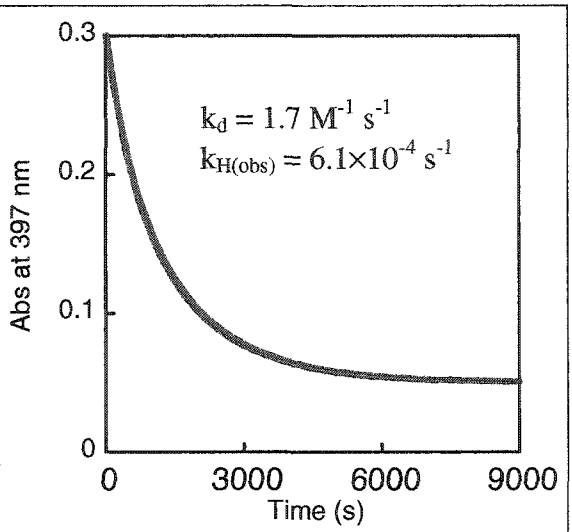

Figure S3(b). Decomposition of 4-Me-PINO radical in HOAc at 25 °C. $[Co(III)]_0$ = 0.500 mM and [4-Me-NHPI] = 7.50 mM.

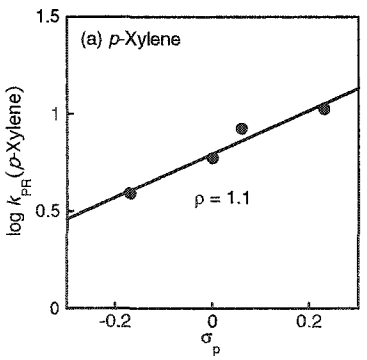

Figure S4(a). Hammett plot for the reaction of substituted PINO radicals with p-xylene in HOAc at 25 °C.

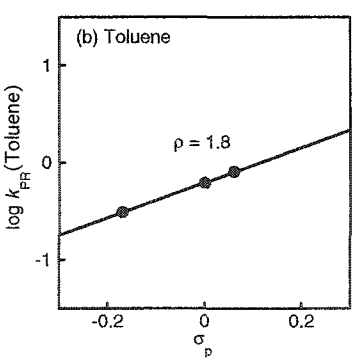

Figure S4(b). Hammett plot for the reaction of substituted PINO radicals with toluene in HOAc at 25 °C.

Table S1. Rate Constants of the Reaction between PINO• and 4-Me-NHPI with CF_3COOH in HOAc

$[CF_3COOH]$ / mmol L^{-1}	k_{obs} / s^{-1}
0	2.06
78	2.06
249	2.09

$[PINO•]_0 = 0.2$ mmol L^{-1}, $[4\text{-Me-NHPI}]_0 = 2$ mmol L^{-1}, $[NHPI]_0 = 2$ mmol L^{-1} in HOAc at 25 °C.

Table S2. Rate Constants for the Hydrogen Abstraction of 4-Substituted PINO Radicals with Toluene and Toluene-d_8 in HOAc at 25 °C

4-X-PINO•	$_{PR}$ (Toluene) / L mol^{-1} s^{-1}	$_{PR}$ (Toluene-d_8) / L mol^{-1} s^{-1}	k_H/k_D
F	0.810 ± 0.005	$(3.14 \pm 0.07) \times 10^{-2}$	25.8
H [a]	0.620 ± 0.005	$(2.29 \pm 0.03) \times 10^{-2}$	27.1
Me	0.310 ± 0.009	$(1.44 \pm 0.02) \times 10^{-2}$	21.5

[a] Ref. 5.

GENERAL CONCLUSIONS

Methyltrioxorhenium (MTO) was found to be an active catalyst for two reactions: one is the reduction of hydronium ions by Eu_{aq}^{2+} to evolve H_2; the other is reduction of perchlorate ions to chloride ions by Eu_{aq}^{2+} or Cr_{aq}^{2+} in acidic solution. In order to understand the reaction mechanism, kinetic studies were carried out and rate constants were obtained. Stepwise schemes were proposed to agree with all the experimental data. In the hydrogen evolution reaction, a yellow metastable Re(IV) species was produced and characterized spectrophotometrically by an intense charge transfer band at 410 nm. After that, a rhenium(V) hydride complex was postulated in the scheme to generate H_2 by a proton-hydride reaction, with which the reaction avoids the formation of the thermodynamically unfavorable intermediate H•. Under similar conditions, Cr^{2+} ions do not evolve H_2, despite $E°_{Cr} \sim E°_{Eu}$. In addition, no H_2 formation were observed in the presence of perchlorate ions because the reaction between methyldioxorhenium (MDO) and perchlorate ions has a much faster rate than that of hydrogen evolution.

A six-coordinate rhenium(V) compound MeReO(edt)(bpym) was prepared, characterized, and investigated for oxygen atom transfer reactions between picoline N-oxide and triarylphosphines. We found it is a good catalyst for the reaction, even though it is less active than those five-coordinate rhenium(V) dithiolato compounds. All the kinetic experiments were studied in benzene. The results showed that the reaction has a first-order dependence on both rhenium and picoline N-oxide. Triarylphosphines were found to inhibit the reaction, and those phosphines with more electron-donating groups in *para* positions had slower reaction rates. The importance of this study is that it proves a hypothesis: there should

be a steric requirement for the potential catalyst in the oxygen transfer reactions, which is the necessary existence of an open coordination site on rhenium center.

In the last chapter, we studied three different types of reactions of phthalimide N-oxyl radicals (PINO•) and N-hydroxylphthalimide (NHPI) derivatives. First, the self-decomposition of PINO• follows second-order kinetics. However, when excess of 4-Me-NHPI are used in the system, it was found that H-atom abstraction competes with the self-decomposition of 4-Me-PINO•. Second, the hydrogen atom self-exchange reactions between PINO• and substituted NHPI were found to follow H-atom transfer rather than the stepwise electron-proton transfer pathway. Last, the investigations of hydrogen abstraction from *para*-xylene and toluene by PINO• show large kinetic isotope effects, with the reaction becoming slower when the ring substituent on PINO• is more electron donating.

ACKNOWLEDGEMENTS

I would like to thank Professor James H. Espenson for his guidance and encouragement throughout my graduate career. His inspiration and devotion to science will always motivate me for my future life.

I would also like to thank previous and present group members for their assistance on daily work and insightful scientific discussions, especially Michael J. Vasbinder, Dr. Nobuyoshi Koshino and Dr. Basudeb Saha.

My appreciation also goes to my committee members for their help over my graduate study.

I am also thankful to Dr. Dave Scott and Dr. Shu Xu for assistance in NMR spectroscopy, to Dr. Arkady Ellen for analyzing crystal data, and to people in Engineering Service of Ames Lab for providing the instruments for hydrogen evolution measurements.

I would like to give my special appreciations to my husband and parents for their love, understanding and support in my whole life.

This work was performed at Ames Laboratory under Contract No W-7405-ENG-82 with the U.S. Department of Energy. The United States government has assigned the DOE Report number IS-T 2125 to this thesis.